The Pennsylvania State University

The Graduate School

THE ROLE OF DEFECT CHEMISTRY IN DC RESISTANCE DEGRADATION OF LEAD ZIRCONATE TITANATE THIN FILMS

A Dissertation in

Materials Science and Engineering

by

Betul Akkopru-Akgun

Submitted in Partial Fulfillment
of the Requirements
for the Degree of

Doctor of Philosophy

December 2019

The dissertation of Betul Akkopru-Akgun was reviewed and approved* by the following:

Susan Trolier-McKinstry
Professor of Ceramic Science and Engineering and Electrical Engineering
Dissertation Co-Adviser
Co-Chair of Committee

Michael T. Lanagan
Professor of Engineering Science and Mechanics and Materials Science and Engineering
Dissertation Co-Adviser
Co-Chair of Committee

Clive A. Randall
Professor of Materials Science and Engineering

Suzanne Mohney
Professor of Materials Science and Engineering and Electrical Engineering

Zoubeida Ounaies
Professor of Mechanical Engineering

John C. Mauro
Graduate Program Chair, Professor of Materials Science and Engineering

*Signatures are on file in the Graduate School.

ABSTRACT

This thesis describes the roles of defect chemistry and internal electric fields on the long-term stability of the properties of piezoelectric films. The correlation between defect chemistry, aging, leakage currents, and time dependent dielectric breakdown was studied for Nb and Mn doped $PbZr_{0.52}Ti_{0.48}O_3$ (PZT) thin films. It was demonstrated that the magnitude of the internal field is much higher in Mn doped PZT (PMZT) films compared to Nb doped PZT (PNZT) films after poling in the temperature range of 25-200°C under an electric field of -240 kV/cm. The development of the internal field is thermally activated, with activation energies from 0.5±0.06 to 0.8±0.1 eV in Mn doped films and from 0.8±0.1 to 1.2±0.2 eV in Nb doped films. The different activation energies for imprint suggests that the physical mechanism underlying the evolution of the internal field in PMZT and PNZT films differs; the enhanced internal field upon poling is attributed to (1) alignment of oxygen vacancy – acceptor ion defect dipoles ($(Mn''_{Ti} - V_O^{\bullet\bullet})^x$, $(Mn'_{Ti} - V_O^{\bullet\bullet})'$)) in PMZT films, and (2) thermionic injection of electron charges and charge trapping in PNZT films. In either case, the internal field reduces back switching, enhances the remanent piezoelectric properties, and dramatically improves the aging behavior. PMZT films exhibited the greatest enhancement, with reduced high temperature (180°C) aging rates of 2-3%/decade due to improved stability of the poled state. In contrast, PNZT films showed significantly larger high temperature aging rates (15.5%/decade) in the piezoelectric coefficient, demonstrating that the fully poled state was not retained with time.

The correlation between defect chemistry, leakage currents, and time dependent dielectric breakdown was also studied for $PbZr_{0.52}Ti_{0.48}O_3$ (PZT) films doped with 0.5, 1, 2, or 4% Nb. As the samples are nearly intrinsic, signatures for both hole hopping between Pb^{2+} and Pb^{3+} and electron trapping by Ti^{4+} were observed. For all doping levels, the dominant conduction mechanism transitioned from Poole-Frenkel emission at lower electric fields to Schottky emission at higher electric fields. The electric field for this transition diminishes from 172 to 82 kV/cm with decreasing Nb concentration. The concomitant modification of Schottky barrier height from 1.24 to 0.95 eV with decreasing Nb concentration is attributed to Fermi level pinning via oxygen vacancies. The DC resistance degradation was controlled by Schottky emission from 250-400 kV/cm; the lifetime of the films increases with increasing Nb level. The effective Schottky barrier height for 2% Nb doped PZT films decreased from 1.12 to 0.85 eV during degradation. This is related to the migration of oxygen vacancies towards the cathode, accompanied by the observation of Ti^{3+} near the cathode. Furthermore, the electric field range over which Schottky conduction increased with degradation. The mechanisms for time-dependent dielectric breakdown in PZT films will thus be a strong function of the initial film defect chemistry.

The electrical reliability of lead zirconate titanate (PZT) films was improved by incorporating Mn; the time dependent dielectric breakdown lifetimes and the associated activation energy both remarkably increased with Mn concentration. The correlation between the defect chemistry and the resistance degradation was studied to understand the physical mechanism(s) responsible for enhanced electrical reliability. At lower electric fields, Poole-Frenkel emission was responsible for the leakage current. Beyond a

threshold electric field, Schottky emission controlled the leakage. After degrading 2 mol% Mn doped PZT film under an electric field of 350 kV/cm at 180°C for 12 h, no significant change in potential barrier height for injecting electrons from the cathode into the anode was observed. This suggests that the degradation is mostly controlled by Poole-Frenkel conduction via some combination of hole migration between lead vacancies, small polaron hopping between Mn sites and hole hopping between Pb^{2+} and Pb^{3+}. The oxygen vacancy concentration after degrading PZT films under an electric field of 350 kV/cm at 180°C for 12 h was found to be $1x10^{20}$ cm^{-3} for 2 mol% Mn doped PZT films. No variation in the valence state of Ti near the cathode was observed in degraded Mn doped PZT films. Additionally, thermally stimulated depolarization current results did not show any depolarization peak arising from relaxation of trapped electrons on Ti^{4+}. This suggests that multivalent Mn provides trap sites for electrons and holes; free electron generation due to compensation of oxygen vacancies at the cathode and free hole formation at the anode region might be suppressed by the valence changes from Mn^{3+} to Mn^{2+} and Mn^{2+} to Mn^{3+} respectively.

Finally, the role of interfacial defect chemistry in time dependent breakdown and associated charge transport mechanisms was investigated for $Pb_{0.99}(Zr_{0.52}Ti_{0.48})_{0.98}Nb_{0.02}O_3$ (PNZT) films. Electrical degradation was strongly dependent on the sign of the electric field; a significant increase in the median time to failure from 4.8±0.7 to 7.6±0.4 hours was observed when the top electrode was biased negatively compared to the bottom electrode. The improvement in electrical reliability of Pt/PNZT/Pt films is attributed to (1) a $V_O^{\bullet\bullet}$ distribution across the film due to PbO non-stoichiometry, and (2) Ti/Zr segregation in PNZT films. Compositional mapping

indicates that PbO loss is more severe near the bottom electrode, leading to a $V_O^{\bullet\bullet}$ gradient across the film thickness. Upon degradation, $V_O^{\bullet\bullet}$ migration towards the bottom Pt electrode is enhanced. The concentration of $V_O^{\bullet\bullet}$ accumulated near the bottom Pt interface (6.2×10^{18} /cm^3) after degradation under an electric field of 350 kV/cm for 12 h was two times higher than that near the top Pt/PNZT interface (3.8×10^{18} /cm^3). The $V_O^{\bullet\bullet}$ accumulation near the bottom Pt/PNZT interface causes severe band bending and a decrease in potential barrier height, which in turn accelerates the electron injection, followed by electron trapping by Ti^{4+}. This causes a dramatic increase in the leakage current upon degradation. In contrast to the bottom Pt/PNZT interface, only a small decrease in potential barrier height for electron injection was observed at the top Pt/PNZT interface following degradation. It is also possible that a Zr-rich layer near the top interface reduces electron trapping by Ti^{4+}.

TABLE OF CONTENTS

LIST of FIGURES

LIST of TABLES

Acknowledgments

First and foremost, I would like to thank my advisor, Professor Susan Trolier-McKinstry, who is the best advisor, teacher, and mentor I could have ever wish for. She is always ready to take out of her personal time to meet her students. Her endless support, guidance, and generosity in time over my PhD years at Penn State are amazing and invaluable for me. Her dedication, enthusiasm and hard work always inspired me to be a good scientist and keep me motivated to contribute the field. Professor Trolier-McKintsry, I wholeheartedly appreciate for your mentorship, helping me improve and everything you have thought me to reach my goals. I truly cannot put my gratitude into words. I always feel lucky to have you as a role model for my future and be proud of a member of STM family.

Secondly, I would like to thank my co-advisor Professor Michael T. Lanagan for his guidance, invaluable insights, perspective, being open to the questions; no matter what was the level of question and even for teaching me how to do some electrical characterization techniques like van der Pauw method during my first year of PhD. He is always approachable with a big smile and open to discussion and interpretation of the experimental data over the years. His wise and prompt solutions to the experimental difficulties always improved the quality of the research.

I then wish to thank Professor Clive Randall, who I think of as my third advisor, for extremely valuable recommendations, enlightening discussions on electrical degradation phenomena in electroceramics. He let me involve in his group to learn and implement some electrical characterization techniques like TSDC and DLTS on PZT thin films. His contribution to the literature over the last 30 years guided us to explore

more about the correlation between the defect chemistry and the electrical degradation in PZT films. A special thanks goes to Thorsten Bayer and Kosuke Tsuji who thought me how to perform in-situ impedance analysis and deep level transient spectroscopy. I consider myself incredibly lucky to be surrounded by smart scientists. Thank you very much for long working hours, helpful discussions, and for your support. I believe this work would not be possible without your help.

I would also like to express my sincere appreciation to the rest of the members of my committee, Professor Suzanne Mohney and Professor Zoubeida Ounaies for their useful feedback, thoughtful suggestions, and outside perspectives to improve the quality of the thesis.

I would also like to thank the members of the STM, Randall, and Lanagan group for always being supportive, and helping me solve some troubleshooting problems, providing an environment that supports brainstorming on complicated data sets.

Many thanks to the MSC technical team; Julia Anderson, Amanda Baker, Vince Bojan, Trevor Clark, Maria DiCola, Bill Drawl, Beth Jones, Kathy Gehowski, Bangzhi Lui, Tim Klinger, Mike Labella, Jeff Long, Shane Miller, Nichole Wonderling, Steve Perini, Ke Wang, and Max Wetherington for helping me overcome technical difficulties as well as for trainings on the instruments. A special thanks also goes to Sandra Elder, April Benson, Joanne Aller, Donna Lucas, and Susie Sherlock for helping with the scheduling meetings, conferences, and all non-technical details.

I gratefully acknowledge National Science Foundation as well as Center for Dielectrics and Piezoelectrics under Grant Nos. IIP-1841453 and IIP-1841466 for funding this study.

I would also like to thank my parents for their endless support from 12000 miles away. They always offered help to take care of my son during my studies and to be with me whenever I went through difficult times. Without your encouragement, understanding and believing in me, I couldn't be the person I am today. Thank you very much for your love, support, and sacrifice in your personal times throughout my PhD years.

Finally, I would like to thank my husband, Mahir Akgun, for his endless support, love, encouragement, inspiration and countless advice whenever I feel stumped. He always encouraged me to grow as a scientist and person who I am today. He is proud of my academic achievements and most of the time gets more excited about my work than I do myself. I believe half of those achievements are belong to him. Mahir, you are the best husband, dad and lifetime friend I could ever wish for. Words cannot express the gratitude I have for you. I always feel so lucky to have you in my life. I'd like to dedicate this thesis to my lovely husband and sons, Arel and Arden Nova.

Chapter 1

Introduction and thesis organization

Utilization of microelectromechanical systems (MEMS) devices has dramatically increased the magnitude of the electric field distributed across lead zirconate titanate (PZT) piezoelectric films relative to typical fields applied to bulk PZT ceramics. As a result, the electrical reliability, including both DC resistance degradation and the stability of properties is of great concern. Therefore, it is important to understand the nature and concentration of defects as well as associated charge transport mechanisms leading to the leakage current and electrical degradation in PZT films in order to control electrical breakdown and device failure.

In general, electrons, holes, and mobile ions all contribute to the charge transport in PZT films; motion of these carriers, in turn, influence aging, retention loss, and electrical degradation. The equilibrium concentration of defects is determined by the nature of the dopants (acceptor, donor, fixed valence, redox-reactive), annealing atmosphere (PO_2 or P_{PbO}) and processing temperature. The volatility of PbO upon processing of PZT films is typically uncontrolled, and hence adds complexity to the defect chemistry in PZT films. When PbO(g) evaporates, charge compensation occurs by formation of oxygen and lead vacancies. It is believed that migration of oxygen vacancies and subsequent redistribution of charges in PZT films are primarily responsible for electrical degradation in PZT ceramics.

As a mixed electronic and ionic conductor, PZT has a band gap of 3.4 eV,[1] with multiple in-gap states introduced by defects.[1-8] The valence band consists of O *2p* and Pb

6s states, while the conduction band is made up of the unfilled d states of Ti^{4+}.[9] The presence of lone electron pairs (6s electrons) allows Pb^{2+} sites to act as shallow acceptor levels for holes. Early deep level transient spectroscopy (DLTS) studies reported by Smyth et al. confirmed that the Pb^{2+}/Pb^{3+} level is located approximately 0.26-0.3 eV above the valence band edge.[10] Lead vacancies, created due to evaporation of PbO(g) also introduce singly and doubly ionized lead vacancies that lie 0.9 and 1.4 eV above the valence band, respectively.[11-12] In the same way, introduction of acceptor ions creates additional impurity levels in the PZT energy band diagram. Redox active Mn ions produce two distinct impurity levels; (1) $Mn^{2+/}Mn^{3+}$ and (2) $Mn^{3+/}Mn^{4+}$ with ionization energies of 1.9 and 1.2 eV, respectively.[13] The main electron trapping centers in PZT are $Ti^{4+/}Ti^{3+}$,[10, 14-15] which produces a level about 1 eV below the conduction band, and oxygen vacancies, which are shallow traps located about 0.2 eV below the conduction band.[1] These defect levels are shown in Figure 1.1.

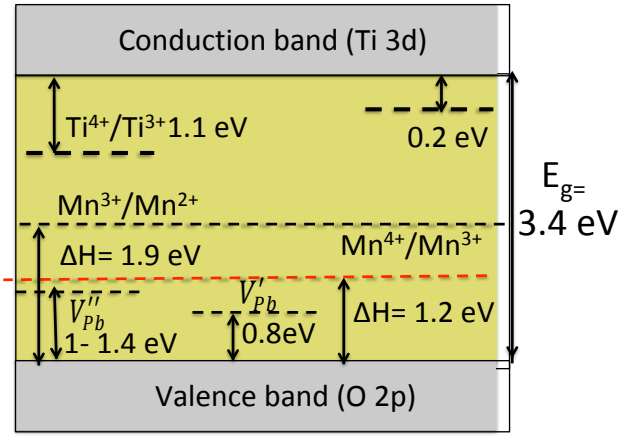

Figure 1.1 *Schematic representation of defect states in energy band diagram of PZT*

In contrast to PZT ceramics, electronic/ionic transport and the relevant defect chemistry are less well understood in PZT films. While, in principle, understanding of degradation in bulk PZT ceramics is a resource to the thin film community, there are a number of important differences that influence the defect chemistry and the charge

transport mechanisms responsible for DC resistance degradation. Three of the critical disparities are (1) most films have extremely fine grain sizes (< 200 nm), leading to a substantially higher fracture toughness than would be characteristic of bulk ceramics, which reduces the likelihood of electromechanical failure mechanisms, with subsequent dielectric breakdown. (2) The processing of thin films is typically conducted under conditions where the sample is not in thermodynamic equilibrium; this can result in higher point defect concentrations and metastable structures and (3) interfaces have a much stronger influence on point defect chemistry in films than in bulk materials; the equilibrium concentration of a point defect is strongly dependent on formation energy of defects at the interface. Moreover, as feature size is scaled down, the diffusion length over which defects must move to induce degradation becomes shorter. Thus, in order to understand the resistance degradation mechanism in PZT thin films, information about the charge transport mechanisms and related defect chemistry in PZT thin films is crucial. This dissertation examines the role of defect chemistry on the aging of ferroelectric properties and the resistance degradation in PZT thin films.

The roles of defect chemistry and internal electric fields on the long-term stability of the properties of piezoelectric films are presented in Chapter 2. The physical origin of the internal field is explored and the link between imprint and defect chemistry is studied. The stability of the developed imprint and the functional properties of the films at high temperatures is presented.

The correlation between defect chemistry, leakage currents, and time dependent dielectric breakdown in $PbZr_{0.52}Ti_{0.48}O_3$ (PZT) films doped with 0.5, 1, 2, or 4% Nb is presented in Chapter 3. A combination of techniques like DLTS, thermally stimulated

depolarization current (TSDC), and in-situ impedance measurements assist in determination of the major carrier type and associated charge transport mechanisms in Nb doped PZT films. The migration of oxygen vacancy and redistribution of charges, which takes place during degradation is discussed.

In Chapter 4, the role of redox active Mn in modifying the defect structure and associated charge transport mechanism is studied. Charge injection from the electrodes and subsequent transport of charge in Mn doped PZT films are discussed. This chapter provides information about how to engineer defect chemistry to control the leakage current rise upon electrical degradation and thereby improve lifetime of PZT films.

Chapter 5 discusses using Thermally Stimulated Depolarization Current (TSDC) to identify the type of defects contributing to dc resistance degradation in PZT films. The changes in defect concentrations and their distributions during electrical degradation in undoped, donor (Nb) and acceptor (Mn) doped PZT films are examined using TSDC.

Chapter 6 provides experimental evidence to demonstrate how the pristine state interfacial defect chemistry influences the transport mechanism upon electrical degradation in Nb doped PZT films. The role of PbO stoichiometry and Ti/Zr segregation on the conduction properties of the PZT/Pt is discussed.

Chapter 7 summarizes the significant findings from this study. A proposed future work section, including some preliminary data, describes possible pathways to understand the effect of DC resistance degradation on both the intrinsic and extrinsic properties of PZT films.

1.2 References

[1]Scott J.F. "Device physics of ferroelectric thin film memories," *Jpn. J. Appl. Phys.* 38: 2272-74 (1999).

[2]Warren W.L., Dimos D., Waser R.M., "Degradation mechanisms in ferroelectric and high-permittivity perovskites," *MRS Bulletin*, 40-45 (1996).

[3]Donnelly N.J. and Randall C.A., "Pb loss in Pb(Zr,Ti)O_3 ceramics observed by in situ ionic conductivity measurements," *J. Appl. Phys.*, 109: 104107-1-6 (2011).

[4]Waser R., Klee M., "Theory of conduction and breakdown in perovskite thin films," Integrated Ferroelectr. 2: 23-40 (1992).

[5]Boukamp B.A., Pham M.T.N., Blank D.H.A., and Bouwmeester H.J.M., "Ionic and electronic conductivity in lead-zirconate-titanate (PZT)," *Solid State Ionics*, 170:239 (2004).

[6]Slouka C., Kainz T., Navickas E., Walch G., Hutter H., Reichmann K., "The effect of acceptor and donor doping on oxygen vacancy concentrations in lead zirconate titanate (PZT)," *Materials*, 9: 945-1-22 (2016).

[7]Nagaraj B., Aggarwal S., Song T.K., Sawhney T., and Ramesh R.," Leakage current mechanisms in lead-based thin-film ferroelectric capacitors," *Phys. Rev. B*, 59: 16022 (1999).

[8]Slouka C., Andrejs L., and Fleig J., "Defect chemistry and transport properties of Nd doped Pb(Zr_xTi_{1-x})O_3," *J. Electroceram.*, 33: 221-39 (2014).

[9]Matsutani A., Luo Z.J., Pojprapai S., Hoffman M., Pezzotti G., "Visualization of highly graded oxygen vacancy profiles in lead-zirconate-titanate by spectrally resolved cathodolumiescence spectroscopy," *Appl. Phys. Lett.*, 95: 202903-1-3 (2009).

[10]Robertson J., Warren W.L., Tuttle B.A., Dimos D., and Smyth D.M., "Shallow Pb^{3+} hole traps in lead zirconate titanate ferroelectrics," *Appl. Phys. Lett.,* 63: 1519–21 (2012).

[11]Dih J. and Fulrath R.M., "Electrical conductivity in lead zirconate-titanate ceramics," *J. Am. Ceram. Soc.* 61: 448-51 (1978).

[12]Guiffard B., Boucher E., Eyraud L., Lebrun L., Guyomar D., "Influence of donor co-doping by niobium or fluorine on the conductivity of Mn doped and Mg doped PZT ceramics," *J. Eur. Cer. Soc.* 25: 2487-90 (2005).

[13]Wechsler B.A., and Klein M.B., "Thermodynamic point defect model of barium titanate and application to the photorefractive effect," *J. Opt. Soc. Am. B- Optical Phys*, 5: 1711–23 (1988).
[14]Smyth D.M., "Defect structure in perovskite titanates," *Current Opinion in Solid State & Mater. Sci.,* 1: 692-697 (1996).

[15]Raymond M.V., Smyth D.M., "Defects and charge transport in perovskite ferroelectrics," *J. Phys. Chem. Solids*, 57: 1507-1511 (1996).

Chapter 2

The effect of imprint on remanent piezoelectric properties and ferroelectric aging of $PbZr_{0.52}Ti_{0.48}O_3$ thin films

Chapter 2 of the thesis has been published previously in Journal of American Ceramic Society, 2019; 102:5328-41.

2.1 Introduction

Ferroelectric thin films are finding increased usage in a wide variety of microelectromechanical (MEMS) devices, including ink jet printers, adjustable optics, ultrasound transducers, resonators, energy harvesters, etc.[1-4] Significant work has been done on deposition techniques and device fabrication technology over the last two decades[5-9]; however, there are comparatively few reports on long-term ferroelectric aging of these materials.[10-12] Thus, an understanding of the fundamental materials science that underpins the stability of the properties is lacking.

Aging in ferroelectric ceramics can be defined as the change of piezoelectric and dielectric properties with time, under zero external stress and isothermal conditions.[10] It originates from stabilization of the local domain structure and immobilization of domain walls, both of which reduce the extrinsic contributions to properties over time.[13] There are four principal mechanisms that restrict domain wall motion and change the local domain configuration, and consequently cause aging. These are: (1) migration of impurities and vacancies to domain walls to lower the wall energy (domain wall immobilization),[14] (2) accumulation of charge at grain boundaries; the resulting internal field stabilizes the polarization direction, (an interface effect)[15] (3) alignment of defects to decrease the dipolar energy (volume or bulk effect),[16] and (4) ferroelastic switching

from a poled state to relieve local strains. In bulk ceramics, aging is often dominated by rearrangement of charged defects that stabilize the domain configuration through an electric or elastic field. This results in a decrease in the dielectric and piezoelectric properties over time.[14-19] The short-range motion of charged point defects (mainly oxygen vacancies), contributes to the reorientation of defect dipoles, while long-range motion of mobile ionic or electronic carriers results in formation of a space charge layer.[17, 18] Therefore, aging and degradation of ferroelectric ceramics is intimately related to conduction.

Since the discovery of aging in bulk ferroelectrics in the 1950s,[13] significant effort has been spent on investigating the mechanisms for aging and their dependence on the concentration and type of defects and the associated charge transport mechanism.[10, 18, 20-23] In general, the defect chemistry is a function of oxygen partial pressure, temperature, and doping.[24] In particular, the dopant type and concentration play important roles in the aging rate. It is well known that oxygen vacancies help immobilize domain walls. Hard dopants like Fe or Mn in lead zirconate titanate (PZT) generate oxygen vacancies, which act to stabilize domain walls through mechanisms such as direct pinning of the wall and/or development of a preferred polarization direction. This will increase the aging rate.[25-27] Soft doping with niobium, on the other hand, lowers the aging rate relative to acceptor-doped and undoped PZT.[28]

The enhancement of domain wall mobility in soft materials has been explained in several ways: (i) reduction in space charge accumulation at domain walls (e.g. donor doping also decreases the hole concentration) (ii) donor dopants compensate acceptor ions which are naturally present in the material and thus minimize the adverse effect of

acceptor ions on aging, (iii) compensation of lead vacancies by donor ions reduces the internal stress in the material so that domain walls becomes more mobile.[17, 50] In mixed dopant systems, where both acceptors and donors are introduced, the relative and total concentrations of dopants determine the dominant aging mechanism. The presence of acceptor ions even at small concentrations in highly donor doped PZT ceramics generates localized oxygen vacancies that act to increase aging rate.[29]

To diminish aging in ferroelectric thin films, a mechanism that restricts depolarization is required, e.g. by creating a preferred polarization state. This is known as imprint and is characterized by a shift in the polarization – electric field (P-E) hysteresis loop along the field axis.[30] There are two commonly used methods to introduce imprint in PZT thin films: (1) hot poling,[31] and (2) poling while illuminating under UV radiation.[31] The first method uses thermal energy to align defect dipoles along the polarization direction while the second method utilizes UV radiation to develop or redistribute space charge layers.[32-34] Both mechanisms generate internal electrical fields, leading to stabilization of the domain configuration along the polarization direction.

Different mechanisms have been proposed to explain imprint in PZT films; (1) the bulk screening model,[32] (2) the interface screening model,[31] and (3) the defect-dipole alignment model.[35] The bulk and interface screening models both assume the presence of a thin layer at the interface between the electrode and ferroelectric where the spontaneous polarization is suppressed and electronic charges are trapped.[35] In the bulk screening model, imprint is ascribed to the depolarizing field due to incomplete screening associated with the presence of a non-ferroelectric layer between the electrode and ferroelectric film.[36] In the interface screening model, on the other hand, an electrical field

arises in the interfacial layer to compensate the depolarization field, leading to either charge injection from the electrode into the bulk of the film or charge separation within the interfacial layer.[35] Although both models have been successful in describing the UV-induced imprint phenomena in PZT films, only the interface screening can be reasonably used to describe the imprint behavior in hot-poled ferroelectric films.[35]

In contrast, imprint can also develop in ferroelectric films due to defect-dipole alignment in a poling field associated with oxygen vacancy migration around acceptor ions. [35, 37] Introducing acceptor ions increases the vacancy concentration while addition of donors favors negatively charged cation vacancies. Since the oxygen vacancy concentration decreases after donor doping, an enhancement in the internal field is expected after doping with acceptor, rather than donor ions.[38]

Since imprint in PZT films is linked in at least some cases to defect-dipole alignment, the effect of doping on imprint is crucial to understanding the link between imprint and aging. The objective of this study is to understand how defect chemistry and internal electric fields develop in piezoelectric films, as well as the effect of these parameters on the long-term stability of the properties. For this purpose, Mn and Nb doped $PbZr_{0.52}Ti_{0.48}O_3$ thin films were deposited on platinized Si substrate using spin coating of a sol-gel solution. All samples were characterized by X-ray diffraction and field emission scanning electron microscopy to ensure that no second phases develop. Then, the ferroelectric and dielectric properties were examined before and after poling at 25-200°C. The poling conditions (poling time, magnitude of the electric field, and temperature) were used to modulate the remanent polarization and the degree of imprint

developed.[12, 39] High temperature aging at 180°C was performed to investigate the stability of the developed imprint and the functional properties of the films.

2.2 Preparation of Mn and Nb doped PZT thin films

Sol Preparation

Two series of PZT thin film solutions with Mn and Nb doping levels from 0.5-4 mol.% were prepared from lead acetate trihydrate ($Pb(CH_3COO)_2 \cdot 3H_2O$, Sigma-Aldrich), zirconium (IV) propoxide ($Zr(OCH_2CH_2CH_3)_4$, Sigma-Aldrich), titanium (IV) isopropoxide ($Ti(OCH(CH_3)_2)_4$, Sigma-Aldrich), manganese (II) acetate tetrahydrate ($(CH_3COO)_2Mn \cdot 4H_2O$, Sigma-Aldrich) and niobium (V) ethoxide ($Nb(OCH_2CH_3)_5$, Sigma-Aldrich), 2-methoxyethanol ($CH_3OCH_2CH_2OH$, Sigma-Aldrich), acetylacetone ($CH_3COCH_2COCH_3$, Sigma-Aldrich) and acetic acid (CH_3COOH, Sigma-Aldrich). Solutions with a Zr/Ti ratio of 52/48 were prepared using 10 mol% Pb excess to compensate for lead loss during heat treatment. The preparation of precursor solutions is similar to that described elsewhere.[40]

For preparation of Mn-doped PZT films, 20g of lead acetate trihydrate and 0.058-0.47 g of manganese acetate were dissolved in 120 mL of 2-methoxyethanol (2-MOE) under Ar in a rotary evaporator flask placed in an oil bath at 120°C. The solution mixture was then dried under vacuum until complete precipitation occurred. In a separate beaker, 11.2g of zirconium n-propoxide and 6.48g of titanium iso-propoxide were dissolved in 150 mL of 2-MOE and stirred for 30 min in a glove box. The resultant solution was slowly added into the Pb/Mn powders in the heated flask; the solution mixture was refluxed for 2 h under Ar at 120 °C. Following refluxing, the solution was vacuum distilled and then diluted with 2-MOE (5 vol %) and acetylacetone (22.5 vol %) to

achieve the desired solution molarity of 0.40 M. The Mn doping concentration in solution was estimated as $Pb_{\left(1.1-\frac{1}{2}x\right)}\ Zr_{0.52(1-x)}\ Ti_{0.48(1-x)}\ Mn_x\ O_{3.1}$, x = 0.005–0.04.

The processing of Nb-doped PZT solutions is very similar that used for Mn-doped PZT films. The only difference is that the $Nb(OC_2H_5)_5$ was added to the Ti/Zr/2-MOE solution and stirred for 30 min in the glove box. The solution composition was batched as $Pb_{\left(1.1-\frac{1}{2}x\right)}\ Zr_{0.52(1-x)}\ Ti_{0.48(1-x)}\ Nb_xO_{3.1}$, where x = 0.005–0.04. Subsequent steps were identical to those used in the processing of Mn doped PZT thin films, where the Zr/Ti/Nb solution was added to the Pb-containing powder and refluxed at 120°C to obtain the final solution.

Coating Process

Silicon substrates with a thick thermal SiO_2 barrier layer, 200 Å of Ti and 1500 Å of Pt (Nova Electronic Materials, Inc., Richardson, TX) were used in this study. Prior to coating, the substrates were exposed to rapid thermal processing at 500°C for 60 s to remove surface moisture. Doped PZT films were prepared via spin coating. First, the solution was dispensed onto the substrate through a 0.1μm polytetrafluoroethylene (PTFE, Restek) syringe filter. Then a single layer was spun at 1500 rpm for 30 s. Each layer underwent two pyrolysis treatments for 3 min at 250 and 450°C, respectively. The film was then crystallized at 700°C for 60 s by rapid thermal annealing (RTA). The process was repeated 6 times until a desired thickness of 0.4 μm was reached. Finally, a single PbO layer was coated onto the surface of PZT films and then heat treated at 700°C in air, to remove surface pyrochlore. Residual PbO was then removed by immersing the sample in a 4M acetic acid solution for 60 s.

2.3 Materials Characterization

Glancing Incidence X-ray Diffraction (GIXRD) was performed to examine the structure and orientation of the films using an X'Pert Pro MPD diffractometer (PANalytical, Almelo, The Netherlands). The x-ray source was Cu *Kα* radiation, with an accelerating voltage of 40 kV. The step size and hold time at each step was 0.02° and 10s, respectively. X-ray diffraction patterns were recorded between 10° and 80° 2θ.

The coating morphology was examined using a Leo 1530 model field emission scanning electron microscope (FESEM) (LEO Electron Microscopy Ltd., Cambridge, England) operated at 5 kV. Surface images were obtained in secondary electron imaging mode. The film thickness was measured using an Alpha-Step 500 Surface Profilometer (Tencor, Portsmouth, NH).

For electrical characterization, Pt top electrodes with diameters ranging from 200 μm to 1 mm were prepared by double layer photolithography and lift off processing. For this purpose, ~100 nm thick Pt films were sputter deposited on the PZT surface (CMS-18 Sputter System, Kurt J. Lesker Company, Pittsburgh, PA). After liftoff, the patterned Pt top electrodes were post-annealed at temperatures in the range of 500 to 750°C. The bottom Pt electrode was exposed using buffered HF to etch the PZT layers. The low field dielectric properties of the PZT films were determined using an LCR meter (Hewlett-Packard 4284A Precision, Agilent Technologies, Inc., Palo Alto, CA). All measurements were performed at 1 kHz with an oscillation voltage of 0.03 V. Hysteresis measurements were made using a Precision Multiferroic Analyzer (Radiant Technologies, Inc., Albuquerque, NM) using a triangular waveform and a frequency of 100 Hz. The longitudinal piezoelectric coefficient ($d_{33, f}$) of the PZT films was determined by double

beam laser interferometry (AixACCT DBLI). Prior to measurements, the samples were first poled at temperatures from 25 to 200°C using an HP 6200B dc power supply (Agilent Technology, Palo Alto, CA) with a DC electrical field five times higher than the coercive field for 30 min.

The first order reversal curves method (FORC) was used to determine the reversible and irreversible FORC distributions.[41] First order reversal curves were taken using a homemade polarization measurement system with voltage amplifiers (BOP 1000M, Kepco and TREK 609C-6, Piezotronics, Inc.). The films were initially pre-poled under an electric field of -240 kV/cm at 25 and 150°C for 30 min. Then, a family of P-E hysteresis loops (40 different loops) was recorded using an electric field cycle from a negative saturation field $-E_{max}$ to a field α_i where α_i changes from $-E_{max}$ to $+E_{max}$. The instantaneous descending electric field was β_i, The polarization was measured for α_i from $-E_{max}+ n\Delta E$, n= 2 to 40 and β_i from $-E_{max}+ k\Delta E$, k=0, 1, 2, …, n, respectively. The irreversible and reversible FORC distributions are defined for ($\alpha_i \in \alpha$) and ($\beta_i \in \beta$) as:[41]

$$p(\alpha,\beta) = \frac{1}{2}\frac{\partial^2 P(\alpha,\beta)}{\partial\alpha\,\partial\beta} \qquad \text{Equation 2.1}$$

$$p_{rev}(\alpha) = \lim_{\beta\to\alpha-}\frac{1}{2}\frac{\partial P(\alpha,\beta)}{\partial\beta} \qquad \text{Equation 2.2}$$

where α and β are the up- and down- switching fields of some population of hysterons, respectively. For α>β, the hysterons are irreversible and for α=β, the hysterons are reversible.

Aging measurements

Before the aging test, samples were poled at 150°C under an electric field of 240 kV/cm for 30 min. Then, the samples were aged at zero field under closed circuit conditions at 180°C. High temperatures were used to accelerate the aging process. The piezoelectric response, $d_{33,f}$, was then measured at room temperature as a function of the time spent aging at elevated temperature. The time variation of $d_{33,f}$ follows a well-known logarithmic law. The percent change of piezoelectric response (d_{33}) per decade of time (e.g. one order of magnitude change) was calculated using the following relationship with time.

$$d_{33,f}(t) = d_{33,f}(t_0) - r \log(t) \qquad \text{Equation 2.3}$$

where $d_{33,f}(t)$ is the longitudinal piezoelectric coefficient measured after an aging time t, $d_{33,f}(t_0)$ is longitudinal piezoelectric coefficient at t_0, $(t_0 < t)$, and r is the rate of decay. Similarly, P-E hysteresis measurements were conducted following different aging times to monitor the change in the magnitude of imprint for the PMZT and PNZT films.

2.4 Results and Discussion

2.4.1 Phase identification and microstructure of PZT thin films

The surface morphology and structure of Mn and Nb doped PZT films after annealing at 700°C in O_2 were studied by FESEM and GIXRD. Figure 2.1 shows that all films have the perovskite structure.[42] No peaks corresponding to secondary phases such as excess PbO or pyrochlore were observed in the XRD patterns, suggesting that at most trace amounts of secondary phases exist in either set. As shown in Figure 2.1, the films with low Mn and Nb concentrations are approximately randomly oriented. With increasing Mn concentration, XRD peaks shifted towards higher angles, indicating

decreased out-of-plane lattice parameters for the PMZT films. The results for the Mn-doped film are comparable to those reported by Zhu et al.[43] The same group reported no change in lattice parameter with Nb doping.[44]

Figure 2.2 exhibits FESEM surface micrographs of the Mn and Nb doped PZT films grown on Pt/Ti/SiO_2/Si substrates. As shown there, both Mn and Nb doped PZT

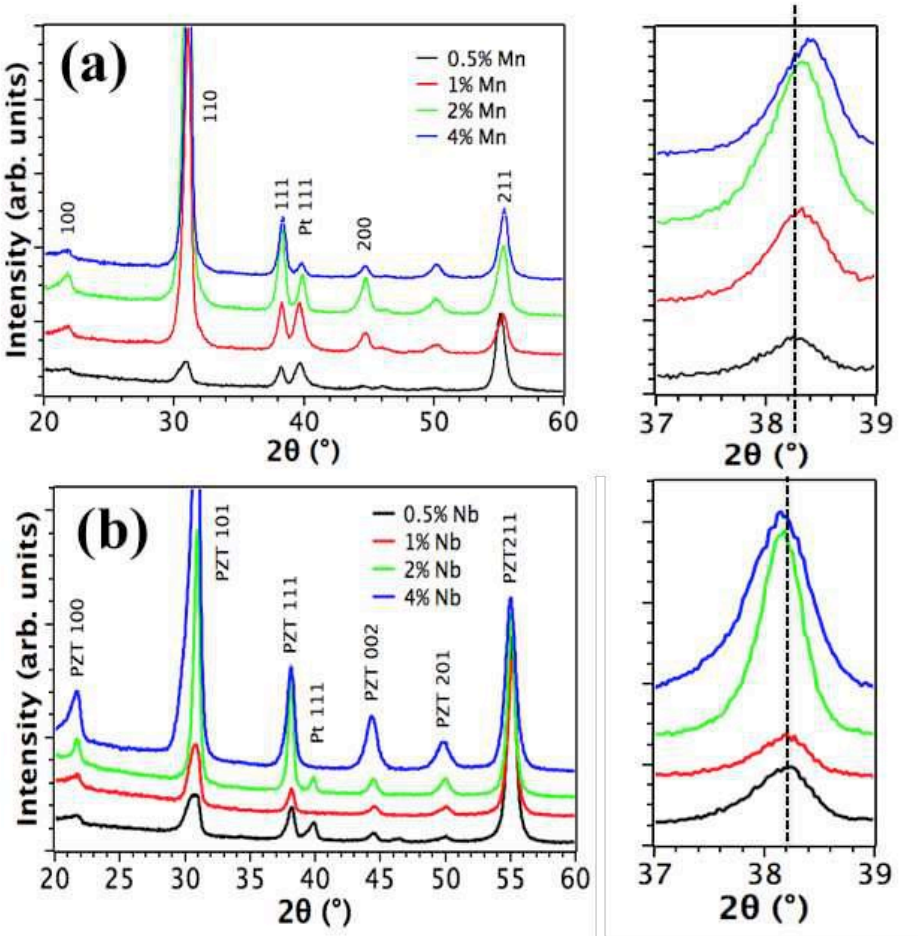

Figure 2.1 *Glancing XRD diffraction patterns of (a) Mn and (b) Nb doped PZT films. All films were smooth, homogeneous and of high density; no crack formation was observed. SEM results confirmed that the grain size in both Mn and Nb doped PZT films is similar and varies from 30-150 nm.*

2.4.2 Thermal imprint in Mn and Nb doped PZT films

The high field dielectric response of 1% Mn and 1% Nb doped PZT films before and after poling at 25 and 150°C for 30 min was analyzed using the irreversible FORC distributions, where α and β are the up- and down- switching fields of some population of hysterons, respectively, as shown in Figure 2.3 The appearance of periodic features along the α=β line of Figure 3 is an artifact arising from the algorithm used for calculation. In

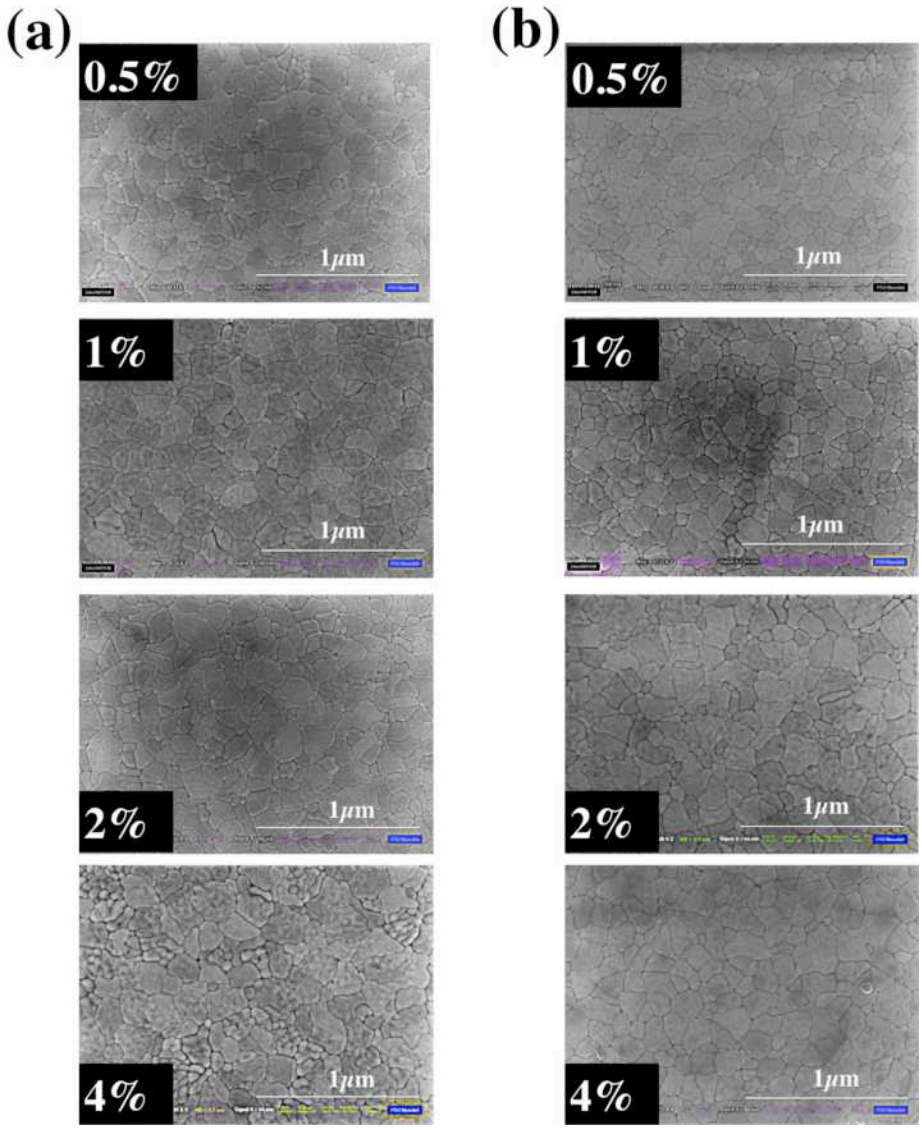

Figure 2.2 *Top surface FESEM images of (a) Mn, and (b) Nb doped PZT films.*

unpoled Mn doped PZT films, the irreversible FORC distribution was broadened, which means that up and down switching fields for the hysterons show more variability. It is probable that this is a result of the fact that incorporation of Mn into PZT generates defect dipoles, which change the local electric/elastic field, modulating the switching of the

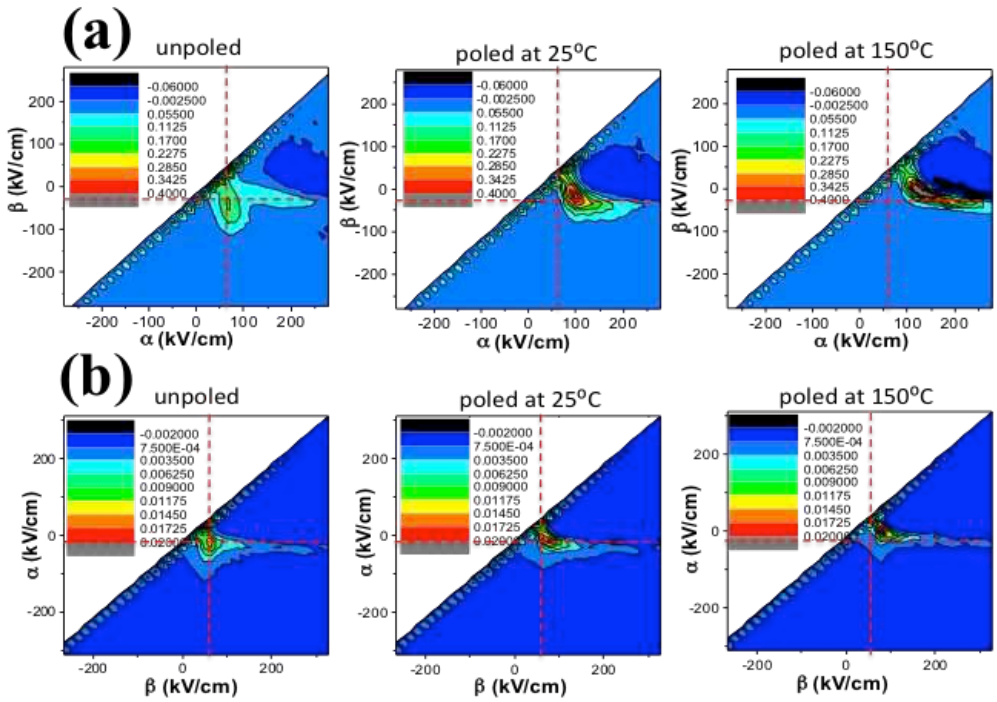

Figure 2.3 *The irreversible FORC distributions of the (a) 1% Mn and (b) 1% Nb doped PZT films before and after poling at 25 and 150°C.*

hysterons. Since Nb doped PZT films have a low concentration of defect dipoles involving oxygen vacancies, the FORC distribution is very sharply peaked. After poling, the distribution of switching fields becomes sharper for both Mn and Nb doped films. Additionally, the up- and down-switching fields for the hysterons shifts further from the $\alpha = -\beta$ line, consistent with the development of imprint. This shift is more noticeable in Mn doped PZT films, compared to their Nb doped counterparts, indicating a higher magnitude of imprint in PMZT films. Mn doped PZT films have higher concentration of defect dipoles (acceptor ions and oxygen vacancies) that can be aligned along the

polarization direction during poling to introduce imprint.[30]

Figure 2.4 shows the effect of imprint on the reversible FORC distributions. It is seen that poling of both Mn and Nb doped films shifts the reversible FORC distributions

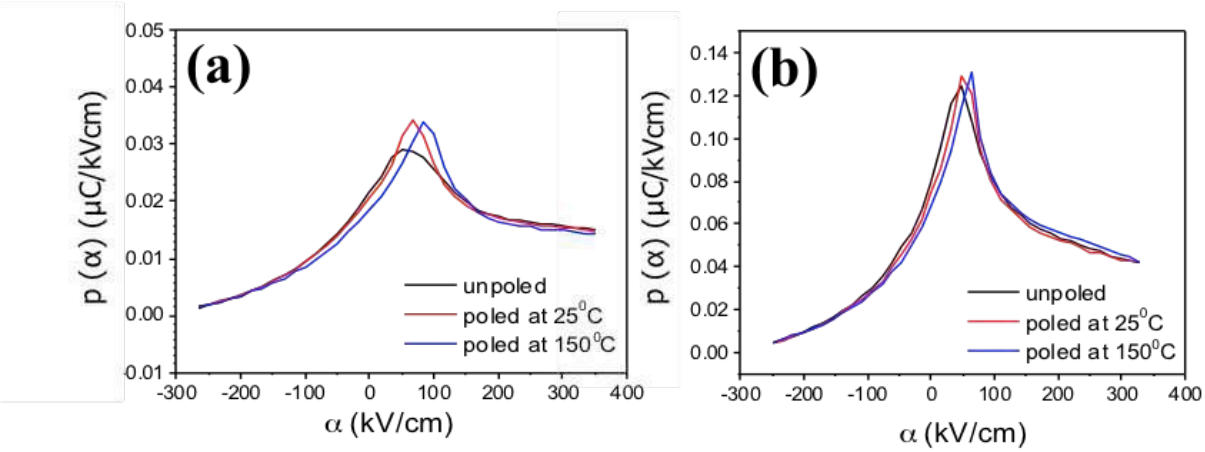

Figure 2.4 *Reversible FORC distributions of (a) 1% Mn doped and (b) 1% Nb doped PZT films*

along the field axis, another indication of imprint in the PZT films. The degree of imprint was enhanced as the poling temperature increased. For PMZT films, the internal field is 14 and 28 kV/cm after poling at 25 or 150°C, respectively. For PNZT films, on the other hand, the magnitude of internal field was smaller; it is 7 kV/cm after poling at 25°C and it increased to 14 kV/cm after poling at 150°C. Furthermore, the maximum in the reversible FORC distribution increases after poling; this is most noticeable in Mn doped PZT films after hot poling. This increase is presumably related to the restoring force provided by the imprint field. The restoring force tends to align domains perturbed by the electric field, making the response more reversible and increasing the intensity of the reversible FORC distribution.

The effect of thermal imprint on the ferroelectric properties of Mn and Nb doped films was also investigated by P-E hysteresis measurements; the findings are in

agreement with the FORC results. Figure 2.5 shows the hysteresis loops of unpoled and poled PZT thin films doped with 1 mol.% Nb or Mn, measured up to 400 kV/cm. As

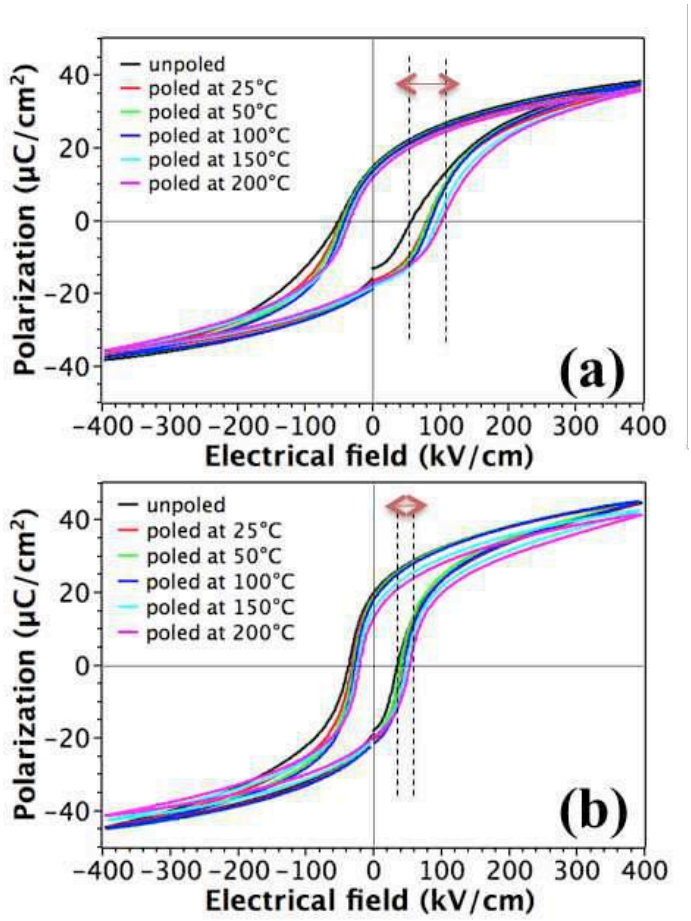

Figure 2.5 *Variation of P-E hysteresis loop of (a) 1% Mn and (b) 1% Nb doped PZT films after poling at different temperatures*

shown in Figure 2.5, the hysteresis loops of both films move to positive voltages after poling at -240 kV/cm (such that the direction of poling field is pointed from the top to the bottom electrode). The shift becomes more noticeable as the poling temperature increases. It is apparent that films poled at room temperature under these conditions have nearly symmetrical hysteresis loops, as do films that were originally unpoled. However, as the poling temperature is increased to 200°C, a strong imprint progressively develops. This is manifested primarily as a left-right shift on the loop, without significant

degradation in the switchable polarization (Figure 2.5). In the same way, there is no strong evidence for development of significant levels of leakage at either electrode following the high temperature poling.

Figure 6 exhibits the level of imprint in PMZT and PNZT films as a function of poling temperature. The magnitude of imprint was determined from the voltage shifts in P-E hysteresis loops. The internal field can be defined as,

$$E_i = \frac{+E_c - |-E_c|}{2} \qquad \text{Equation 2.4}$$

where E_i is the internal field, $+E_c$ is the positive coercive field, and $-E_c$ is the negative

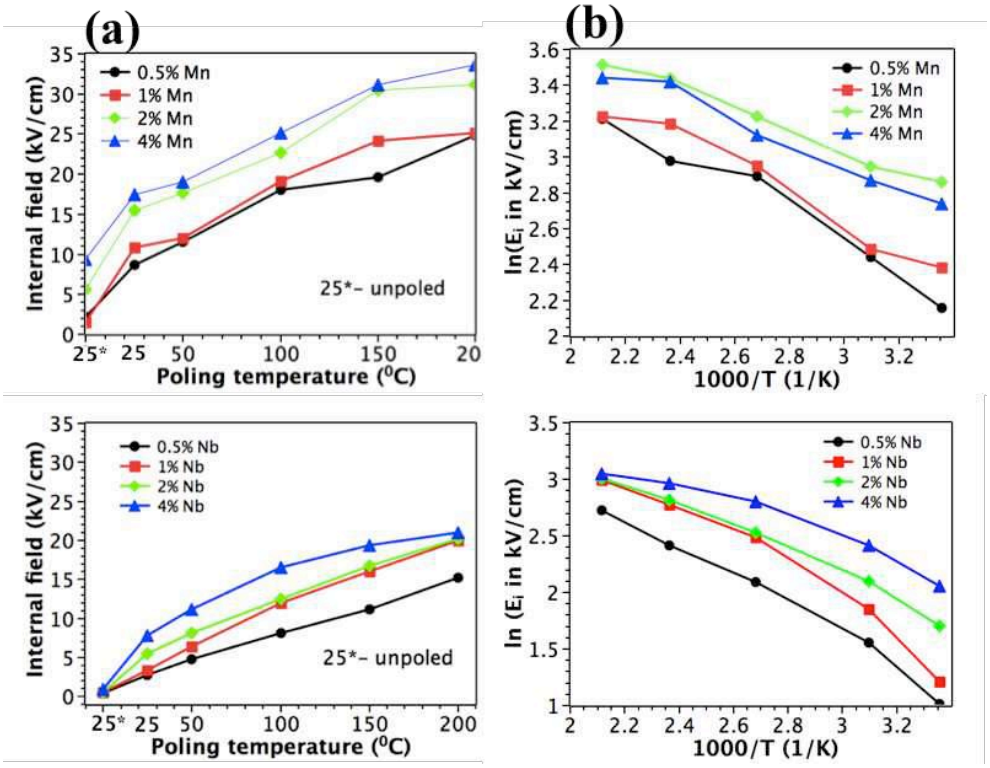

Figure 2.6 *Variation of the magnitude of internal field in (a) Mn and (b) Nb doped PZT films determined from P-E loops performed after poling at different temperatures.* ***Activation energies for internal field were calculated from the slope of the graphs.***

coercive field. As shown in Figure 2.6, the response of PNZT and PMZT films to poling is considerably different. For PMZT and PNZT films, the internal fields ranged from 3 to 32 kV/cm and 0.5 to 18 kV/cm, respectively. For all dopant levels and poling

temperatures, the magnitude of imprint was higher in the PMZT films. The temperature dependence of the voltage shift in the P-E hysteresis was found to follow an Arrhenius-like behavior for both donor and acceptor doped PZT films. It should be noted that the high temperature data points for Mn doped PZT films and the 25°C data point for Nb doped PZT films deviate from purely Arrheniius-like behavior with a single activation energy. Since the estimated activation energies vary only slightly when these data points are excluded, the data points were retained, and their influence on the activation energy is included within the error bars. As shown in Figure 6b, the activation energies (E_a) extracted from the slopes of the Arrhenius plots for Mn doped PZT films ranged between 0.5±0.06 and 0.8±0.1 eV. These are much lower than E_a for their Nb doped counterparts (0.8±0.1 to 1.2±0.2 eV).

Addition of Mn on the perovskite Zr/Ti site in PZT can create defect dipoles such as $(Mn''_{Ti} - V_O^{\bullet\bullet})^x$, $(Mn'_{Ti} - V_O^{\bullet\bullet})'$ when it is ionically compensated by oxygen vacancies. Additionally, evaporation of PbO could, in principle, lead to formation of $(V''_{Pb} - V_O^{\bullet\bullet})^x$ defect associates. Oxygen vacancies are the most mobile ions in PZT and short-range migration of oxygen vacancies around the acceptor can generate an internal field in PZT films at poling temperatures and fields.[45-46] Presumably, the concentration of defect associates increases with Mn concentration in the PZT, enhancing the propensity of defect dipole alignment upon thermal poling of PZT films. Indeed, the E_a for imprint in Mn doped PZT films varies between 0.5 and 0.8 eV, which is close to the activation energy required for migration of oxygen vacancies (Table 1).[47] This suggests that imprint in Mn doped PZT films is governed via defect dipole alignment rather than injecting and/or trapping of electronic charges (Figure 10b). To further support this hypothesis,

leakage current measurements were conducted to explore the dominant conduction mechanism over the range of temperatures used for development of imprint in PMZT films (Figure 2.7). It was found that the leakage current is controlled via Schottky emission and that the potential barrier height for thermionic injection of electronic charges varies between 0.72 to 1.12 eV. It is notable that the Schottky barrier heights generally exceeds E_a for imprint in Mn doped PZT films (Table 2.2).

Table 2.1 *Activation energies for imprint in PMZT and PNZT films.*

PMZT films	***0.5% Mn***	***1% Mn***	***2% Mn***	***4% Mn***
E_a *(eV)*	0.8±0.1	0.7±0.1	0.6±0.1	0.5±0.06
PNZT films	***0.5% Nb***	***1% Nb***	***2% Nb***	***4% Nb***
E_a *(eV)*	1.2±0.2	1.2±0.2	0.9±0.1	0.8±0.1

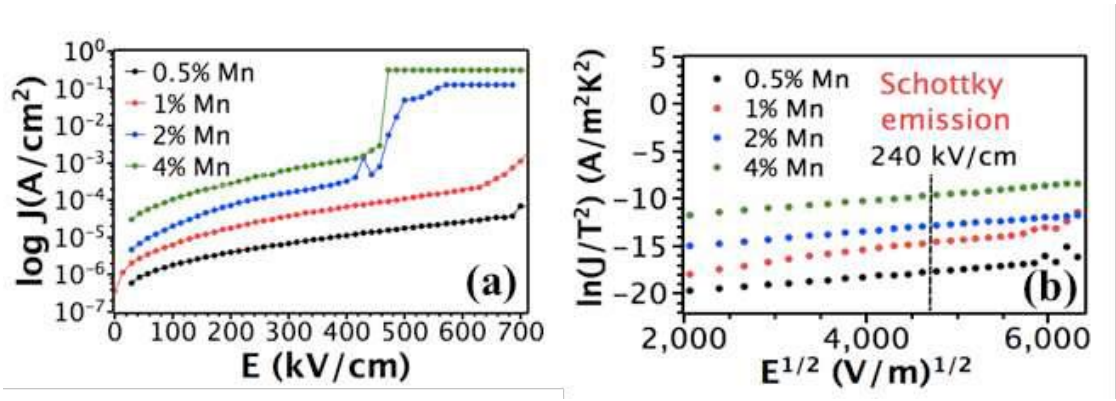

Figure 2.7 (a) *The variation of leakage current density with electric field in Mn doped PZT films (b) Fitting of the leakage current-voltage data for distinct electric fields in Mn doped PZT thin films.*

Table 2.2 *Schottky barrier heights in PMZT and PNZT films*

PMZT films	*0.5% Mn*	*1% Mn*	*2% Mn*	*4% Mn*
Φ_B *(eV)*	1.17±0.04	1.06±0.05	0.84±0.03	0.72±0.04
PNZT films	***0.5% Nb***	***1% Nb***	***2% Nb***	***4% Nb***
Φ_B *(eV)*	0.95±0.05	1.07±0.03	1.15±0.04	1.24±0.04

In contrast to Mn doped PZT films, the activation energy for imprint in Nb doped PZT films (0.8±0.1 to 1.2±0.2 eV) (Table 2.1) was much higher than the activation

energy required for migration of oxygen vacancies (0.5-0.6 eV). It is intriguing that, particularly in the case of the lower Nb concentrations, the activation energy for imprint is comparable to the activation energy for failure of many undoped PZT films.[48] The higher activation energies for imprint in PNZT films suggest that defect dipole alignment is not the only mechanism contributing to imprint. Indeed, the only source for generation of oxygen vacancies in Nb doped PZT films is evaporation of PbO upon annealing at temperatures higher than 450°C, which could lead to formation of $(V_{Pb}'' - V_O^{\bullet\bullet})^x$ dipoles. The oxygen vacancy concentration reduces with increasing Nb levels in PZT films, which would suppress the internal field originating from defect dipole alignment upon thermal poling. However, it was found that the magnitude of imprint increases at higher Nb concentrations. This strongly suggests that defect dipole alignment model alone cannot explain the magnitude of imprint observed in Nb doped PZT films.

It is possible that charge injection, the propensity for long-range migration of oxygen vacancies, or differences in the original film stoichiometry can also contribute to the observed imprint.[35, 49] To explore the contribution of electronic charges to the built in internal field, leakage current measurements were conducted on Nb doped PZT films. For lower Nb concentrations (0.5% and 1% Nb), the conduction is mainly controlled by Schottky emission in the temperature and electric field (240 kV/cm) range used to create an internal field in PZT films (Figure 2.8). It is intriguing that the potential barrier height for thermoionic emission of electrons from the electrode into the PNZT is approximately 1 eV (Table 2.2), which is comparable to the activation energy (1.2±0.2 eV) for generation of imprint in PZT films. Furthermore, impedance measurements were conducted to explore defect sites at which injected electronic charges could be trapped.

Figure 2.9 shows the temperature dependence of the modulus and conductivity for 1% Nb doped PZT films. The calculated activation energy for Nb doped PZT film is 1.1 ± 0.06 eV, which is attributed to electron trapping by Ti^{4+}.[26, 50]

$$Ti^{4+} + e' \rightarrow Ti^{3+} \qquad \text{Equation 2.5}$$

It is believed that imprint in 0.5 and 1% Nb doped PZT films results from electron injection from the electrode into the dielectric with subsequent electron trapping by Ti^{4+} site

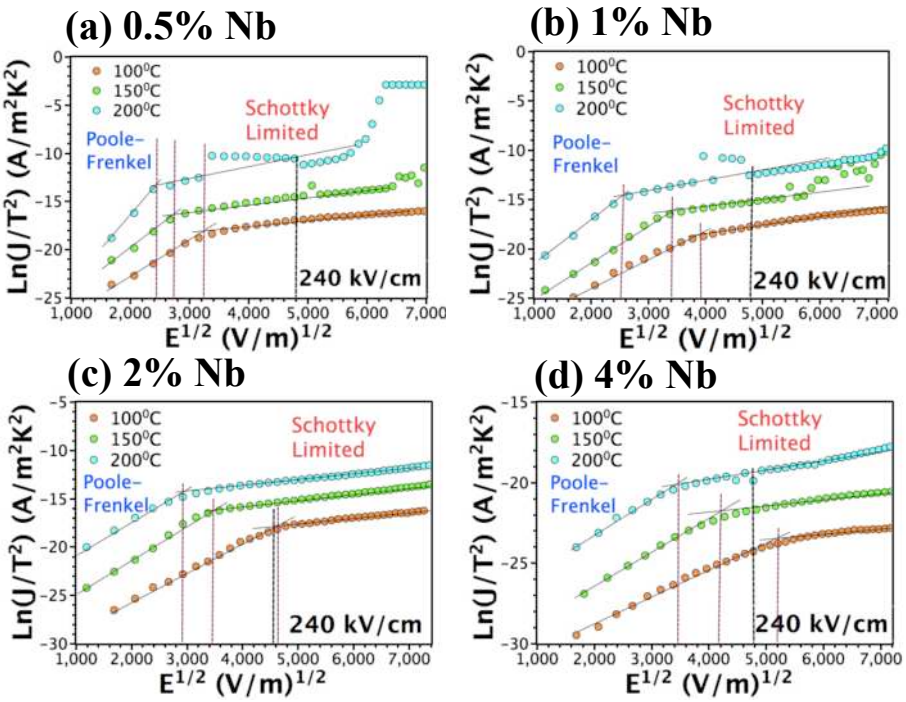

Figure 2.8 *Fitting of the leakage current-voltage data for distinct temperatures in (a) 0.5%, (b)1% Nb, (c) 2% Nb, and (d) 4% Nb doped PZT thin films.*

(Figure 2.10a). With an increase in Nb concentration, Poole-Frenkel emission starts contributing to the electronic conduction below 150°C, leading to a discrepancy between the imprint E_a (0.8-0.9 eV) and the calculated Schottky barrier height (1.15-1.24 eV).

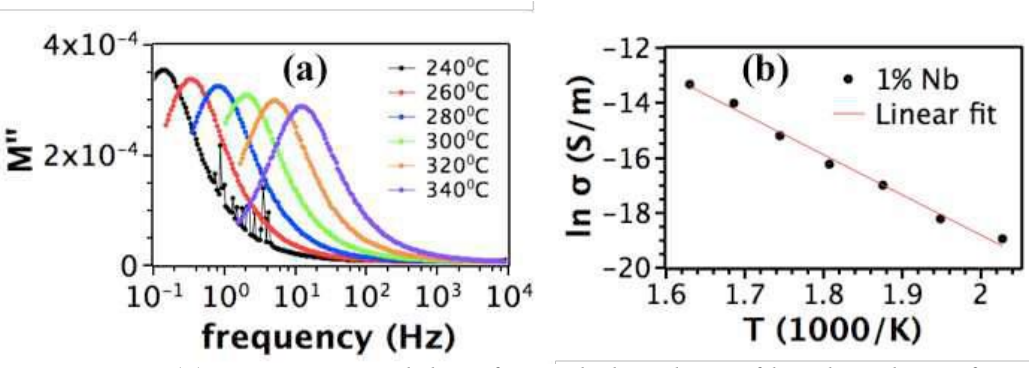

Figure 2.9 *(a) Imaginary modulus of 1% Nb doped PZT film plotted as a function of frequency at different temperatures. (b) Change in conductivity of 1% Nb doped PZT films with temperatures.*

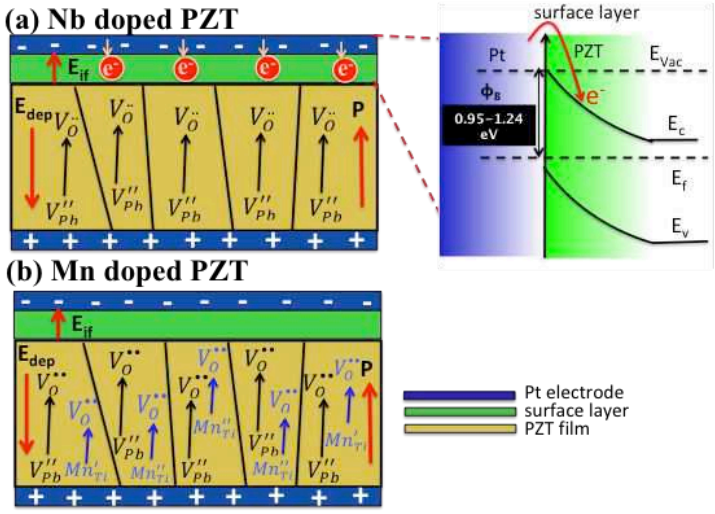

Figure 2.10 *Schematic representations of physical models for development of imprint in (a) Nb doped, (b) Mn doped PZT films.*

It was found that the internal field has a significant effect on the remanent piezoelectric properties, such as the longitudinal piezoelectric coefficient ($d_{33,f}$). Figure 2.11(a) and 2.11(b) show the longitudinal piezoelectric coefficients of 1% Mn and 1% Nb doped PZT films after poling at temperatures ranging from 25 to 200°C. The data were taken by driving the film with a unipolar field parallel to the poling direction to progressively higher electric fields in the range of 50-150 kV/cm. There are several key points that are apparent from these figures. First, the films that had been poled at room temperature or 50°C had relatively smaller remanent $d_{33,f}$ coefficients than those poled at

higher temperatures. When driven to progressively higher electric fields (> 50 kV/cm), the films repole, producing hysteretic responses. In contrast, films poled at higher temperatures showed larger remanent $d_{33,f}$ values, and substantially less hysteresis in the instantaneous $d_{33,f}$ as a function of the drive field. This indicates that the net polarization in the PMZT and PNZT films poled at higher temperatures are more stable than the ones poled at room temperature. Secondly, the maximum value of the $d_{33,f}$ observed was larger for higher poling temperatures. For 1% Mn doped PZT film, the remanent $d_{33,f}$ value after poling at 25°C is 66 pm/V, increasing to 75±2, 85±2, 90±2, and 92±3 pm/V after poling the sample at 50, 100, 150, and 200°C. Similarly, the 1%Nb doped PZT film poled at 25°C has a remanent $d_{33,f}$ of 80 pm/V; the remanent $d_{33,f}$ increased to 84±1, 92±1, 96±1, and 98±2 pm/V after poling the sample at 50, 100, 150, and 200°C. These results are consistent with better alignment of the polarization along the electric field direction upon poling.[11]

Figure 2.11(c) and Figure 2.11(d) exhibit the change in $d_{33,f}$ with internal field for PZT-based films with different Mn and Nb concentrations. It was observed that the internal field improves the $d_{33,f}$ for both PMZT and PNZT films. However, the enhancement in $d_{33,f}$ due to imprint is more obvious in PMZT films, where larger internal fields can be introduced (Figure 2.11). As shown in Figure 2.11(c), the longitudinal piezoelectric coefficient of 4% Mn doped PZT films is almost doubled after poling at 200°C. For 4% Nb doped PZT films, on the other hand, $d_{33,f}$ only increased by ~30% relative to its 25°C-poled counterpart. The larger increase in $d_{33,f}$ after poling at high temperatures in Mn doped PZT films can be attributed to an enhanced internal field due to alignment of defect dipoles ($(Mn_{Ti}'' - V_O^{\bullet\bullet})^x$, $(Mn_{Ti}' - V_O^{\bullet\bullet})'$) along the polarization

direction during poling.

Another finding of Figure 2.11(c) and (d) is that for both Mn and Nb doped films, the internal field and corresponding $d_{33,f}$ increased with doping concentration. As reported in the literature, the alignment of oxygen vacancy and acceptor ion defect dipoles during poling introduces imprint in PZT ceramics.[51-52] When oxygen vacancies

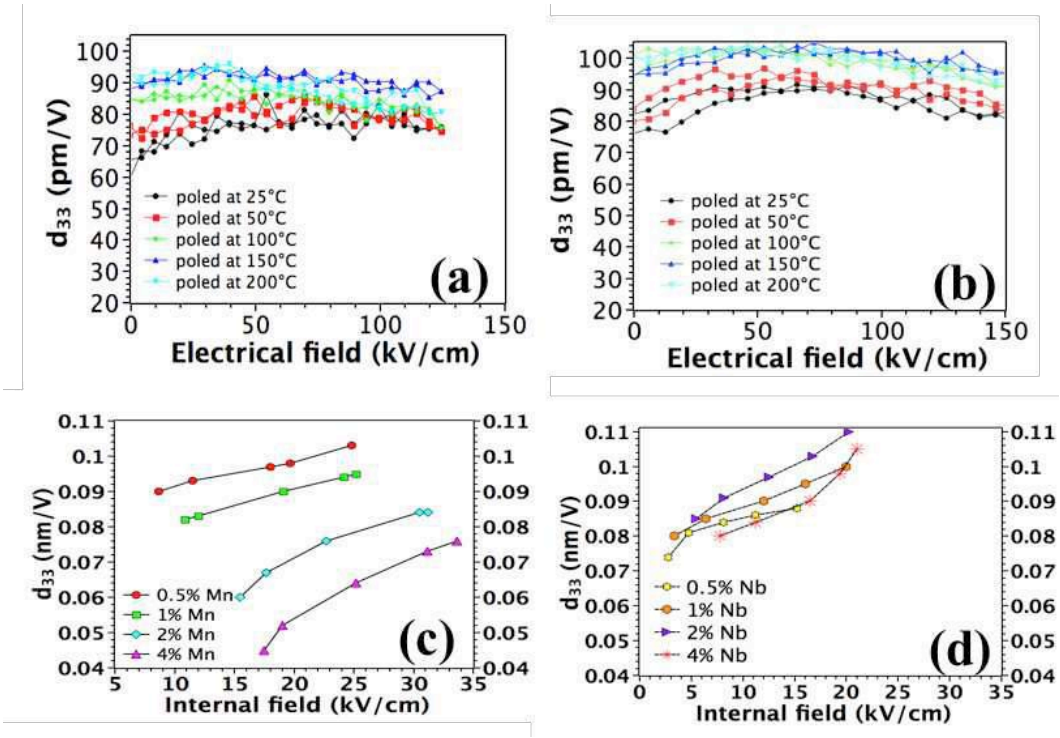

Figure 2.11 *Variation of the magnitude of longitudinal piezoelectric coefficient $d_{33,f}$ of (a) 1% Mn doped, (b) 1%Nb doped PZT films after poling at 25, 50, 100, 150, and 200°C, (c) 0.5, 1, 2, 4% Mn, (d) 0.5, 1, 2, 4% Nb doped PZT films after poling at 150°C*

either move around an acceptor center to produce a defect dipole, or migrate long distances to produce space charge, it results in formation of internal field in PZT films, which in turn enhances the piezoelectric properties. Since the oxygen vacancy concentration increases as higher concentrations of Mn are introduced into PZT films, an enhanced internal field and $d_{33,f}$ are expected. However, in the case of Nb doped PZT films, the increase in internal field and $d_{33,f}$ cannot be explained based on the defect

dipole alignment model since the oxygen vacancy concentration decreases after donor doping. It is believed that internal field in Nb doped PZT films results from both thermoionic emission of charges and Poole-Frenkel emission from traps. With increasing Nb concentration, the contribution of bulk charge transport mechanisms like electron trapping at Ti^{4+} sites (trap energy of 1 eV) to internal field increases, leading to a higher magnitude of the imprint field in PZT films.

2.4.3 The stability of imprinted state in Mn and Nb doped PZT films

The stability of the imprinted state in the PMZT and PNZT films induced by poling the samples at 25-200°C was examined under high field. P-E hysteresis measurements were made on equivalent electrodes immediately after poling at 150°C and 1, 2, 4, 6, or 24 h after the poling. Figure 2.12 exhibits the change in the magnitude of imprint in PMZT films as a function of time after poling. The samples were aged at 180°C to increase the aging rate, as it was very slow at room temperature. The magnitude of imprint was calculated from the shifts along the electric field axis in P-E hysteresis loops. As shown in Figure 2.12, the stability of the imprint with aging time at 180°C showed significant differences for Mn and Nb doped PZT films. For Mn doped PZT films, the magnitude of imprint slightly decreased after 24h, indicating that voltage shift is mostly conserved. For Nb doped PZT films, on the other hand, the imprint gradually decreased with time and completely disappeared after 24h at 180°C. The difference in stability of imprint is consistent with the hypothesis that the mechanism for inducing imprint in Mn and Nb doped PZT films differs. The physical origin of imprint in Mn doped PZT films arises from alignment of defect dipoles like $(Mn''_{Ti} - V_O^{\bullet\bullet})^x$, $(Mn'_{Ti} - V_O^{\bullet\bullet})'$ along the polarization direction. A strong defect association between singly ionized

manganese ions Mn'_{Ti} and $V_O^{\bullet\bullet}$ due to Jahn-Teller distortion[53] significantly improves the stability of these defect complexes upon thermal aging at 180°C, and hence the poled state is mostly preserved. For Nb doped PZT films, on the other hand, the induced imprint is mostly due to injection or/and trapping of electronic charges rather than

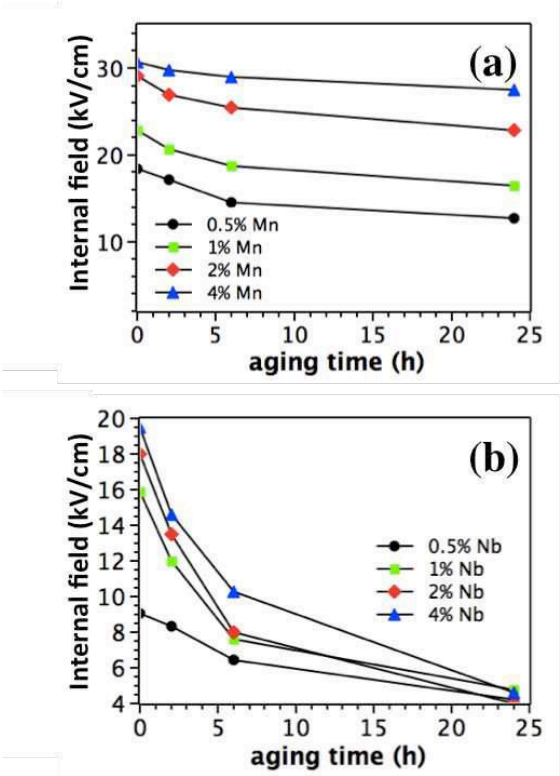

Figure 2.12 *Time stability of imprint in (a) Mn-, (b) Nb-doped PZT films for aging at 180°C*

movement of oxygen vacancies. These trapped charges tend to relax upon thermal aging, leading to reduction of imprint in Nb doped PZT films on aging at 180°C.

As expected, the internal field improves the stability of the remanent piezoelectric properties. As shown in Figure 2.13, the imprint in Mn doped PZT films leads to dramatic reductions in aging. The 180°C aging rate of 0.5% Mn doped PZT film is 6.8%/decade and this rate decreases to 4.4, 3.1, and 2.3%/ decade for 1, 2, and 4% Mn doped PZT films, respectively. The reduction in high temperature aging rates is attributed to improved stability of the poled state.

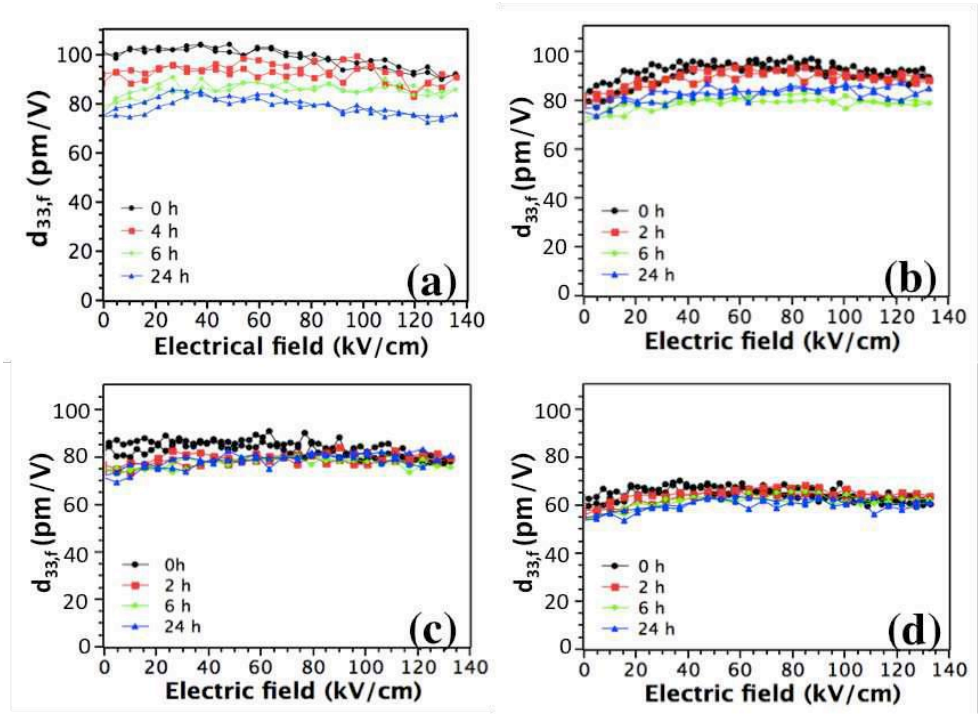

Figure 2.13 *Time stability of $d_{33,f}$ in (a) 0.5, (b)1, (c) 2, (d) 4% Mn-doped PZT films following aging at 180 °C.*

In contrast, PNZT films showed significantly larger high temperature $d_{33,f}$ aging rates, demonstrating that the fully poled state was not retained with time (Figure 2.14). 0.5, 1, 2, and 4% Nb doped PZT films had 180°C aging rates of 13.6, 13.1, 7.6, and 6.8%/decade, respectively. The sharp decrease in the piezoelectric properties is the result of polarization loss due to backswitching of the ferroelectric domains.[7] Imprint reduces aging more effectively in acceptor doped PZT films, with respect to donor doped ones, following a high temperature poling step.

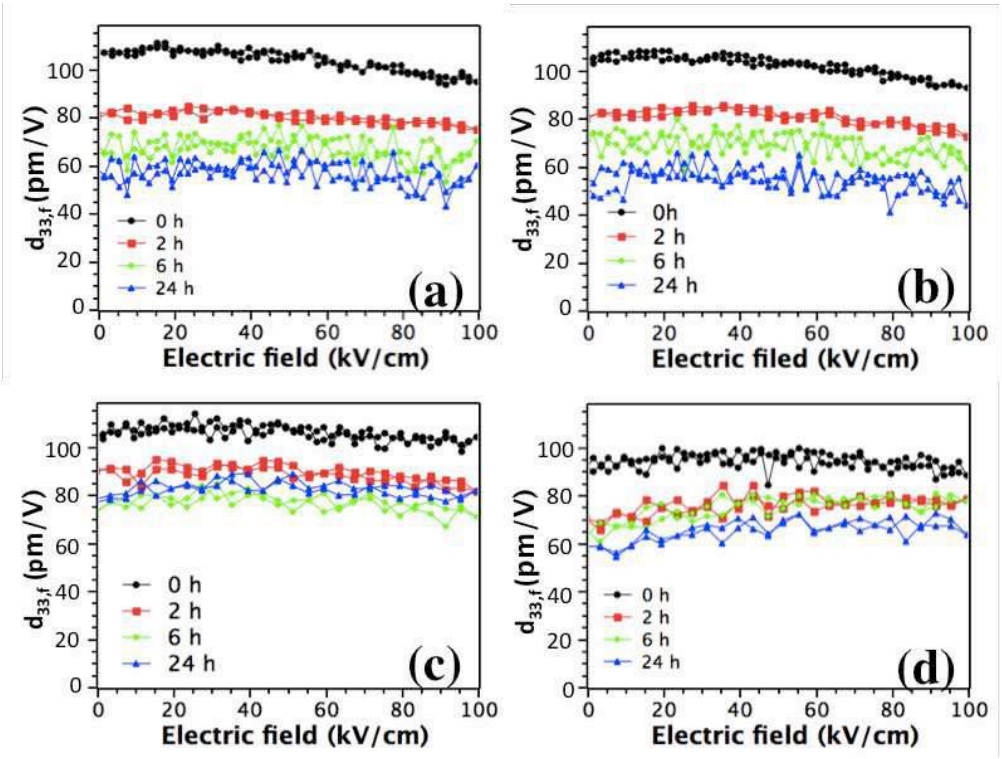

Figure 2.14 *Time stability of $d_{33,f}$ in (a) 0.5, (b)1, (c) 2, (d) 4% Nb-doped PZT film following aging at 180 °C.*

2.5 Conclusions

The development of internal fields and their effect on the remanent piezoelectric properties and aging were studied in Mn and Nb doped PZT (Zr/Ti: 52/48) thin films. Crack free, homogenous, and smooth films were obtained by chemical solution deposition. Both Mn and Nb doped films are approximately randomly oriented.

Both Mn and Nb doped PZT films develop imprint on poling. For all dopant levels and poling temperatures, the magnitude of imprint was found to be higher in PMZT films; the internal field changed from 3 to 32 kV/cm and 0.5 to 18 kV/cm for PMZT and PNZT films, respectively, for poling at temperatures from 25 °C to 200 °C. The enhanced internal field in the PMZT films was attributed to higher oxygen vacancy concentrations on Mn doping. In PMZT films, the E_a for the development of imprint

varied from 0.5±0.06 to 0.8±0.1 eV as a function of [Mn], suggesting that the movement of oxygen vacancies and orientation of defect dipoles are responsible for the imprint developed. Higher E_a (0.8±0.1-1.2±0.2 eV) were characteristic of the development of imprint in PNZT films. Thermionic emission of electrons and subsequent electron trapping by Ti^{4+} trap sites are likely to be the origin of the imprint in PNZT films. The contribution of charge trapping processes to the internal field increases at higher Nb levels, leading to a reduction in the E_a for imprint.

The presence of an internal field improves the $d_{33,f}$ in both PMZT and PNZT films. However, the enhancement in $d_{33,f}$ due to imprint is more obvious in PMZT films, where larger internal fields can be introduced during poling. It was also found that imprint reduces aging more effectively in Mn doped PZT films, relative to Nb doped ones, following a high temperature poling step. This is attributed to enhanced stability of the poled state in acceptor doped films due to a strong defect association between singly ionized manganese ions Mn'_{Ti} and $V_O^{\bullet\bullet}$ (casued by the Jahn-Teller distortion). The higher aging rate in PNZT films is associated with loss of the internal field due to relaxation of trapped charges during aging.

2.6 References

[1]Muralt P., Ledermann N., Baborowski J., Barzegar A., Gentil S., Belgacem B., Petitgrand S., Bosseboeuf A., Setter N., "Piezoelectric micromachined ultrasonic transducers based on PZT thin films," *IEEE Trans. Ultrason. Ferroelectr. Freq. Control*, 52: 2276-88 (2005).

[2]Morimoto K., Kanno I., Wasa K., Kotera H., "High-efficiency piezoelectric energy harvesters of *c*-axis-oriented epitaxial PZT films transferred onto stainless steel cantilevers," *Sensors and Actuators A.* 163: 428-32 (2010).

[3]Funakubo H., Dekkers M., Sambri A., Gariglio S., Shklyarevskiy I., and Rijnders G., "Epitaxial PZT films for MEMS printing applications," *MRS Bull.*, 37, 1030-8 (2002).

[4]Pulskamp J.S., Polcawich R.G., Rudy R.Q., Bedair S.S., Proie R.M., Ivanov T., Smith G.L.," Piezoelectric PZT MEMS technologies for small-scale robotics and RF applications," MRS Bull 37:1062-70 (2012).

[5]Trolier-McKinstry S., Muralt P., "Thin Film Piezoelectrics for MEMS," *J. Electrocer.*, 12: 7-17 (2004).

[6]Muralt P., Kholkin A., Kohli M., Maeder T., "Piezoelectric actuation of PZT thin-film diaphragms at static and resonant conditions," *Sensors and Actuators A*, 53: 398-404 (1996).

[7]Shepard Jr J.F., Moses P.J., Trolier-McKinstry S., "The wafer flexure technique for the determination of the transverse piezoelectric coefficient (d_{31}) of PZT thin films," *Sensors and Actuators A*, 71 C: 133-138 (1998).

[8]Damjanovic D., "Ferroelectric, dielectric and piezoelectric properties of ferroelectric thin films and ceramics," *Rep. Prog. Phys.,* 61: 1267-1324 (1998).

[9]Setter N., Damjanovic D., Eng L., Fox G., Gevorgian S., Hong S., Kingon A., Kohlstedt H., Park N.Y., Stephenson G.B., Stolitchnov I., Taganstev A.K., Taylor D.V., Yamada T., and Streiffer S., "Ferroelectric thin films: review of materials, properties, and applications," *J. Appl. Phys.*, 100: 051606-1-46 (2006).

[10]Schulze W.A., Ogino K., "Review of literature on aging of dielectrics," *Ferroelectrics*, 87: 361-377 (1988).

[11]Polcawich R.G., Trolier-McKinstry S., "Piezoelectric and dielectric reliability of lead zirconate titanate thin films," *J. Mater. Res*., 15: 2505-2513 (2000).

[12]Kholkin A.L., Tagantsev A.K., Colla E.L., Taylor D.V., Setter N., "Piezoelectric and dielectric aging in $Pb(Zr,Ti)O_3$ films and bulk ceramics," *Integrated Ferroelectrics*, 15: 317-324 (1997).

[13]Drougard M.E. and Young D.R., "Domain clamping effect in barium titanate single crystals," *Phys. Rev.,* 94: 1561-1564 (1954).

[14]Postnikov V.S., Pavlov V.S., and Turkov S.K., "Internal friction in ferroelectrics due to interaction of domain boundaries and point defects," *J. Phys. Chem. Sol.* 31: 1785-91 (1970).

[15]Takahashi M., "Space charge effect in lead zirconate titanate ceramics caused by the addition of impurities," *Jpn. J. Appl. Phys.,* 9: 1236-46 (1970).

[16]Robels U. and Arlt G., "Domain wall clamping in ferroelectrics by orientation of defects," *J. Appl. Phys.*, 73: 3454-60 (1993).

[17]Morozov M.I. and Damjanovic D., "Charge migration in $Pb(Zr,Ti)O_3$ ceramics and its relation to ageing, hardening, and softening," *J. Appl. Phys.,* 107: 034106 (2010).

[18]Carl K. and Hardtl K.H., "Electrical after-effects in $Pb(Zr,Ti)O_3$ ceramics," *Ferroelectrics*, 17: 473-486 (1978).

[19]Jonker G.H., "Nature of aging in ferroelectric ceramics", *J. Am. Ceram. Soc.*, 55: 57-58 (1972).

[20]McQuarrie M.C. and Buessem W.R., "The aging effect in barium titanate," *Ceram. Bull.*, 34: 402-406 (1955).

[21]Thomann H., "Stabilization effects in piezoelectric lead titanate zirconate ceramics," *Ferroelectrics*, 4: 141-146 (1972).

[22]Arlt G. and Neumann H., "Internal bias in ferroelectric ceramics: origin and time dependence," *Ferroelectrics*, 87: 109-120 (1988).

[23]Glaum J., Genenko Y.A., Kungl H., Schmitt L.A., and Granzow T., "De-aging of Fe-doped lead-zirconate-titanate ceramics by electric field cycling: 180°- vs. non-180° domain wall processes," *J. Appl. Phys.,* 112: 034103 (2012).

[24]Smyth D.M., "Defect structure in perovskite titanates," *Current Opinion in Solid State & Mater. Sci.,* 1: 692-697 (1996).

[25]Smyth D.M., "Ionic transport in ferroelectrics", *Ferroelectrics*, 151: 115-124 (1994).

[26]Raymond M.V., Smyth D.M., "Defects and charge transport in perovskite ferroelectrics," *J. Phys. Chem. Solids*, 57: 1507-1511 (1996).

[27]Newnham R.E., "Review article: electroceramics," *Reports on Progress in Physics*, 52: 123-156 (1989).

[28]Jaffe B., Cook W.R., and Jaffe H., Piezoelectric Ceramics: Academic, New York, p. 139 (1971).

[29]Scholz J.R., "Aging rates in PZT ferroelectrics with mixed acceptor-donor dopants," MS thesis, Penn State University, p.55 (2009).

[30]Polcawich R.G., Trolier-McKinstry S., "Piezoelectric and dielectric reliability of lead zirconate titanate thin films," *J. Mater. Res.*, 15: 2505-2513 (2000).

[31]Warren W.L., Dimos D., Pike G.E., Tuttle B.A., and Raymond M.V., "Voltage shifts and imprint in ferroelectric capacitors," *Appl. Phys. Lett.*, 67: 866-868 (1995).

[32]Dimos D., Warren W.L., Sinclair M.B., Tuttle B.A., and Schwartz R.W., "Photoinduced hysteresis changes and optical storage in (Pb, La)(Zr,Ti)O_3 thin films and ceramics," *J. Appl. Phys.*, 76: 4305-4315 (1994).

[33]Warren W.L., Dimos D., Pike G.E., Vanheusden K., and Ramesh R., "Alignment of defect dipoles in polycrystalline ferroelectrics," *Appl. Phys. Lett.*, 67: 1689-1691 (1995).

[34]Kholkin A.L., and Setter N., "Photoinduced poling of lead titanate zirconate thin films," *Appl. Phys. Lett.*, 71: 2854-2856 (1997).

[35]Grossmann M., Lohse O., Bolten D., Boettger U., and Schneller T., "The interface screening model as origin of imprint in $PbZr_xTi_{1-x}O_3$ thin films. I. dopant, illumination, and bias dependence," *J. Appl. Phys.*, 92: 2680-2687 (2002).

[36]Koval V., Viola G., and Tan Y., Ferroelectric Materials: Synthesis and Characterization: Biasing Effects in Ferroic Materials Intech., p. 205-245 (2015).

[37]Boettger U., Braeuhaus D., Waser R., "The influence of non-ferroelectric interface layers and inclusions on the imprint behavior of ferroelectric thin film capacitors," Proceedings of the *Sixteenth IEEE International Symposium on the Applications of Ferroelectrics*, 32-34 (2007).

[38]Takahashi S.," Effects of impurity doping in lead zirconate-titanate ceramics," *Ferroelectrics*, 4: 143-156 (1982).

[39]Zhang Q. and Whatmore R.W., "Improved ferroelectric and pyroelectric properties in Mn-doped lead zirconate titanate thin films," *J. Appl. Phys.*, 94: 5228-33 (2003).

[40]Wolf R.A. and Trolier-McKinstry S., "Temperature dependence of the piezoelectric response in lead zirconate titanate films," *J. Appl. Phys.*, 95: 1397-1406 (2004).

[41]Fujii I. Dielectric nonlinearity of ferroelectrics. Ph.D. thesis, Penn State University. 2010. p 22.

[42]Kurchania R., Milne S.J., Characterization of sol-gel $Pb(Zr_{0.53}Ti_{0.47})O_3$ films in the thickness range 0.25–10 μm," *J. Mater. Res.*, 14: 1852-1859 (1998).

[43]Zhu W., Fujii I., Ren W., Trolier-McKinstry S., "Influence of Mn doping on domain wall motion in $Pb(Zr_{0.52}Ti_{0.48})O_3$ films," *J. Appl. Phys.*, 109: 064105 (2011).

[44]Zhu W., Fujii I., Ren W., Trolier-McKinstry S., "Domain wall motion in A and B site donor-doped $Pb(Zr_{0.52}Ti_{0.48})O_3$ Films," *J. Am. Ceram. Soc.*, 95: 2906-13 (2012).

[45]Chan N.H., Smyth D.M., "Defect chemistry of donor-doped $BaTiO_3$," *J. Am. Ceram. Soc.*, 67: 285-288 (1984).

[46]Warren W.L., Tuttle B.A., Dimos D., Pike G.E., Al-Shareef H.N., Ramesh R., Evans J.T., "Voltage shifts and defect-dipoles in ferroelectric capacitors," *Jpn J. Appl. Phys.*, 35: 1521-30 (1996).

[47]Boukamp B.A., Pham M.T.N., Blank D.H.A., Bouwmeester H.J.M., "Ionic and electronic conductivity in lead-zirconate-titanate (PZT)," *Solid State Ionics*, 170:239-54 (2004).

[48]Garten L., "Residual ferroelectricity, piezoelectricity, and flexoelectricity on barium strontium titanate tunable dielectrics," Ph.D. Thesis, Penn State University, p. 152 (2014).

[49]Grossmann M., Lohse O., Schneller T., Bolten D., Boettger U., Rodriguez Contreas J., Kohlstedt H., Waser R., "Imprint in ferroelectric $Pb(Zr,Ti)O_3$ thin films with thin $SrRuO_3$ layers at the electrodes," *Integ. Ferroelec.*, 37: 205-214 (2001).

[50]Robertson J., Warren W.L., Tuttle B.A., Dimos D., and Smyth D.M., "Shallow Pb^{3+} hole traps in lead zirconate titanate ferroelectrics," *Appl. Phys. Lett.,* 63: 1519–21 (2012).

[51]Carim A.H., Tuttle B.A., Doughty D.H. and Martinez S.L., "Microstructure of solution-processed lead zirconate titanate (PZT) thin films," *J. Am. Ceram. Soc.*, 74: 1455-58 (1991).

[52]Tuttle B.A., Headley T.J., Bunker B.C., Schwartz R.W., Zender T.J., Hernandez C.L., Goodnow D.C., Tissot R.J., Michael J. and Carim A.H., "Microstructural evolution of $Pb(Zr, Ti)O_3$ thin films prepared by hybrid metallo-organic decomposition," *J. Mater. Res.*, 7: 1876-82 (1992).

[53]Ng Y.S., Alexander S.M., "Structural studies of manganese stabilised lead-zirconate-titanate," *Ferroelectrics*, 51: 81-86 (1983).

Chapter 3

Leakage current characteristics and DC resistance degradation mechanisms in Nb doped PZT films

3.1 Introduction

Ferroelectric thin films are leading candidates for use in piezoelectric microelectromechanical systems (piezoMEMS), including ink jet printers, adjustable optics, ultrasound transducers, resonators, energy harvesters, etc.[1-4] In addition to their high dielectric and piezoelectric properties, films for piezoMEMS must exhibit high insulation resistance and acceptable lifetimes. In particular, resistance degradation can ultimately lead to failure in a device that previously withstood a given set of voltage, stress, and temperature conditions. Degradation in perovskite-type ceramics is often due to the field-driven migration of oxygen vacancies (exacerbated at elevated temperatures) and subsequent accumulation of oxygen vacancies near the cathode region.[5-8]

PZT films have been reported to exhibit different conduction mechanisms depending on the microstructure, thickness, bulk or interface defect chemistry, and electrode materials. In particular, the leakage current behavior in PZT films has been described by (1) bulk-limited conduction mechanisms such as Poole-Frenkel emission[9-10] or Space Charge Limited Conduction,[11] (2) interface-limited conduction mechanisms such as Schottky emission,[12-13] and tunneling.[13] Stolichnov et al. postulated a conduction mechanism that involves both bulk- and electrode interface-control.[14] It is possible that the contradictory results in the literature arise from (1) limited knowledge of cation stoichiometry due to PbO loss upon annealing, and (2) a difference in carrier type in PZT

films; some reports presume p-type conductivity, whereas others assume that an n-type layer is created at the surface due to accumulation of oxygen vacancies, though the bulk remains p-type, (3) variations in process conditions that produce different interface and surface trap states.

PZT films have a band gap of ~3.5 eV, but due to the existence of hole and electron trap levels, there can be some electronic conduction.[15] Bulk PZT shows p-type conductivity mediated by defects at lead-site; hole conduction is associated with either hole trapping by Pb^{2+} sites or hole migration between lead vacancies.[16] For the first case, a shallow hole trap with an activation energy of 0.26 eV was attributed to Pb^{3+} centers.[17] Zhao et al. also ascribed p-type conduction in degraded PMN-PT single crystals to hole migration between lead vacancies ($p \sim 2[V''_{Pb}]$).[18-19] On the other hand, electrons can also be trapped at Ti^{4+} sites, inducing small polaron hopping conduction between Ti^{3+} and Ti^{4+} sites.[20, 21]

In contrast to perovskites like $BaTiO_3$ and $SrTiO_3$,[22-24] mixed electronic and ionic transport and the relevant defect chemistry are less well understood in PZT. In doped $SrTiO_3$, a local equilibrium model was proposed to explain the correlation between local oxygen vacancy concentrations, electronic carrier density and charge transport.[8] Field driven oxygen vacancy migration towards the cathode upon resistance degradation leads to the cathode region becoming enriched and the anode region depleted in oxygen vacancies upon resistance degradation. As a result, in degraded Fe doped $SrTiO_3$ single crystals, a high concentration of Ti^{3+} was observed near the cathode.[25]

By analogy, it is believed that leakage currents in PZT films depend on changes in electronic carrier densities and the associated transport mechanisms near electrode/film

interfaces.[26] In particular, the PZT/electrode contact plays a critical role in charge transport and resistance degradation of PZT films when Schottky emission dominates the leakage current.[27-28] PZT/Pt contacts can be rectifying only if PZT is an n-type semiconductor. The Fermi level of PZT lies near the middle of the band gap. This makes charge injection from an electrode into the bulk of the film nearly impossible (E_f~1.85 eV). Some earlier studies suggested that charge injection would be possible in the presence of surface and interface states that modify the barrier height.[29] For example, the Schottky barrier height of PZT films is lowered on annealing under reducing atmospheres, as the resulting higher oxygen vacancy concentrations pin the Fermi level. However, contradictory reports in the literature suggest that the work functions of metal and PZT control the dominant conduction mechanism.[30-31]

With limited and contradictory reports of local defect chemistry and the related charge transport mechanisms in PZT films, it is difficult to design highly reliable piezoelectric materials. The major questions that need to be answered are: (1) the major carrier type in PZT films, (2) the dominant conduction mechanisms, and (3) the changes in local interfacial defect chemistry and charge transport mechanisms which take place during degradation. Thus, in this study, the bulk oxygen vacancy concentration was controlled by introducing different concentrations of Nb into PZT films. Then, the effect of oxygen vacancy concentration on the dominant conduction mechanism as well as resistance degradation of PZT films was investigated. The lifetimes of PZT films with different oxygen vacancy concentrations were assessed using Highly Accelerated Lifetime Testing (HALT). In-situ impedance analysis was performed to understand the variation in local conductivity and associated charge transport mechanisms during

degradation. The variation in the interfacial defect chemistry with migration of oxygen vacancies upon degradation was explored by Electron Energy Loss Spectroscopy (EELS). Additionally, the nature and density of charge carriers were established using Deep Level Transient Spectroscopy (DLTS) and Thermally Stimulated Depolarization Current (TSDC).

3.2. Experimental Procedure

Donor-doped (Nb) lead zirconate titanate (PZT) thin films with dopant concentrations varying between 0.5 to 4 mol% were grown on commercial $Pt/Ti/SiO_2/Si$ substrates (Nova Electronic Materials, Flower Mound, TX) via chemical solution deposition. Solutions with a Zr/Ti ratio of 52/48 were prepared using 10 mol% Pb excess to compensate for lead loss during heat treatment. The preparation of solutions is similar to that described elsewhere.[32] The Nb doping concentration in solution was calculated presuming B site occupancy to reach final film compositions of: $Pb_{\left(1-\frac{1}{2}x\right)}\ Zr_{0.52(1-x)}\ Ti_{0.48(1-x)}\ Nb_x\ O_3$, where x = 0.005–0.04.

To grow the film, PZT solution was dispensed on platinized silicon substrates and spun at 1500 rpm for 30s. Then, each layer was exposed to two subsequent pyrolysis treatments for 3 min at 250 and 450°C, respectively. The film was then crystallized at 700°C for 60 s by rapid thermal annealing (RTA) using a ramp rate of 50°C/sec. in an O_2 flow. The coating and drying process, as well as rapid thermal treatments were repeated until a desired thickness of 350-400 nm was reached. Finally, a PbO layer was coated onto the surface of the PZT films and annealed at 700°C in air, to remove surface pyrochlore. Remaining PbO was then removed by immersing the sample in a 4M acetic

acid solution for 60 s. More details on the film orientation and grain size are available elsewhere.[32]

For electrical characterization, Pt top electrodes with diameters ranging from 200 μm to 1 mm were used. Pt top electrodes were prepared by double layer photolithography and lift off processing. For this purpose, ~100 nm thick Pt films were sputter deposited on the PZT surface (CMS-18 Sputter System, Kurt J. Lesker Company, Pittsburgh, PA) over a resist stack with a re-entrant profile. After liftoff, the samples were post-annealed at 650°C for 1 min by RTA using a ramp rate of 50°C/sec in an O_2 flow.

The microstructure and local composition were studied using a TITAN transmission electron microscope (TEM) with an operating voltage of 300 kV. Electron energy-loss spectroscopy (EELS) was performed using a Gatan Enfina parallel electron energy-loss spectrometer attached to the TITAN TEM microscope. The energy resolution measured from the zero-loss peak full width at half maximum (FWHM) was 1.3 eV. EELS were recorded in TEM-diffraction mode with a collection angle of 14 mrad and convergence angle of 3 mrad.

Leakage current measurements were performed using a 4140 pico-Ampere Meter/DC Voltage Source (Hewlett Packard) in order to understand the steady state condition before current-voltage measurements. Measurements of current were made 60 seconds after any change in voltage to allow the current to stabilize. The field range utilized was up to 500 kV/cm for both voltage polarities.

TSDC measurements were performed using a HP 4140b PA meter at temperatures ranging from 25 to 300°C. The noise level measured under open-circuit conditions was on the order of pico-amps from 50-600°C. First, the sample was heated to a poling

temperature (T_p) and then it was poled under a DC field to orient or move defects. After poling the sample at T_p for 3, 6, or 12 h, the sample was cooled down to T_0 under field to freeze the defect dipoles, space charges, and trapped charges into the poled state. Finally, the sample was heated at a constant heating rate and the relaxation current was monitored with a pA meter. No bias voltage was applied during measurements.

Highly accelerated lifetime testing, HALT, was used to determine the lifetime of Nb doped PZT films and probe the degradation mechanisms. The films were sectioned into 1x1 cm squares which were mounted into DIP packages with silver paste. The top Pt electrodes were wirebonded to the contact pads of the package with gold wire. Capacitance and dielectric loss measurements were done before and after wirebonding to ensure no degradation occured during wirebonding. Eight equivalent 400 μm diameter top platinum electrodes were used to monitor the current across the PZT films versus time for each HALT condition. The HALT measurements were conducted at temperatures from 150 - 200°C with dc electric fields of 300 – 450 kV/cm. The applied electric field was directed from the top to the bottom electrode. The resulting data were treated using the empirical relationship suggested by Prokopowicz and Vaskas:[33]

$$\frac{t_1}{t_2} = \left(\frac{V_2}{V_1}\right)^n \exp\left[\frac{E_a}{k}\left(\frac{1}{T_1} - \frac{1}{T_2}\right)\right] \qquad \text{Equation 3.1}$$

where t is median time to failure (MTF), V is voltage, k is Boltzmann's constant, E_a, is activation energy, and T is temperature. For this study, the device failure was defined as the time the leakage current increased by two orders of magnitude with respect to the steady state leakage current. Weibull analysis was used to calculate the median time to failure, MTF.

To assess the presence of shallow trap sites, Charge based Deep Level Transient

Spectroscopy (Q-DLTS) measurements were conducted. The magnitude of the Q-DLTS signal is $\Delta Q = Q(t_2) - Q(t_1)$, where t_1 and t_2 are discharging durations. The ΔQ signal was monitored as a function of temperature and electric field for a constant rate window $\tau_m = (t_2 - t_1) - ln(t_2/t_1)$. The charge released within Δt is described based on Equation 2.[34]

$$Q(t) = Q_0[\exp(-e_p t_1) - \exp(-e_p t_2)] \qquad \text{Equation 3.2}$$

where $Q_0 = \int_0^\infty Q_0(t)dt$. For hole trap sites, $e_p = \sigma \nu_{th} N_c \exp(-E_a/kT)$ is the hole emission rate, $\nu_{th} = \sqrt{\frac{3kT}{m_e}}$ = electron thermal velocity, $N_C = 2(\frac{3kT}{m_e})^{3/2}$ = effective density of states in the conduction band, m_p^* is the effective mass of the hole or electron and σ is the capture cross section extracted from the intercept of ln $(\tau_m^{-1}/\Gamma T^2)$ versus 1000/T.[34]

In-situ impedance analysis was performed using an Agilent E4980A (or 4284A) Precision LCR Meter (Santa Rosa, CA). The initial, undegraded state was measured using a l00 mV AC amplitude at 201 log-spaced frequencies between 2MHz and 0.01 Hz. A DC voltage of 40 kV/cm was then applied at 320°C and simultaneous impedance measurements were acquired until the degradation process was completed. The DC voltage was turned off to monitor the variation in impedance during the recovery process, as shown in Figure 3.1.

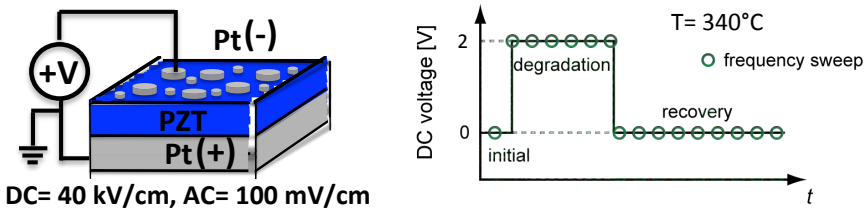

Figure 3.1 *Experimental setup for in-situ impedance analysis*

3.3. Results and Discussion

Figure 3.2 presents the characteristic leakage current response from a 2% Nb PNZT thin film capacitor under a DC bias field of 150 kV/cm at 100°C. Three main regions can be distinguished easily in Figure 3.2: the (1) initial charging current, (2) intermediate leakage regime, and (3) DC resistance degradation regime.

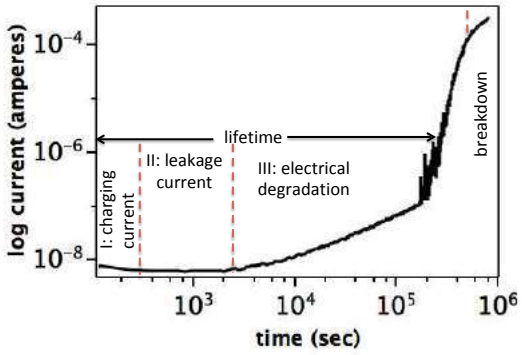

Figure 3.2 *Characteristic leakage current response of a 2% Nb-doped PNZT film as a function of time under a DC bias field of 150 kV/cm and a temperature of 100°C. The applied electric field was directed from the top to the bottom electrode.*

3.3.1 Dielectric relaxation

The initial decrease in leakage current in regime 1 is attributed to dielectric relaxation, which can be described by the empirical Curie-Von Schweidler law:[35]

$$I_R(t) = I_{min} + I_0 t^{-n} \qquad \text{Equation 3.3}$$

Such a dielectric relaxation might arise due to three different mechanisms; (1) space charge polarization (Maxwell-Wagner polarization) that appears due to inhomogeneous electrical conductivity with a wide distribution of relaxation times,[36] (2) charge trapping and space charge formation near the cathode region that diminish the electrical field and injected current according to equation 1,[37] and (3) a superposition of Debye-type relaxation with a distribution of relaxation times.[38] I_{relax} tends to disappear as the degradation time, voltage, and temperature rise. In this study, a temperature range of 50-

200°C together with duration time of 60s at each voltage increment was used to ensure that the contribution of relaxation currents could be neglected.

3.3.2 Leakage regime or (current analysis or characteristics)

In order to determine the dominant conduction mechanism in these films, the I-V results in the leakage regime were fit to the equations for various conduction mechanisms. The steady-state conduction in this temperature and voltage range is non-Ohmic. The best fit for the current-voltage relation was obtained for J vs. $E^{1/2}$ as shown in Figure 3.3. This implies that the leakage current is governed by either Schottky emission or Poole-Frenkel emission.[39]

In the case of Schottky emission, the carriers are emitted from the electrode into the conduction band of the PZT films as a result of lowered barrier height due to strong interaction of the image force and the applied field. The Schottky conduction model for reverse biased Schottky interface is described by:

$$\ln\left(\frac{J_{Sch}}{T^2}\right) = lnA^{**} - \frac{q\Phi_B^{Sch}}{k_B T} + \frac{q\sqrt{qE/4\varepsilon_0\varepsilon_\infty \pi}}{k_B T} \qquad \text{Equation 3.4}$$

where A is the Richardson constant, ε_∞ is the high frequency permittivity, $\Phi_B^{Sch}{}_B$ is the barrier height, and q is the charge per carrier.

In comparison, Poole-Frenkel emission is field-assisted thermionic emission of trapped carriers into a band; the electric field reduces the barrier to emit carriers from the defect sites. The leakage current for the Poole-Frenkel process is given by:

$$\ln\left(\frac{J_{P-F}}{E}\right) = lnC_T - \frac{q\Phi_B^{P-F}}{k_B T} + \frac{q\sqrt{qE/\varepsilon_0\varepsilon_\infty \pi}}{k_B T} \qquad \text{Equation 3.5}$$

where C_T is a constant, ε_∞ is the high frequency permittivity, and Φ_B^{P-F} is the depth of the trap. One distinction between Poole-Frenkel and Schottky effects is that the magnitude of

barrier lowering in Poole-Frenkel emission ($q\sqrt{qE/\varepsilon_0\varepsilon_r\pi}$) is twice that of the Schottky barrier lowering coefficient ($q\sqrt{qE/4\varepsilon_0\varepsilon_r\pi}$) as the distance between the escaping carrier and trap site in the case of Poole-Frenkel emission is half that between the emitted carrier and image charge.[40]

Figure 3.3 shows the fit of the I-V results to the equations for various conduction mechanisms. For Schottky conduction, ln (J/T^2) should be proportional to $E^{1/2}$, while for Poole-Frenkel conduction, ln (J/E) is proportional to $E^{1/2}$. As shown in Figure 3, both plots showed good linearity. From the slope of these plots, the permittivity of the film at optical frequencies was obtained. Table 1 demonstrates that at lower electric fields, the refractive index obtained from the Poole-Frenkel plot ranged from 1.9 to 2.4, while at higher fields that obtained from Schottky plot varies between 1.8 and 2. As PZT has a refractive index near 2.25,[41] the dominant conduction mechanism of the film is believed to be Poole-Frenkel emission (bulk controlled) at lower electric fields and Schottky emission (interface controlled) at higher electric fields. Thus, at lower electric fields, trap-filling is responsible for the leakage current. Beyond a threshold voltage, the applied electric field lowers the barrier height for electron injection into the conduction band, giving rise to a sudden increase in leakage current. The electric field for transition from Poole-Frenkel to Schottky emission varies increases with increasing Nb concentration. A mix of Poole-Frenkel and Schottky emission conduction mechanisms in PZT and BST films were previously reported by Mihara et al.[9] and Bouyssou et al.,[60] respectively.

The variation in Poole-Frenkel and Schottky regimes with Nb concentration can be explained based on the defect chemistry of PZT films. PZT is a well-known p-type wide band gap semiconductor due to the presence of unintentionally doped acceptor ions and PbO loss during high temperature processing. For undoped PZT films, the

electroneutrality condition can be expressed by:

$$2[V_O^{\bullet\bullet}] + [h^{\bullet}] = 2[V_{Pb}''] + [A'_{Ti,Zr}] \qquad \text{Equation 3.6}$$

where $V_O^{\bullet\bullet}$ and V_{Pb}'' are oxygen and lead vacancies, respectively; $h^{\bullet}$ is a hole and $A'_{Ti,Zr}$ is an acceptor impurity. This unintentional incorporation of acceptor species and/or lead vacancies generates holes and oxygen vacancies for charge compensation that can increase conductivity.

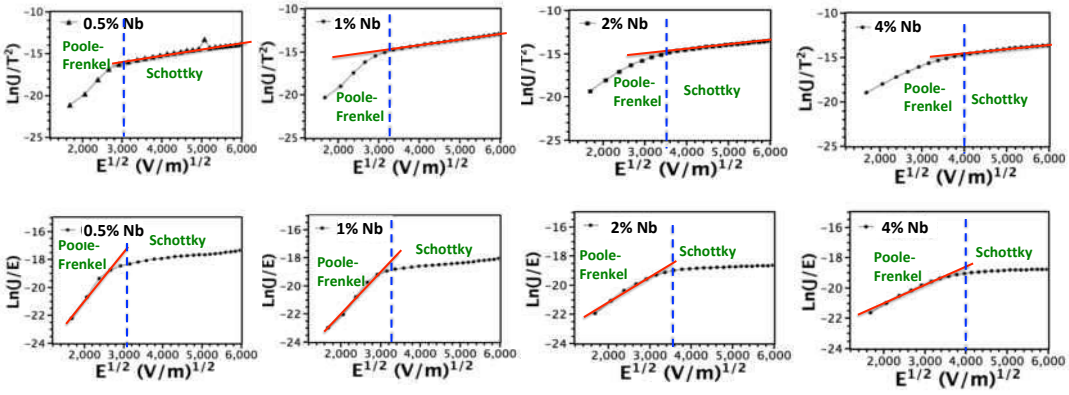

Figure 3.3 *Fitting of the leakage current-voltage data for distinct electric fields in 0.5, 1, 2, and 4% Nb doped PZT thin films.*

Table 3.1 *Refractive index values for Nb doped PZT thin films. For each case, there is a transition from Poole-Frenkel to Schottky conduction as a function of electric field. Reasonable values for the high frequency permittivity are shown in red to denote the change in mechanism.*

	0.5% Nb		1% Nb		2% Nb		4% Nb	
Field (kV/cm)	**≤ 82**	**≥ 82**	**≤ 115**	**≥ 115**	**≤ 144**	**≥ 144**	**≤ 172**	**≥ 172**
Schottky	0.8±0.01	1.8±0.05	0.9±0.04	1.9±0.07	0.7±0.03	1.8±0.04	0.7±0.04	2±0.06
Poole-Frenkel	2.1±0.06	11.7±0.06	1.9±0.07	9.8±0.05	2.3±0.08	12.7±0.05	2.4±0.08	14.6±0.09

When Nb^{5+} is incorporated into PZT films, it is accommodated on the B-site of the lattice (replacing Ti^{4+} or Zr^{4+}). This decreases the concentration of mobile defects such as oxygen vacancies and holes via:

$$Nb_2O_5 + V_O^{\bullet\bullet} \xrightarrow{2(TiO_2)} 2Nb_{Ti}^{\bullet} + 4O_O \qquad \text{Equation 3.7}$$

$$2[V_O^{\bullet\bullet}] + [Nb_{Ti}^{\bullet}] + [h^{\bullet}] = 2[V_{Pb}''] + [e']$$ Equation 3.8

The role of oxygen vacancies on Schottky barrier formation is crucial in PZT films. Since the work function of Pt (Φ_{Pt}=5.3 eV) is greater than the work function of PZT (Φ_{PZT}=3.5 eV)[42], a Schottky barrier can be formed only if the PZT surface acts as a n-type semiconductor. Oxygen vacancies can accumulate near the interface during deposition of the electrode or annealing under a reducing atmosphere. Free electrons charge compensate the ionized oxygen vacancies and can make the interface n-type (though the bulk of the PZT film remains p-type) and leads to formation of a Schottky type contact.[40]

$$O_O^X \rightarrow V_O^{\bullet\bullet} + \frac{1}{2} O_2(g) + 2\, e'$$ Equation 3.9

Since, the concentration of oxygen vacancies diminishes with increasing Nb concentration, both the initial hole concentration and the number of interface states declines; this should increase the Schottky barrier height.

Schottky regime

To calculate the Schottky barrier height, first the Richardson constant, A*, was extracted from the intercept of the Ln (J/T^2) versus 1/T at a given field. Then, the Schottky barrier height (Φ_B) was determined from the intercept of Ln (J/T^2) vs. $E^{1/2}$ as shown in Figure 3. Φ_B is estimated to be 0.95±0.05, eV 1.07±0.03 eV, 1.15±0.04 eV, and 1.24±0.04 eV for 0.5, 1, 2, and 4% doped PZT films, respectively. In all cases, Φ_B is lower than the theoretical value, E_f-E_{VB}= 1.6-1.95 eV, calculated based on the metal work function and the electron affinity of PZT. [43-44]

For the PZT/Pt interface, the work function of Pt determines the Fermi level at the interface that controls the potential barrier height for injection of holes and electrons.

However, large variations in the contact potential were found depending on the defect chemistry at the metal/PZT interface.[31, 45-46]

Robertson and Chen described the effect of surface/interface states on the Schottky barrier height using the equation derived by Cowley and Sze.[47]

$$\phi_{Bn} = S(\phi_m - \chi) + (1 - S)(E_g - \phi_0) \quad \text{Equation 3.10}$$

where Φ_m is the metal work function, χ is the electron affinity of the semiconductor, E_g is the semiconductor band gap, and ϕ_0 is the charge neutrality level below which all surface states must be occupied to maintain charge neutrality at the surface. When S=1, which is known as Schottky limit, the barrier height can be defined by the difference between the metal work function and the semiconductor affinity (Equation 3.11).

$$\phi_{Bn} = (\phi_m - \chi) \quad \text{Equation 3.11}$$

S=0, which is known as the Bardeen limit, corresponds to full Fermi level pinning due to presence of a high concentration of surface/interface states. In this case, the barrier height is the difference between the conduction band edge and ϕ_0. In most cases, the density of surface states is moderate and the barrier heights will be somewhere between the Schottky and the Bardeen limits. It was shown that oxidation and reduction of the PZT/Pt interface lead to changes in E_f of more than 1 eV.[48] Reduction of the oxide surface creates a high concentration of defects, most likely oxygen vacancies, at the PZT/Pt interface that pin the Fermi energy level. This strongly affects the potential contact barrier at the interfaces and is responsible for asymmetry in the contact properties in PZT films. The significant difference between the theoretical and experimental values found in this study suggests that the barrier height is not only affected by the work functions of Pt and PZT, but also by the surface/interface states. The most likely

candidate for such a defect state is oxygen vacancies. It is well known that even donor doped PZT films have some oxygen vacancies due to evaporation of PbO upon annealing. This leads to formation of an n-type PZT layer at the interface and shifts the Fermi level to higher energies.

The near interfacial oxygen vacancy concentration depends on many experimental parameters, such as the annealing temperature and atmosphere, deposition parameters, as well as impurity type and level in PZT films. The addition of Nb into PZT films decreases the concentration of mobile oxygen vacancies. In other work, TSDC measurements on these PZT films show that the oxygen vacancy concentration decreases from $2.3\text{x}10^{19}$ /cm^3 to $2.7\text{x}10^{18}$ /cm^3 as the Nb level increased from 0.5 to 4%.[49] The effect of oxygen vacancy concentration on pinning E_f and the magnitude of potential barrier height was estimated using a model proposed by Cowley and Sze.[47]

$$\phi_{Bn} = \left[S\left(\phi_m - \chi\right) + (1-S)\left(E_g - \phi_0\right)\right] + \{\frac{S^2C}{2} - S^{\frac{3}{2}}[C\left(\phi_m - \chi\right) + (1-S)\left(E_g - \phi_0\right)\frac{C}{S} - \frac{C}{S}\left(E_g - E_F + kT\right) + \frac{C^2S}{4}]^{1/2}\} \quad \text{Equation 3.12}$$

where $C = \frac{2q\delta^2 N_D \mathcal{E}_S}{\varepsilon_r^2}$, $S = \frac{\varepsilon_r}{q\delta_i N_i + \varepsilon_r}$, ε_r and ε_S are the interface and bulk permittivity, δ is the thickness of the interface layer separating interface charges from the bulk, N_i and N_D are the density of gap states and dopants, respectively.

Using this phenomenological approach, the dependence of Schottky barrier height on the density of interface states (oxygen vacancy concentration) was calculated. The parameters used for ϕ_m=2.6 eV, δ=0.4 nm, S=0.35, $\mathcal{E}_S$=400$\mathcal{E}_0$ are the same as those used by Robertsen and Chen.[39] The results are presented in Table 3.2 and Figure 3.4. The estimated potential barrier heights were very close to the experimental values. A variation

in the barrier height between 0.88 and 1.29 eV can occur by changing the concentration of oxygen vacancies or interface states. At higher Nb doping levels, the Schottky barrier is high since the density of interface states (oxygen vacancies) that can develop band bending is low. As the Nb concentration decreases, the defect concentration is strongly reduced, leading to a lower Schottky barrier height of 0.95 eV. This is reasonable as oxygen vacancies in PZT create electronic states close to the conduction band, and are therefore expected to modify the Schottky barrier through pinning of the Fermi level. This enhances the probability of electron injection from the cathode to the PZT (reverse-biased junction), which is believed to be a rate-limiting step for the conduction.

Table 3.2 *Experimental and calculated Schottky barrier heights of Nb doped PZT films*

	N_D (cm^{-3})	C (eV)	Calculated barrier height (eV)	Experimental barrier height (eV)
0.5% Nb	$2.3x10^{19}$	2.3	0.88±0.04	0.95±0.05
1% Nb	$1.1x10^{19}$	1.1	1.05±0.04	1.07±0.03
2% Nb	$6.2x10^{18}$	0.62	1.19±0.07	1.15±0.04
4% Nb	$2.7x10^{18}$	0.27	1.29±0.06	1.24±0.04

Poole-Frenkel Regime

At lower electric fields, the leakage current is dominated by Poole-Frenkel conduction, in which either an electron trapped at a defect site is thermally excited into the conduction band or a hole escapes into the valence band. This conduction mechanism involves the sequential hopping of trapped electrons or holes between defect sites and can be thermally and field activated. To sustain the flow of current arising from the emission of the trapped charges, the Pt/PZT interface needs to act as an Ohmic-like contact at lower electric fields. This could be possible by either trap mediated Ohmic injection, as proposed by Chiang and Wager for insulators[61], which involves initial trap mediated

thermoionic-field emission, followed by trap-to-trap emission, and trap emission to the PZT valence or conduction band to supply enough electrons or holes for continuous trap refilling or is associated with the initial Zr/Ti gradients in the film, such that the film can be considered as being a series of high resistance-low resistance states in series with each other. Further study is needed to understand the validity of these proposed mechanisms in PZT films.

Figure 3.5a shows the temperature dependence of conductivity at constant electric fields for 2% Nb doped PZT films. From the slopes in Figure 3.5a, ionization energies were extracted for different electric fields. As shown in Figure 3.4b, trap ionization energies of 0.28 ± 0.04 eV and 1.1 ± 0.04 eV were extracted for low (≤100°C) and high (≥150°C) temperature ranges, respectively.

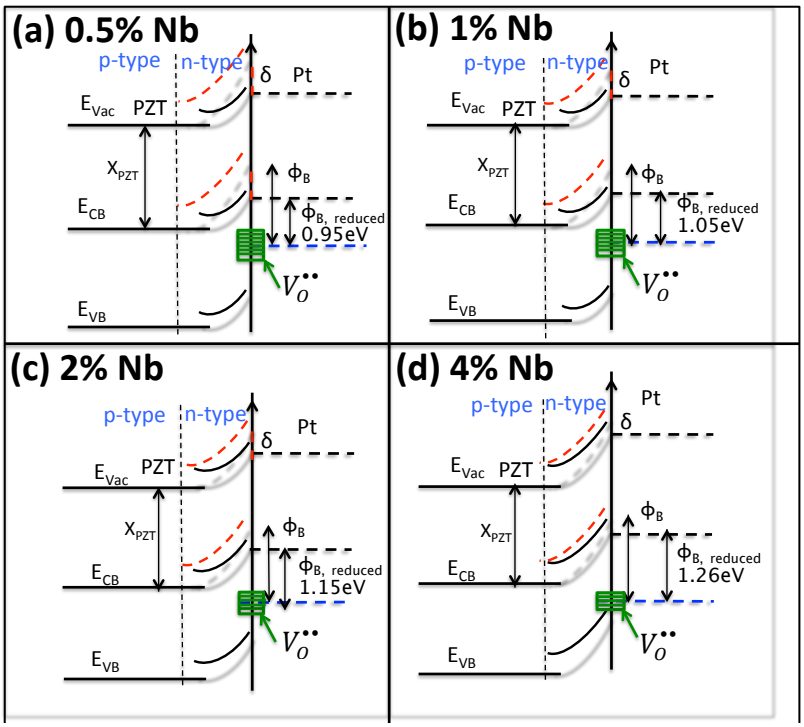

Figure 3.4 *Experimentally determined energy band diagrams for the PNZT/Pt interface. The dashed red line for the bands shows the unmodified band edge. δ represents the magnitude of band bending due to Fermi level pinning via interface states (shown in green).*

Since only steady-state leakage resistance is being considered, the leakage currents should be dominated by the motion of holes or/and electrons rather than oxygen

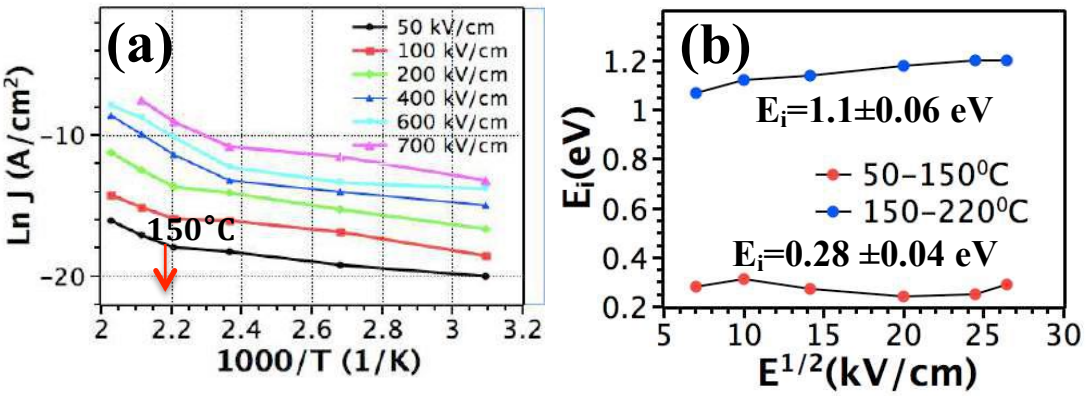

Figure 3.5 *(a) Temperature dependence of conductivity for different electric fields, (b) Trap ionization energies for different electric fields to extract zero field ionization energy*

vacancies. The relatively small activation energy of ~0.28 eV is likely to be related to a trap-mediated hole mobility.

Figure 3.6 depicts the DLTS signals at different discharging durations for 2% Nb doped PZT films. The activation for trap sites, E_a, was extracted from the slope of $\ln(\tau_m^{-1}/\Gamma T^2)$ versus 1000/T. E_a was determined to be 0.29±0.05 eV; this energy has previously been associated with hole hopping between Pb^2 and Pb^{3+} sites (Eq. 3.13).[16] No peak was observed in the range 100–300K, suggesting that there isn't another shallow trap site in PNZT films.

$$Pb^{2+} + h^{\bullet} \longrightarrow Pb^{3+} \qquad \text{Equation 3.13}$$

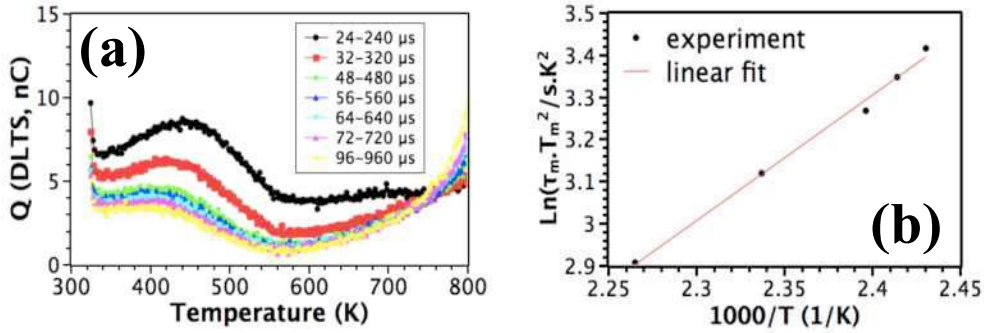

Figure 3.6 *(a) Q-DLTS of 2% Nb doped PZT films at temperatures from 300 to 750 K. The legend on Figure 5a indicates distinct rate windows. DLTS signal was measured at seven different rate windows to resolve emission from different traps, A DLTS peak is generated when the thermal emission rate of the trap is the same as that of the rate window. (b) Arrhenius plot of the DLTS signal.*

For Nb doping levels from 0.5 to 2%, a DLTS peak corresponding to a shallow Pb^{3+} trap level, was observed as shown in Figure 3.7. As expected, the intensity of the DLTS peak depends on the concentration of Nb. For lower Nb levels (0.5%), the DLTS peak intensity, which is directly proportional to the concentration of trap states, is low (Fiure 3.7a). In this work, $\frac{t_1}{t_2} = \alpha = 10$ was kept constant while scanning the rate

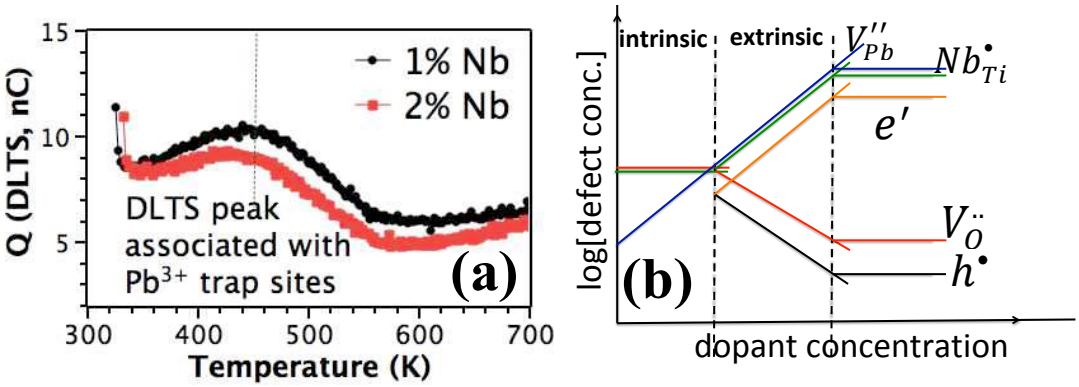

Figure 3.7 (*a) Q-DLTS of 0.5, 1, and 2% Nb doped PZT films, (b) Schematic representation of defect concentrations as a function of Nb doping level in PZT films.*

window $(\tau_m = t_1(\alpha - 1) - \ln\alpha)$. The maximum charge release $\Delta Q(\tau_m)$ is achieved when the rate window equals the emission rate of traps $t_1(\alpha - 1) - \ln\alpha = e_p$. The

magnitude of release charge is then $Q_0[\alpha^{\frac{1}{1-\alpha}} - \alpha^{\frac{\alpha}{1-\alpha}}]$. For $\alpha = 10$, $\Delta Q_{max} = Q_0/1.29$. The density of traps can then be estimated using equation 3.14.

$$N_t = 4\Delta Q_{max}/qAd \qquad \text{Equation 3.14}$$

where q is the electron charge, A is the contact area and d is the thickness of the film.[29] The density of traps was estimated to be $6.8\text{x}10^{17}/\text{cm}^3$, and $3.4\text{x}10^{17}/\text{cm}^3$ for 1 and 2% Nb doped PZT films, respectively. Addition of Nb into PZT films can be either electronically or ionically compensated. The fact that the trap density is around an order of magnitude smaller than the donor density suggests that the preponderance of the compensation is ionic. Of the electronic compensation, the electron concentration rises and hole concentration declines with increasing Nb concentration, which in turn shifts the n-p transition to a higher PO_2 range and temperature (Equation 3.6). This makes hole hopping between Pb^{2+} and Pb^{3+} sites less likely in PZT films (Figure 3.6).

To identify the trap state with an activation energy of 1.1 eV (Figure 3.8), impedance measurements were carried out. Figure 8 exhibits impedance measurement of the pristine 2%Nb doped PZT film at 340°C. The relaxation frequency f(r), is given as

$$f(r) = \frac{1}{2\pi RC} = \frac{\sigma}{2\pi\epsilon_0\epsilon_r} \qquad \text{Equation 3.15}$$

where ε_r is the relative permittivity, σ the conductivity, R is resistance and C is capacitance. Both $Z''(f)$ and $M''(f)$ exhibit a maximum at f(r) (Figure 8); the magnitude of $M''(f)$ can indicate the volume fraction of material with similar conductivity.

Figure 3.8 shows the modulus and impedance results of an undegraded (i.e. the pristine state) 2% Nb doped PNZT film. Only one peak is observed, which indicates a narrow distribution of conductivities. This suggests that oxygen vacancies and other

defects are homogenously distributed. The frequency dependence of the modulus was found to be of the Debye type.

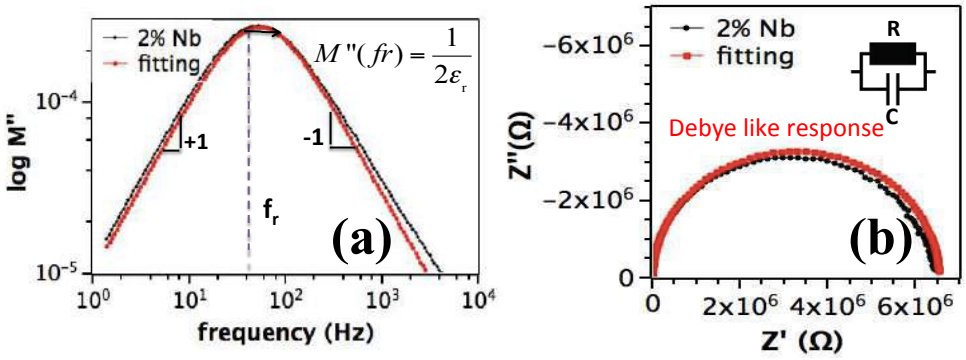

Figure 3.8 *Imaginary (a) modulus, and (b) impedance of 2% Nb doped PZT plotted as a function of frequency for measurements at 340°C. The fit is for a Debye relaxation centered at frequency f_r.*

Figure 3.9 shows the imaginary modulus as a function of frequency for 2% Nb doped PNZT films with different thicknesses. The magnitude of the modulus peak, which is inversely proportional to the permittivity of the PNZT film, is independent of thickness for films from 350 – 1200 nm. This indicates that the modulus peak is associated with bulk charge transport rather than an interface-controlled mechanism.[50]

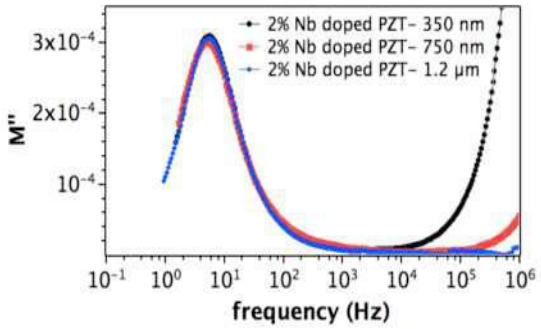

Figure 3.9 *Imaginary modulus of 2% Nb doped PZT with different thicknesses plotted as a function of frequency for measurements at 320°C*

The temperature dependence of the modulus peak was investigated to elucidate the origin of the dominant bulk charge transport mechanism, as shown in Figure 3.10.

The calculated activation energy for Nb doped PZT film is 1.08 ± 0.05 eV, which is attributed to electron trapping by Ti^{4+}.[20]

$$Ti^{4+} + e' \rightarrow Ti^{3+} \qquad \text{Equation 3.16}$$

The activation energies and trap states determined from the DLTS measurements and impedance analyses; (1)~0.28 eV for hole hopping between Pb^{2+} and Pb^{3+} sites and (2) 1.08 eV for electron trapping via Ti^{4+} are consistent with the trap states determined from the leakage current measurements.

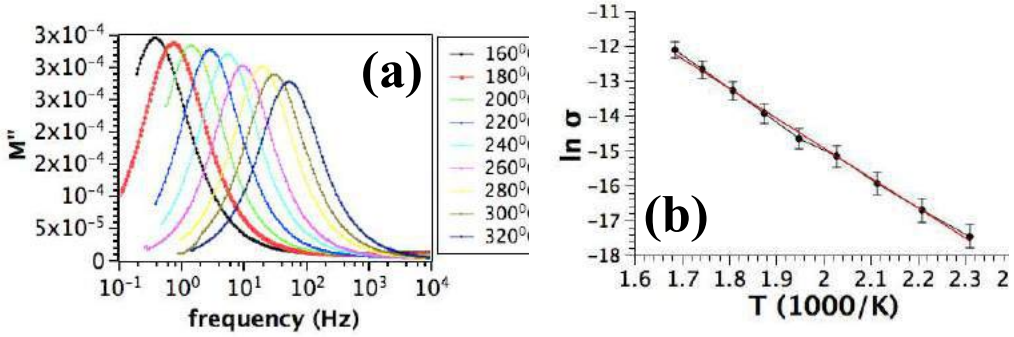

Figure 3.10 (a) *Imaginary modulus of pristine 2% Nb doped PZT films plotted as a function of frequency at different temperatures.* **(b)** *Change in conductivity of pristine 2% Nb doped PZT films with temperature.*

3.3.3 Resistance degradation

Figure 3.11a exhibits the evolution of HALT data for a single 2% Nb doped PNZT capacitor under an electric field of 400 kV/cm at 180°C. The failure time is quite long given the very aggressive measurement conditions utilized. This suggests that the failure process is a comparatively slow one. Thus, it is speculated that failure might be related to (1) drift of oxygen vacancies or/and (2) moving/injection some defects to one of the electrodes.

In order to prove this hypothesis, TSDC measurements were conducted on 2% Nb doped PZT films after degrading under an electric field of 400 kV/cm for 3, 6, or 12 h at 180°C (Figure 3.11b). Comparing Figure 3.11a and Figure 3.11b, it can be seen that the

TSDC peak at 200°C continues to grow with increasing degradation time. As reported elsewhere,[49] the current maximum shifts to higher temperatures for a giving heating rate with increasing poling field, suggesting that the TSDC peak corresponds to depolarization of space charges. An activation energy of 0.73±0.03 eV was found, which is attributed to movement of oxygen vacancies.[49] The migration of oxygen vacancies as well as the possible dissociation of defect dipoles, $(V''_{Pb} - V_O^{\bullet\bullet})^X$ upon electrical degradation gives rise to the ionic space charge peak. With further increasing degradation time, a second TSDC peak started to emerge at around 280°C. This peak has an activation energy of 0.18 eV, and is associated with electron hopping between Ti^{4+} and Ti^{3+} sites.[22, 29, 49]

The growth of the TSDC peaks with degradation time is consistent with the HALT measurements being controlled by migration and subsequent accumulation of oxygen vacancies near the cathode region.

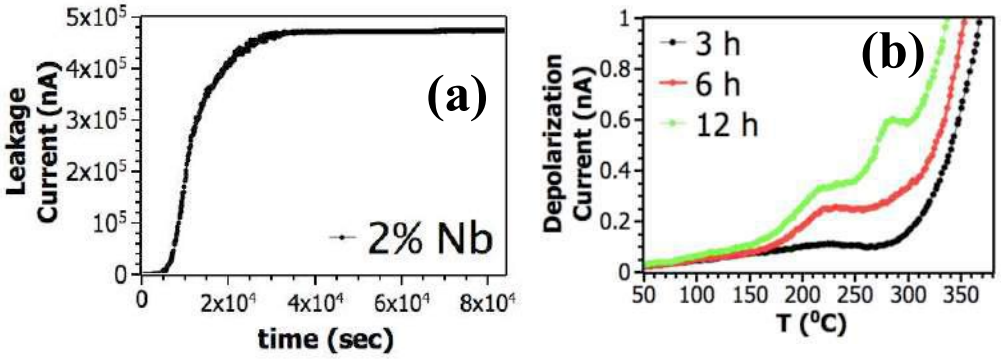

Figure 3.11 (a) *Variation in leakage current with time in 2% Nb doped PZT films,* **(b)** *evaluation of TSDC spectra of 2% Nb doped PZT films after degrading the films for 3, 6, and 28 h. The HALT measurement and degradation study were conducted at 180°C with a DC field of 400 kV/cm.*

Electrical degradation has been extensively studied and modeled by Waser et al.[8] It is believed that resistance degradation is related to long-range motion of oxygen vacancies

under electrical fields.[51-53] In principle, when the oxygen vacancies drift, they can change the field distribution in the sample, and/or modify the Schottky barrier height over time, leading to enhancement in current. Figure 3.12 demonstrates that on degrading 2% Nb doped PZT films at 400 kV/cm and 180°C for 12 h, the width of the Schottky regime increased, accompanied by shrinkage in the field range over which Poole-Frenkel conduction occurred. To understand which Pt/PNZT interface act as a cathode, equivalent Nb doped PZT samples with asymmetric top IrO_2 and bottom Pt electrodes were utilized. Because of the variation in the work function of IrO_2 and Pt, large differences were observed between I-V characteristics of top IrO_2 and bottom Pt contacts. The barrier height for injecting electrons at the cathode decreased from 1.1 to 0.85 eV, which can only be explained by injection of electrons from the electrode into PZT being the rate limiting mechanism for electrical degradation. If the conduction mechanism were governed by injection of holes at the anode then a higher leakage current is expected under an electric field of 400 kV/cm. In contrast to the cathode, no change in the electric field range at which Schottky behavior is dominant, was observed at the anode. Moreover, the potential barrier height didn't change after degrading PZT films at 400 kV/cm and 180°C for 12 h. This indicates that the carriers that dominate the leakage current upon DC resistance degradation are electrons rather than holes. An increased oxygen vacancy concentration near the cathode decreases the barrier for electron injection from the cathode into the film. Near the cathode, the high concentration of oxygen vacancies are charge compensated by electrons via $n \sim 2[V_O^{\bullet\bullet}]$. These electrons could be trapped by Ti^{4+} to create Ti^{3+}.[21, 22]

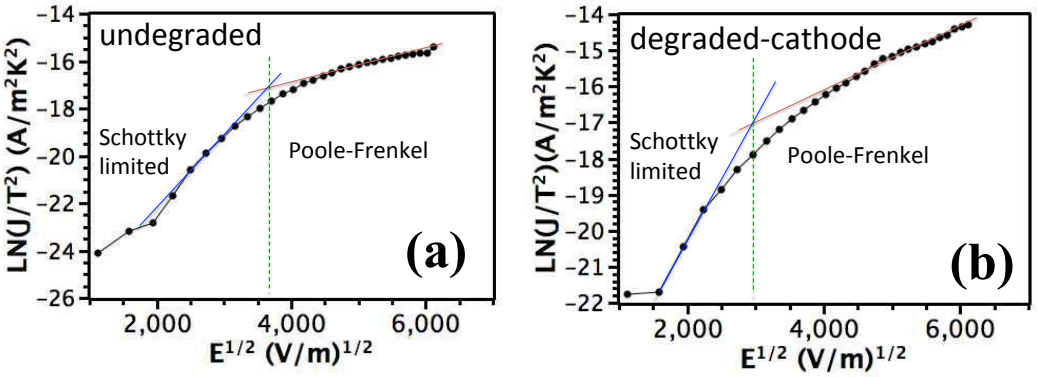

Figure 3.12 *Fitting of the leakage current-voltage data for distinct electric fields in 2% Nb doped PZT thin films (a) before, and (b) after degrading the thin film samples at 180°C with a DC field of 400 kV/cm for 12 h.*

Figure 3.13 shows EELS data for Ti-L edges in a degraded 2% Nb doped PZT film as a function of distance from the cathode. A gradual shift to higher energy loss near the anode was observed for the Ti $L_{2,3}$ edge. Moreover, Ti $L_{2,3}$ data taken close to the cathode shows that the t_{2g} and e_g peaks develop noticeable shoulders (See Figure 13b). Both the chemical shift and the appearance of shoulders imply reduction of Ti^{4+}.[54-55] Thus, there are more trapped electrons near the cathode.

Figure 14 exhibits the effect of Nb doping level on the failure behavior of PZT films. Some pre-breakdown events were observed before final failure. The HALT lifetime of PZT films increases as the Nb concentration increases (See also Table 3.3). This is presumably associated with a reduced concentration of mobile oxygen vacancies as the concentration of Nb in the films rises. Indeed, the effective barrier height gradually

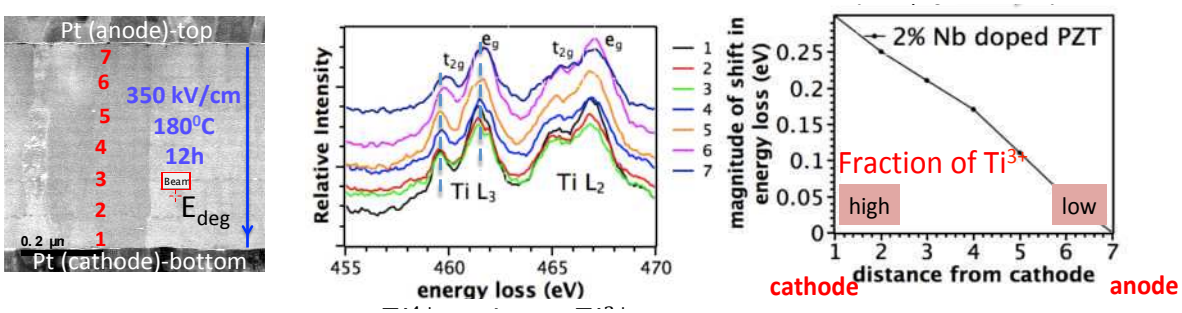

Figure 3.13 *Electron energy loss spectrum from different positions in the 2% Nb doped PZT film as a function of distance from the bottom interface (cathode). Ti $L_{2,3}$ of 2% Nb doped PZT films after degrading at 180°C under electric field of 350 kV/ cm for 12h.*

increases from 0.95 to 1.24 eV with increasing Nb concentration. This significantly increases the threshold electric field required for electron injection from the electrode into the conduction band of bulk PZT films, resulting in a lower degradation rates and longer lifetimes. The HALT activation energies and voltage acceleration factors are illustrated in Figure 3.15. Voltage acceleration factors of 4.2±0.4 and 4.6±0.5 were determined for 1 and 2% Nb doped PZT films, which agrees well with the literature.[56] The calculated activation energies from HALT measurements shown in Table 3.4 are very similar to the effective barrier height values from leakage current measurements (Table 3.2); it gradually increased from 0.95±0.05, 1.07±0.03, 1.15±0.04, and 1.24±0.04 eV with increasing Nb concentrations. This suggests that the lifetime is correlated with Schottky

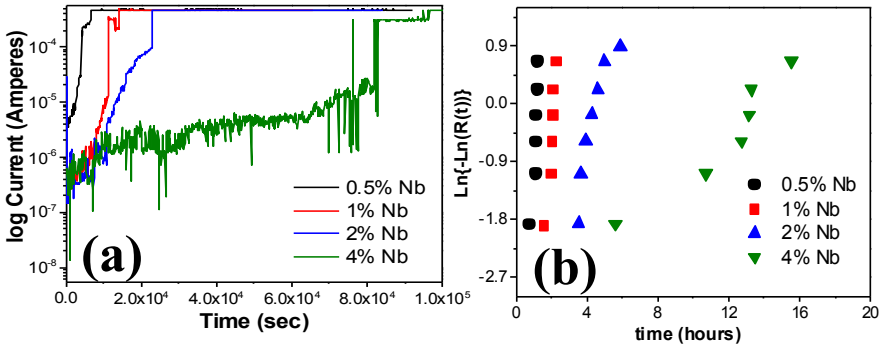

Figure 3.14 *(a) Variation in leakage current with time, (b) the time to failure for 0.5, 1, 2, and 4% Nb doped PZT films. R(t) represents the probability of failure over time. The HALT measurement was conducted at 180°C with a DC field of 400 kV/cm.*

emission. The effective barrier height for conduction increases and the degradation rate

drops with increasing Nb concentrations due to lower oxygen vacancy concentration at higher Nb levels in PZT films.

Table 3.3 *Median time to failure and Weibull parameter for 0.5, 1, 2, and 4% Nb doped PZT films. The HALT measurement was conducted at 180°C with a DC field of 400 kV/cm.*

	$t_{0.5}$ (hours)	Φ_B (eV)	β
0.5% Nb PZT	1.09±0.3	0.95±0.05	4.13±0.18
1% Nb PZT	2.06+0.4	1.07±0.03	3.78±0.11
2% Nb PZT	4.18±0.7	1.15±0.04	7.09±0.25
4% Nb PZT	15.34±1.8	1.24±0.04	3.86±0.13

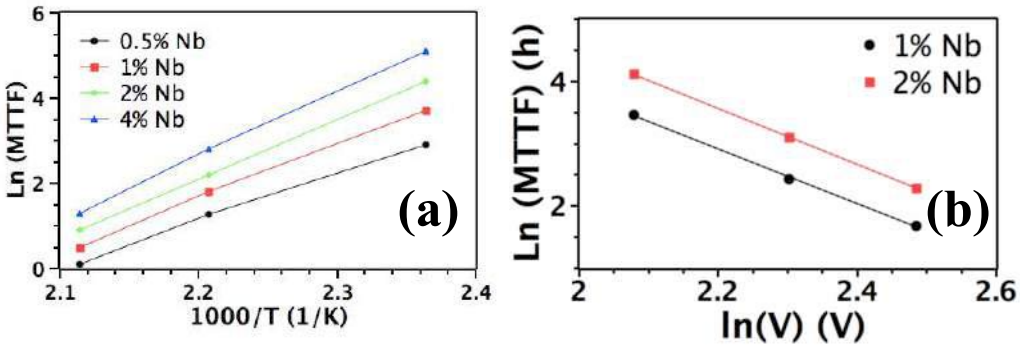

Figure 3.15 *(a) Temperature and (b) voltage dependence of median time to failure (MTF) in 0.5, 1. 2, and 4%Nb doped PZT films.*

Table 3.4 *Activation energies and voltage acceleration factors of 0.5, 1, 2, and 4% Nb doped PZT films.*

	E_a (eV)	**N**
0.5% Nb PZT	0.92±0.06	4.2±0.4
1% Nb PZT	1.06+0.05	4.6±0.5
2% Nb PZT	1.11±0.04	
4% Nb PZT	1.21±0.08	

In-situ Impedance Analysis of Nb doped PZT films

In situ modulus spectroscopy was used to investigate the degradation and recovery process in Nb doped PZT films. Impedance spectroscopy has been extensively utilized to differentiate ionic conduction, electronic conduction, bulk, interface, and grain

boundary effects based on the different time constants for different processes.[57-58] This approach can be used to explore the variation in conductivity profile with a change in defect chemistry of PZT films.[59]

$$\sigma = 2\pi f(r)\epsilon_0\epsilon_r \qquad \text{Equation 3.17}$$

In this technique, a change in f(r) is used to distinguish regions of different conductivities; more conductive regions have a higher relaxation frequency f(r).

The imaginary part of the modulus *M''*(*f*) during the degradation of Nb doped PZT film is shown in Figure 3.16a. The film was degraded at 320°C and DC fields of 40 kV/cm. The AC voltages used for the impedance meaurements was 100 mV. Only some frequency sweeps are shown in this figure for clarity. The pristine state of Nb doped PZT is characterized by one distinct maximum at 8.1 Hz.

The peak of the imaginary modulus widens and moves to higher frequencies with increasing degradation time. Thus, the bulk conductivity escalates throughout the film. No change in the modulus peak intensity was observed at the early stage of the degradation, demonstrating that the permittivity of the film similarly remains constant. After 2860 s of degradation, the magnitude of the modulus peak starts to rise, as illustrated in Figure 3.16a, which implies a reduction in capacitance and could be possibly correlated with a decline in electrode area and relative permittivity due to local breakdown events. The maximum frequency of rhe modulus peak shifts to 480 Hz. After 22000 s of degradation, the shift in modulus peak became very small and the magnitude of conductivity did not change significantly, suggesting that the sample had reached a stable state (Figure 3.16b).

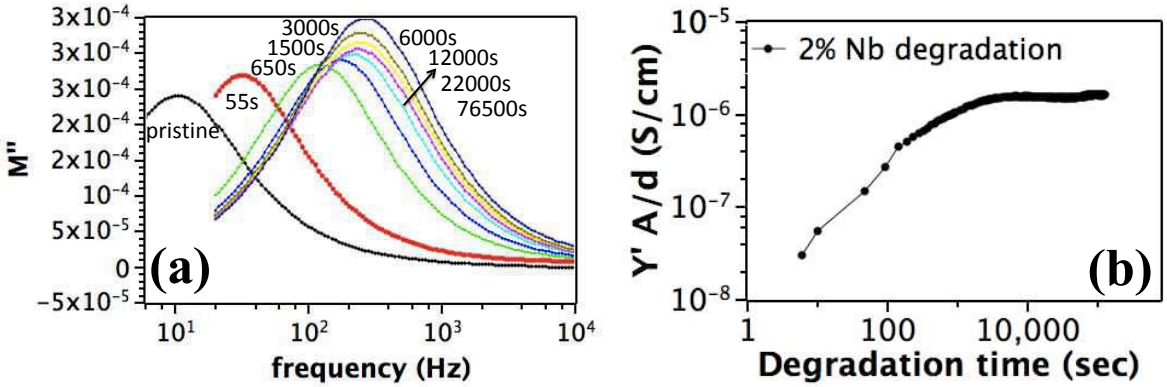

Figure 3.16 (a) *Imaginary modulus plotted as a function of frequency during degradation of 2% Nb doped PZT films at 320°C. The total degradation time is 76500 s, (b) change in admittance of 2% Nb doped PZT films during degradation.*

After reaching a stable degraded state, the imaginary modulus of 2% Nb doped PNZT films as a function of frequency was measured at different temperatures to investigate the temperature dependence of the conductivity (Figure 3.17) with the DC field still applied. The calculated activation energy for 2% Nb doped PNZT film is 1.02 ± 0.06 eV, which is attributed to electron trapping by Ti^{4+}.

$$Ti^{4+} + e' \rightarrow Ti^{3+} \qquad \text{Equation 3.18}$$

The sample was then reheated under the same DC field to 320°C and stabilized for several hours to insure the sample was in the fully degraded state. At that point, the DC field was removed, and the recovery process was tracked as a function of time at 320°C as shown in Figure 3.18. During recovery, no external DC electric field was applied, so charge injection and drift of oxygen vacancies are eliminated. During the recovery process, the modulus peak decreases in relaxation frequency and increases in

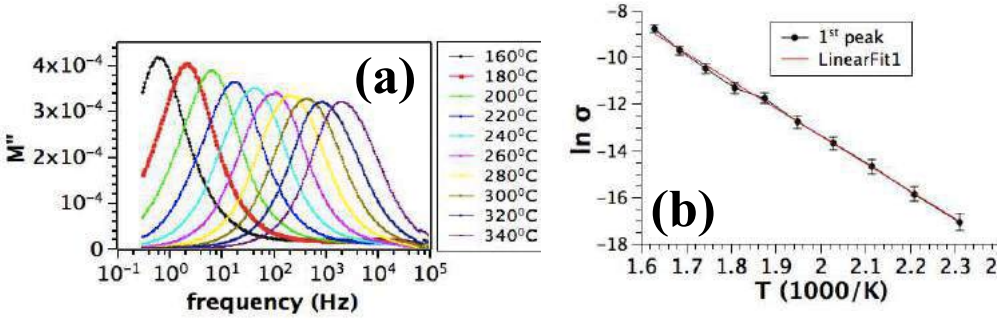

Figure 3.17 *(a) Imaginary modulus of degraded state plotted as a function of frequency at different temperatures. (b) Change in conductivity of 2% Nb doped PZT films with temperature.*

magnitude. However, the modulus peak did not reach its original undegraded position within a recovery time of 76500 s. This indicates that the conductivity of recovered state is still higher than pristine sample after recovery. This suggests that both degradation and recovery are controlled by a slow process like the drift of oxygen vacancies.

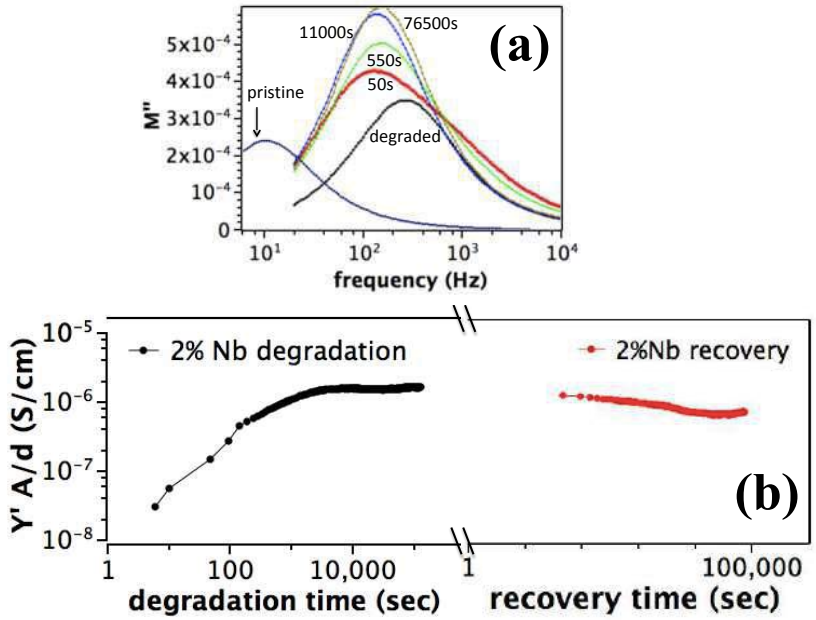

Figure 3.18 (a) *Imaginary modulus plotted as a function of frequency during recovery of 2% Nb doped PZT films at 320°C. The total recovery time is76500 s, (b) change in admittance of 2% Nb doped PZT films during degradation and recovery.*

Conclusions 3.4

Nb doped PZT films with different doping levels were deposited onto Pt/Ti/SiO_2/Si substrates via chemical solution deposition. At lower electric fields, Poole-Frenkel emission was found to be responsible for the increase in leakage current via hole hopping between Pb^{2+} and Pb^{3+} sites and electron trapping by Ti^{4+} sites. Beyond a threshold voltage, Schottky emission starts to control the leakage current. The Schottky barrier height decreased from 1.24 eV to 0.95 eV as the Nb concentration decreased from 4 to 0.5 mol%.

DC resistance degradation was associated with drift of oxygen vacancies. The increased oxygen vacancy concentration near the cathode decreased the barrier for electron injection from the cathode into the bulk of the film from 1.1 to 0.85 eV (after degrading 2% Nb doped PZT films under electric field of 400 kV/cm at 180°C for 12 h). The change in Schottky regime and effective barrier height after degradation suggest that that leakage current increase upon degradation is controlled by Schottky type conduction, indicating that the majority carriers that dominate the leakage current upon DC resistance degradation are electrons rather than holes. TSDC, EELS, and in-situ impedance findings show the appearance of a Ti^{3+} species as a result of a strong reduction of cathode region upon DC resistance degradation.

3.4 References

[1]Wilke R.H., Johnson-Wilke R.L., Cotroneo V., Davis W.N., Reid P.B., Schwartz D.A., Trolier-McKinstry S., "Sputter deposition of PZT piezoelectric films on thin glass substrates for adjustable x-ray optics," *Appl. Opt*., 52: 3412-9 (2013).

[2]Kanno I., Morimoto K., Wasa K., Kotera H., "High efficiency energy harvester of transferred epitaxial PZT films on stainless steel sheets," *Sens. Actuator A- Phys.*, 163: 482-32 (2010).

[3]Su Q-X., Kirby P., Komuro E., Imura M., Zhang Q., Whatmore R., "Thin-film bulk acoustic resonators and filters using ZnO and lead-zirconium-titanate thin films," *IEEE Trans. Microw. Theory Tech.,* 49: 769-78 (2001).

[4]Muralt P., Ledermann N., Baborowski J., Barzegar A., Gentil S., Belgacem B., Petitgrand S., Bosseboeuf A., Setter N., "Piezoelectric micromachined ultrasonic transducers based on PZT thin films," *IEEE Trans. Ultrason. Ferroelectr. Freq. Control*, 52: 2276-88 (2005).

[5]Baiatu T., Waser R., Hardtl K-H "dc Electrical Degradation of Perovskite-Type Titanates: III, A Model of the Mechanism," *J. Am. Ceram. Soc.* 73(6): 1663-73 (2005).

[6]Waser R., Baiatu T., Hardtl K-H, "dc Electrical Degradation of Perovskite-Type Titanates: I, Ceramics," *J. Am. Ceram. Soc.* 73(6): 1645-53 (1990).

[7]Waser R.M., "Electrochemical boundary conditions for resistance degradation of doped alkaline-earth titanates," *J. Am. Ceram. Soc.* 72: 2234-40 (1989).

[8]Waser R., Klee M., "Theory of conduction and breakdown in perovskite thin films," Integrated Ferroelectr. 2: 23-40 (1992).

[9]Mihara T and Watanabe H., "Electronic conduction characteristics of sol-gel ferroelectric $Pb(Zr_{0.4}Ti_{0.6})O_3$ thin-film capacitors," *Jpn. J. Appl. Phys., Part 1* 34: 5664-5673 (1995).

[10]Hu H. and Krupanidhi S.B., "Current-voltage characteristics of ultrafine-grained ferroelectric Pb(Zr, Ti)O_3 thin films," *J. Mater. Res*. 9: 1484-1498 (1994).

[11]Blom P.W.M., Wolf R.M., Cillessen J.F.M., and Krijn M.P.C.M., "Ferroelectric Schottky Diode," *Phys. Rev. Lett*. 73: 2107-10 (1994).

[12]Chen X., Kingon A.I., Al-Shareef H., Bellur K.R., "Electrical transport and dielectric breakdown in Pb(Zr,Ti)O_3 thin films," *Ferroelectrics* 151: 133–138 (1994).

[13]Kurasawa M., Kurihara K., Otani S., Kutami M., "Retention and imprint properties in single-crystalline PLZT thin film capacitors," *Proc. IEEE International Symposium on*

Applications of Ferroelectrics, 2000, ISAF 2000, 21 July–2 August, 2000, vol. 1, pp. 173–176.

[14]Stolichnov, I., Interface-controlled mechanisms of degradation in ferroelectric thin films, PhD Thesis, EPFL, (2000).

[15]Joshi V., Dacruz C.P., Cuchiaro J.D., pas de Araujo C.A., and Zuleeg R., "Analysis of C-V and I-V data of BST thin films," *Integ. Ferroelec*. 14:133-140 (1997).

[16]Robertson J., Warren W.L., Tuttle B.A., Dimos D., and Smyth D.M., "Shallow Pb^{3+} hole traps in lead zirconate titanate ferroelectrics," *Appl. Phys. Lett.,* 63 [11]: 1519–21 (1993).

[17]Baude P.F., Ye C., Polla D.L., "Deep level transient spectroscopy characterization of ferroelectric $Pb(Zr,Ti)O_3$ thin films", *Appl. Phys. Lett.,* 64: 2670-72 (1994).

[18]Zhao S., Zhang S.J., Liu W., Donnelly N.J., Xu Z., and Randall C.A., "Time dependent dc resistance degradation in lead-based perovskites: $0.7Pb(Mg_{1/3}Nb_{2/3})O_3 - 0.3PbTiO_3$," *J. Appl. Phys.* 105: 053705 (2009).

[19]Saremi S., Xu R., Dedon L.R., Mundy J.A., Hsu S-L, Chen Z., Damodaran A.R., Chapman S.P., Evans J.T., and Martin L.W., "Enhanced electrical resistivity and properties via ion bombardment of ferroelectric thin films," *Adv. Mater.* 28: 10750-56 (2016).

[20]Raymond M.V., Smyth D.M., "Defects and charge transport in perovskite ferroelectrics," *J. Phys. Chem. Sol*. 57: 1507-11 (1996).

[21]Robertson J., Warren W.L., Tuttle B.A., "Band states and shallow hole traps in $Pb(Zr,Ti)O_3$ ferroelectrics," J. Appl. Phys. 77, 3975-80 (1995).

[22]Rodewald S., Fleig J., Maier J., "Resistance degradation of iron-doped strontium titanate investigated by spatially resolved conductivity measurements," *J. Am. Ceram. Soc.* 83[8]:1969-76 (2000).

[23]Yoon S-H., Randall C.A., Hur K-H.," Correlation between resistance degradation and thermally stimulated depolarization current in acceptor (Mg)-doped $BaTiO_3$ submicrometer fine-grain ceramics," *J. Am. Ceram. Soc.* 92[8]: 1758-65 (2009).

[24]Warren W.L., Dimos D., Waser R.M., "Degradation mechanisms in ferroelectric and high-permittivity perovskites," *MRS Bulletin*, 40-45 (1996).

[25]Liu W., Randall C.A., "Thermally Stimulated Relaxation in Fe-Doped $SrTiO_3$ Systems: II. Degradation of $SrTiO_3$ Dielectrics," *J. Am. Ceram. Soc.* 91:3251-57 (2008).

[26]Boukamp B.A., Pham M.T.N., Blank D.H.A., and Bouwmeester H.J.M., "Ionic and electronic conductivity in lead-zirconate-titanate (PZT)," *Solid State Ionics*, 170:239 (2004).

[27]Scott J.F. "Device physics of ferroelectric thin film memories," *Jpn. J. Appl. Phys.* 38: 2272-74 (1999).

[28]Wouters D.J., Willems G.J., Maes H.E., "Electrical conductivity in ferroelectric thin films," *Microelectron Eng.* 29: 249-56 (1995).

[29]Dawber M., Scott J.F., "Physics of thin-film ferroelectric oxides," *Integ. Ferroelec.* 38 161-9 (2001).

[30]Stolichnov I. and Tagantsev A., "Space-charge influenced-injection model for conduction in $Pb(Zr_xTi_{1-x})O_3$ thin films," *J. Appl Phys.* 84: 3216-25 (1998).

[31]Dey S.K., Lee J.J., and Alluri P., "Electrical-properties of paraelectric $(Pb_{0.72}La_{0.28})TiO_3$ thin-films with high linear dielectric permittivity-Schottky and ohmic contacts," *Jpn. J. Appl. Phys*., 34: 3134-52 (1995).

[32]Akkopru-Akgun B., Zhu W., Lanagan M.T., Trolier-McKinstry S., "The effect of imprint on remanent piezoelectric properties and ferroelectric aging of Mn or Nb doped $PbZr_{0.52}Ti_{0.48}O_3$ thin films," *J. Am. Soc.* 102: 5328-41 (2019).

[33]Prokopowicz T.I. and Vaskas A.R., "Research and development intrinsic reliability subminiature ceramic capacitors," Final Report Nos. ECOM-90705-F and NTIS AD-864068 (1969).

[34]Lang D.V., "Deep-level transient spectroscopy: A new method to characterize traps in semiconductors," *J. Appl. Phys.,* 45: 3023-32 (1974).

[35]Jonscher A.K., Dielectric Relaxation in Solids, Chelsea Dielectrics Press, London, (1983).

[36]Maxwell C., Electricity and Magnetism, Clarendon Press, Oxford, Vol. 1, 452 (1892).

[37]Wolters D.R. and Zegers-van Duynhoven A.T.A., The Physics and Technology of Amorphous SiO_2, Plenum Press (1988).

[38]Auciello O., Waser R., Science and Technology of Electroceramic Thin Films, 223-248 (1995).

[39]O'Dwyer J., The Theory of Electrical Conduction and Breakdown in Solid Dielectrics, Clarendon Press, Oxford (1973).

[40]Nagaraj B., Aggarwal S., Song T.K., Sawhney T., and Ramesh R.," Leakage current mechanisms in lead-based thin-film ferroelectric capacitors," *Phys. Rev. B*, 59: 16022 (1999).

[41]Trolier-McKinstry S., Chen J., Vedam K., and Newnham R.E., "In situ annealing studies of sol-gel ferroelectric thin films by spectroscopic ellipsometry," *J. Am. Ceram. Soc.,* 78: 1907-13 (1995).

[42]Scott J.F. Ferroelectric memories Springer Verlag Heidelberg, 112-20 (2000).

[43]Scott J. F., Watanabe K., Hartmann A. J. and Lamb R. N., "Device models for PZT/Pt, BST/Pt, SBT/Pt, and SBT/Bi ferroelectric memories," *Ferroelectrics,* 225: 83-90 (1999).

[44]Robertson J. and Chen C.W., Schottky barrier heights of tantalum oxide, barium strontium titanate, lead titanate, and strontium bismuth tantalite," *Appl. Phys. Lett.* 74: 1168-1170 (1999).

[45]Klein A., "Interface Properties of Dielectric Oxides," *J. Am. Ceram. Soc.,* 99 [2]: 369–387 (2016).

[46]Hwang C.S., Lee B.T., Kang C.S., Kim J.W., Lee K.H., Cho H.J., Horii H., Kim W.D., Lee S.I., Roh Y.B., and Lee M.Y., "A comparative study on the electrical conduction mechanisms of $(Ba_{0.5}Sr_{0.5}TiO_3$ thin films on Pt and IrO_2 electrodes," *J. Appl. Phys.* 83: 3703-13 (1998).

[47]Cowley A.M., and Sze S.M., "Surface states and barrier height of metal–semiconductor systems," J. *Appl. Phys.* 36: 3212-20 (1965).

[48]Takatani S., Kushida-Abdelghafar K., Miki H., "Effect of H_2 annealing on a $Pb/PbZr_xTi_{1-}xO_3$ interface studied by x-ray photoelectron spectroscopy," *Jpn. J. Appl. Phys.,* 36: 435-38 (1997).

[49]Akkopru-Akgun B., Marincel D., Bayer T., Tsuji K., Zhu W., Randall C., Lanagan M.T., Trolier-McKinstry S., "Thermally stimulated depolarization current measurements on degraded lead zirconate titanate films to be submitted to Appl. Phys. Lett.

[50]Zubko P., Jung D.J., and Scott J.F., "Electrical characterization of $PbZr_{0.4}Ti_{0.6}O_3$ capacitors," *J. Appl. Phys*. 100: 114113 (2006).

[51]Ossmer H., Slouka C., Andrejs L., Blaha P., Friedbacher G., Fleig J., "Electrocoloration of donor-doped lead zirconate titanate under DC field stress," *Solid State Ionics*, 281: 49-59 (2015).

[52]Slouka C., Kainz T., Navickas E., Walch G., Hutter H., Reichmann K., "The effect of acceptor and donor doping on oxygen vacancy concentrations in lead zirconate titanate (PZT)," *Materials*, 9: 945-1-22 (2016).

[53]Volkl E., Hillebrand P., Fleig J., "Resistance variation in donor-doped PZT stacks with Cu inner electrodes under high field stress," *J. Electroceram.,* 27:66-77 (2011).

[54]Leapman R.D., Grunes L.A., and Fejes P.L., "Study of L_{23} edges in the 3d transition metals and their oxides by electron-energy-loss spectroscopy with comparisons to theory," *Phys. Rev. B* 26: 614 -35(1982).

[55]Otten M.T., Miner B., Rask, J.H. and Buseck P.R., "The determination of Ti, Mn and Fe oxidation states in minerals by electron energy-loss spectroscopy," *Ultramicroscopy* 18: 285-89 (1985).

[56]Garten L., PhD Dissertation, "Residual ferroelectricity, piezoelectricity, and flexoelectricity in barium strontium titanate tunable dielectrics," Penn State University, Ch 8, p 145-156 (2014).

[57]West A.R., Sinclair D.C., and Hirose N., "Characterization of electrical materials, especially ferroelectrics, by impedance spectroscopy," *J. Electroceram.* 1: 65-71 (1997).

[58]Bayer T.J.M., Wang J.-J., Carter J.J., Moballegh A., Baker J., Irving D.L., Dickey E.C., Chen L.-Q., and Randall C.A., "The relation of electrical conductivity profiles and modulus data using the example of STO:Fe single crystals," *Acta Mater.* 117: 252-61 (2016).

[59]Irvine J.T.S., Sinclair D.C., and West A.R., "Electroceramics: Characterization by impedance spectroscopy," *Adv. Mater.* 2, 132-38 (1990).

[60]Bouyssou E., Paolls R.D., Rousseau A., "Systematic tuning of the conduction mechanisms in ferroelectric thin films," *J. Phys. Condens. Matter.* 25: 495901-1-13 (2013).

[61]Chiang T-H., Wager J.F., "Electronic conduction mechanisms in insulators," *IEEE Transactions on Electron Devices*. 65:223-30 (2018).

Chapter 4

The influence of Mn doping on the leakage current mechanisms and resistance degradation behavior in lead zirconate titanate films

4.1 Introduction

The performance and electrical reliability of lead zirconate titanate (PZT) ferroelectric films used in microelectromechanical systems (MEMS) as acoustic sensors,[1] ultrasonic transducers,[2-3] energy harvesting devices,[4-5] actuators,[6] and sensors[7-8] are typically controlled by point defects. The type and concentration of defects in the structure strongly depends on both the nature of the impurities (acceptor, donor, fixed valence, redox-reactive) and the host lattice. The incorporation of impurities into PZT results in formation of lead or oxygen vacancies for ionic compensation and electrons or holes for electronic compensation.[9]

Acceptor type impurities like $Fe^{2+,3+}$, $Mn^{2+,3+}$, Mg^{2+} have lower valence than the B-site cations (Ti^{4+}, Zr^{4+}) they replace. Charge compensation is achieved by generating oxygen vacancies and/or holes in the system. Oxygen vacancies and acceptor ions create defect dipoles represented as $(A''_{Ti} - V_O^{\bullet\bullet})^x$, $(A'_{Ti} - V_O^{\bullet\bullet})'$ in Kroger-Vink notation. Some acceptor ions like $Mn^{2+/3+/4+}$

$$AO_2 \xrightarrow{(TiO_2)} A''_{Ti} + V_O^{\bullet\bullet} + O_O^{\mathrm{x}} \qquad \text{Equation 4.1}$$

$$2[V''_{Pb}\,] + \left[A'_{Ti,Zr}\right] = 2[V_O^{\bullet\bullet}] + [h^{\bullet}] \qquad \text{Equation 4.2}$$

or $Fe^{2+/3+/4+}$ can take multiple valence states. It has been demonstrated that valence state of redox-active acceptor ions varies with the annealing atmosphere. Hayashi et al. showed that processing of Mn doped $PbTiO_3$ in oxidizing atmospheres results in

isovalent doping (Mn^{4+} substituting for Ti^{4+}) and low oxygen vacancy concentrations, whereas annealing under reducing atmosphere leads to aliovalent doping ($Mn^{2+/3+}$ on Ti^{4+}) and higher oxygen vacancy concentrations.[10-11] Thus, the hole or/and oxygen vacancy concentrations can be engineered to govern the electrical properties of PZT films.

In contrast to acceptors, donor type impurities like Nd^{3+} or La^{3+} on the A-site (Pb^{2+}) or Nb^{5+} on the B-site (Ti^{4+}, Zr^{4+}) are either ionically and/or electronically compensated via doubly ionized lead vacancies and electrons, respectively. Incorporation of donor ions into PZT reduces the concentration of oxygen vacancies below the intrinsic level.

$$D_2O_5 + V_O^{\bullet\bullet} \xrightarrow{2(TiO_2)} 2D_{Ti}^{\bullet} + 4O_O \qquad \text{Equation 4.3}$$

$$[D_{Ti}^{\bullet}] + 2[V_O^{\bullet\bullet}] + [h^{\bullet}] = 2[V_{Pb}''] + [e'] \qquad \text{Equation 4.4}$$

Understanding the variation in point defect types and concentrations through aliovalent doping in PZT films is crucial to understand the ionic and electronic conduction mechanisms that contribute electrical degradation of PZT films. Defects are known to contribute to ionic conductivity and may account for electronic conductivity when they are electronically compensated in PZT ceramics. Table 4.1 gives activation energy data for ionic and/or electronic conduction and associated degradation mechanisms observed in different lead-based perovskites. As shown in Table 1, large variations of activation energies and transport mechanisms that control the degradation process have been proposed in the literature.[12-24] This indicates that both the mechanisms responsible for changes over time and the mechanisms responsible for degradation may

Table 4.1 *Reported activation energies in PZT and other lead-based perovskites*

Composition	Method	E_a (eV)	Mechanism	Reference
(Mg, Nb) co-doped PZT bulk (Mn, Nb) co-doped PZT bulk	Impedance measurement	1.05–1.25 eV 1.48 eV	ionic conductivity by $V_O^{\bullet\bullet}$ V_{Pb}'' diffusion	(Ref. 12)
PZT film	HALT	0.78 eV	Ionic migration of $V_O^{\bullet\bullet}$	(Ref. 13)
$Pb(Zr_{0.54},Ti_{0.46})O_3$ film	DLTS	0.27 eV	Hopping between Pb^{2+} and Pb^{3+}	(Ref. 14)
$PbZr_{0.65}Ti_{0.35}O_3$ film	ToF-SIMS-O^{18} tracer diffusion	2.7 eV 0.6 eV	near-surface oxygen tracer diffusivity "bulk" diffusivity	(Ref. 15)
PZT film PNZT film PLZT film	HALT	0.6-1.2 eV	Hole trapping by V_{Pb}'' or acceptor impurities	(Ref. 16)
$PbZr_{1-x}Ti_xO_3$ bulk	EPR	0.26 eV 1 eV	Hopping between Pb^{2+} and Pb^{3+} electron trapping via Ti^{4+} sites	(Ref. 17)
$Pb_{1.01}Ti_{1.00}O_x$ films $Pb_{1.00}Ti_{1.00}O_x$ films $Pb_{1.01}Ti_{1.00}O_x$ films	DLTS	0.25-0.27 eV 0.46-0.50 eV 0.93-1.01 eV	Hopping between Pb^{2+} and Pb^{3+} the ionization of lead vacancies	(Ref. 18)
$(Pb_{1-x}La_x)(Zr_{0.90}Ti_{0.10})_{1-x/4}O_3$	Impedance measurement	0.99–1.21 eV	The ionization of the oxygen vacancies	(Ref. 19)
Nd doped $Pb(Zr_{0.52}Ti_{0.48})O_3$ films	HALT	0.87 eV	Migration of oxygen vacancies	(Ref. 20)
$Pb(Zr,Ti)O_3$	I-V	0.5-0.6 eV	Ionization energy of Ti^{4+} to Ti^{3+}	(Ref. 21)
$(Pb_{1-x}Ba_x)(Zr_{0.95}Ti_{0.05})O_3$	Impedance measurement	0.98-1.28eV	$V_O^{\bullet\bullet}$ trapping level for electrons	(Ref. 22)
Mn doped PMN-PT single crystal	Impedance measurement	0.54 eV	$V_O^{\bullet}$	(Ref. 23)
PMN-PT single crystal	HALT, Impedance measurement, TSDC	0.6 eV 1.4 eV 1.1 eV	Ionic migration of $V_O^{\bullet\bullet}$ hole migration between V_{Pb}'' Electron hopping from deeply localized Ti^{3+}	(Ref. 24)

differ in bulk and thin films as well as differ between acceptor and donor doped PZT films due to variation in defect chemistry and microstructures.

The defect chemistry in PZT films is very difficult to determine precisely due to unknown cation stoichiometry resulting from evaporation of PbO upon annealing at temperatures higher than 400°C. As shown in Table 4.1, a wide variation in activation energy for a failure under a DC bias field was observed depending on the type and concentration of impurity ion as well as on the film stoichiometry.[12-24] In general, acceptor doped PZT films exhibit lower lifetime than their donor doped counterparts since the addition of acceptor ions in perovskite lattice leads to formation of oxygen vacancies;[25] it is believed that the field driven migration of oxygen plays a critical role in DC resistance degradation.[26-27] It was shown in $BaTiO_3$ and $SrTiO_3$ that resistance degradation can be associated with migration of oxygen vacancies and subsequent accumulation near the cathode and depletion near the anode.[26, 28] Surprisingly, Pb based perovskites with redox-active acceptor ions exhibit longer lifetime and lower electrical degradation rates.[24] Enhanced lifetime via introduction of Mn has been reported by Yoon et al. for $BaTiO_3$ ceramics[29-30], Mori et al. for PZT films[31], and Yan et al. for PMN-PT ceramics[32]. Two different mechanisms were proposed to explain the improvement in lifetime via addition of Mn into PZT films; (1) Jahn-Teller distortion of Mn^{3+} retards the dissociation of $Mn'_{Ti} - V_O^{\bullet\bullet}$ defect dipoles and subsequent migration of oxygen vacancies upon electrical degradation,[30] (2) $e' - h^{\bullet}$ trapping; electrons accumulated near the cathode and hole formation in anodic region can be suppressed by introducing Mn into PZT films.[24] Although it is well understood that Mn doping plays a critical role in defect chemistry and resistance degradation, the exact mechanism has not yet been clarified.

In this work, the influence of Mn addition in altering the defect structure and associated charge transport mechanisms has been studied; it has been shown that the variable valence state of acceptor ions can be used to engineer defect types and concentrations in the perovskite lattice. The defect chemistry, including the nature and concentrations as well as migration of mobile point defects under electric field and electronic carrier distributions were explored by in-situ impedance, DLTS (Deep Level Transient Spectroscopy) and TSDC (Thermally Stimulated Depolarization Current). The existence and migration of oxygen vacancies were analyzed by TSDC. The change in interfacial defect chemistry was monitored via Electron Energy Loss Spectroscopy. The dominant conduction mechanism leading to resistance degradation in Mn doped PZT films was explored by I-V measurements. The lifetimes of PZT films with different Mn concentrations were assessed using Highly Accelerated Lifetime Testing (HALT), from which activation energies and voltage acceleration factors were extracted. A physical model was developed to explain the relationship between defect microstructure and macroscopic electrical properties, which is crucial for the design of electrically reliable PiezoMEMS that could function under high electric fields and temperatures during their entire service lifetime.

4.2. Experimental Procedure

Multivalent acceptor-doped (Mn) lead zirconate titanate (PZT) thin films with dopant concentrations varying from 0.5 to 4 mol% were grown on commercial Pt/Ti/SiO_2/Si substrates (Nova Electronic Materials, Flower Mound, TX) via chemical solution deposition. Solutions with a Zr/Ti ratio of 52/48 were prepared using 10 mol% Pb excess to compensate for lead loss during heat treatment. The preparation of solutions

is similar to that described elsewhere.[33] The Mn doping concentration in solution was calculated presuming B site occupancy to reach final film compositions of: $Pb_{\left(1-\frac{1}{2}x\right)}\ Zr_{0.52(1-x)}\ Ti_{0.48(1-x)}\ Mn_xO_3$, where x = 0.005–0.04.

The preparation of the films as well as characterization techniques to assess the structural and electrical properties of Mn doped PZT films were described in Section 3.2.[33]

4.3 Results and Discussion

Figure 4.1 shows the time-dependence leakage current for Mn doped PZT films under an electric field of 400 kV/cm at 180°C. Weibull analysis was performed to attain the distribution of degradation rates and the MTTF, e.g. the center ($t_{0.5}$) of a life distribution (Figure 4.1b). The failure time increases remarkably with Mn concentration in PZT films. The MTTF was found to be 1.47±0.2, 3.9±0.4, 7.9±0.9, and 21.4±0.8 for 0.5, 1, 2, and 4 mol% Mn doped PZT films, respectively (Table 4.2). The activation energy for electrical degradation was determined using the empirical relationship

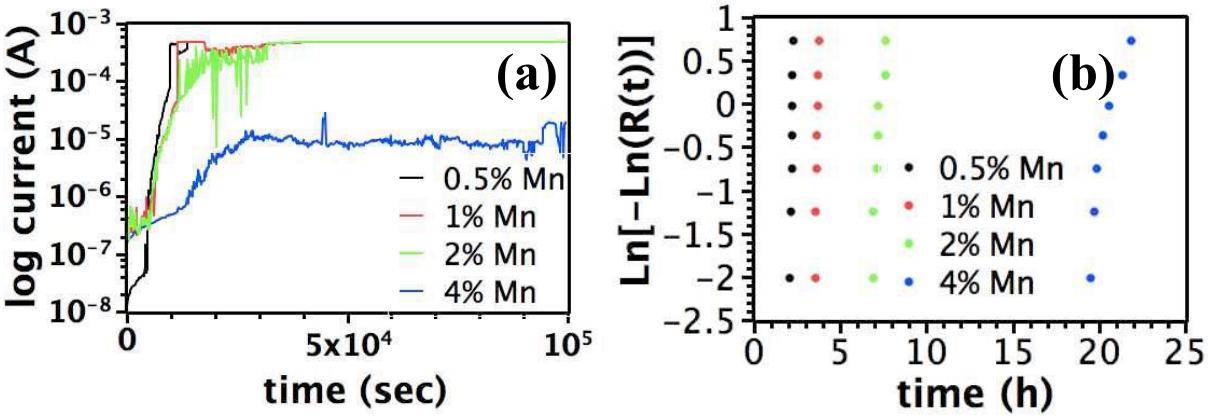

Figure 4.1 *(a) Variation in leakage current with time in, (b) the time to failure for 0.5, 1, 2, and 4% Mn doped PZT films. R(t) represents the probability of failure over time. The HALT measurement was conducted at 180°C with a DC field of 400 kV/cm.*

Table 4.2 *Median time to failure and Weibull fitting parameter 0.5, 1, and 2% Mn doped PZT films. The HALT measurement was conducted at 180°C with a DC field of 400 kV/cm.*

	$t_{0.5}$ (hours)	β
0.5% Mn PZT	1.47±0.2	16.45±0.5
1% Mn PZT	3.9+0.4	11.4±0.3
2% Mn PZT	7.2±0.9	3.5±0.2
4% Mn PZT	21.4±0.8	9.3±0.5

suggested by Prokopowicz and Vaskas.[34] It was found that the activation energy for electrical degradation increases with Mn concentration in PZT films; activation energies of 0.76±0.06, 0.97±0.05, 1.15±0.04, and 1.33±0.06 eV were found for 0.5, 1, 2, and 4 mol% Mn doped PZT films, respectively. (Figure 4.2, Table 4.2). A voltage acceleration factor of 4.8±0.24 and 5.6±0.3 was found for 1 and 2 mol% Mn doped PZT films, which

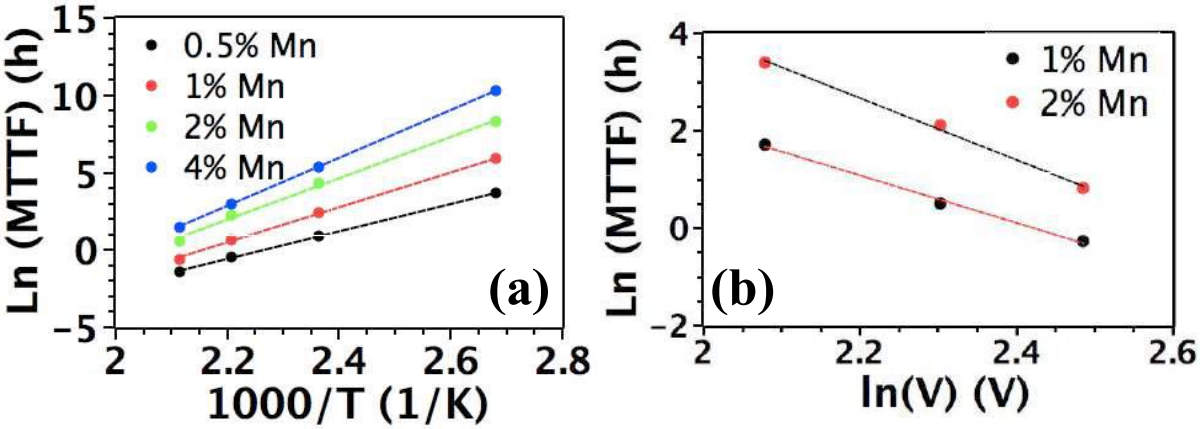

Figure 4.2 *(a) Temperature and (b) voltage dependence of median time to failure (MTF) in 0.5, 1, 2, and 4% Mn doped PZT films.*

Table 4.3 *Activation energies and voltage acceleration factors of 0.5, 1, 2, and 4% Mn doped PZT films.*

	E_a (eV)	N
0.5% Mn PZT	0.76±0.06	
1% Mn PZT	0.97+0.05	4.8±0.24
2% Mn PZT	1.15±0.04	5.6±0.3
4% Mn PZT	1.33±0.06	

similar to the values reported in the literature. [13, 16, 36] Degradation in perovskite-type ceramics is often due to the field driven migration of oxygen vacancies (exacerbated at elevated temperatures) and subsequent accumulation of oxygen vacancies near the cathode region.[26] Thus, it is unexpected to observe higher lifetimes and lower degradation rates in PZT films with higher Mn concentrations, as Mn acceptor ions increase the oxygen vacancy concentration.

$$2[Mn_{Ti}''] + [Mn_{Ti}'] + 2[V_{Pb}''] + [e'] = 2[V_O^{\bullet\bullet}] + [h^{\bullet}] \qquad \text{Equation 4.5}$$

As described above, the enhanced lifetime in Mn doped PZT films can, in principle, be attributed to one of two factors; (1) A strong defect association between singly ionized manganese ions Mn_{Ti}' and $V_O^{\bullet\bullet}$ due to Jahn-Teller distortion significantly reducing migration of oxygen vacancies,[30] (2) $e' - h^{\bullet}$ trapping effect; electrons accumulated at the cathode region and hole formation near the anode due to drift of oxygen vacancies can be suppressed by introducing Mn into the PZT films.[24, 31-32]

To assess the presence of mobile or/and trapped oxygen vacancies, Thermally Stimulated Depolarization Current Measurements (TSDC) were performed on degraded Mn-doped PZT films (Figure 4.3). Only one depolarization current peak was observed around 200°C. The polarization electric field dependence of T_{max} of TSDC peak was studied to explore the physical origin of this peak; the corresponding activation energy was calculated using the initial rise method described elsewhere.[37] It was found that the peak is due to ionic migration of oxygen vacancies with an activation energy of 0.6 eV.[37] Thus, the dissociation of defect dipoles, $(Mn_{Ti}'' - V_O^{\bullet\bullet})^x$, $(Mn_{Ti}' - V_O^{\bullet\bullet})'$, $(V_{Pb}'' - V_O^{\bullet\bullet})^x$, along with the migration of individual oxygen vacancies upon electrical degradation leads to growth of ionic space charge peak. The concentration of oxygen

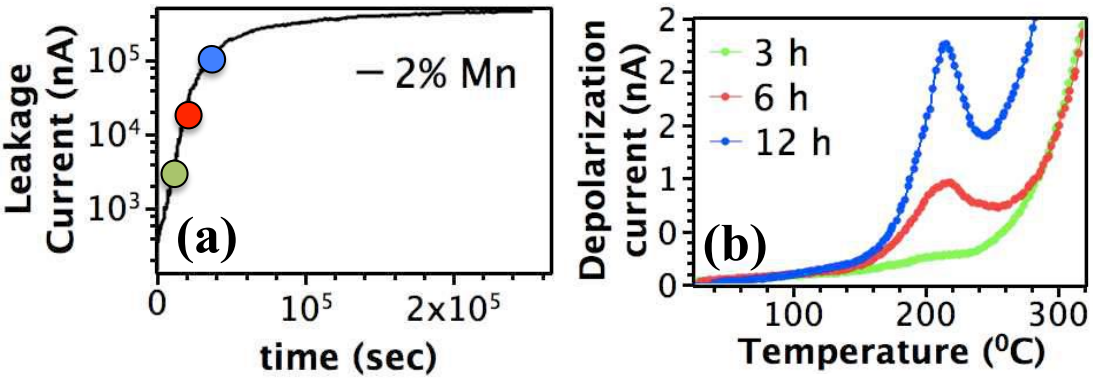

Figure 4.3 *(a) Variation in leakage current with time in 2% Mn doped PZT films, (b) evaluation of TSDC spectra of 2% Mn doped PZT films after degrading the films for 3, 6, or 12 h. The HALT measurement and degradation study were conducted at 180°C with a DC field of 400 kV/cm.*

vacancies increased from $3x10^{19}$ to $5x10^{19}$, $1x10^{20}$, and $2x10^{20}/cm^3$ with increasing Mn concentration from 0.5 to 1, 2, and 4 mol%, respectively, [37] which confirms that the ionic conductivity due to long-range migration of oxygen vacancies was not eliminated due to Jahn-Teller distortions.

Ionic migration and subsequent accumulation of oxygen vacancies under dc field changes the local defect chemistry through the PZT films; electrons are created in the cathodic region, and holes are generated in the anodic region by accumulation and depletion of oxygen vacancies, respectively. This results in an exponential increase in leakage current and lowering of the barrier for injection from the cathode into the film. The compensating electrons can be trapped at Ti^{4+} to create Ti^{3+} ions.[17] Electron accumulation due to migration of oxygen vacancies in Nb doped PZT films was confirmed by increased concentration of Ti^{3+} near the cathode region.[38]

In contrast to the findings for Nb doped PZT films, no variation in valence state of Ti towards to cathode region was observed in Mn doped films. Figure 4.4 depicts a series of Ti-L edges from diferent positions in 2 mol% Mn doped PZT film as a function of

distance from the cathode. Prior to EELS analysis, the film was severely degraded under an electric field of 400 kV/cm for 12 h. No apparent chemical shift is observed from a series of EELS spectra taken from cathodic region to anodic region, implying that there is

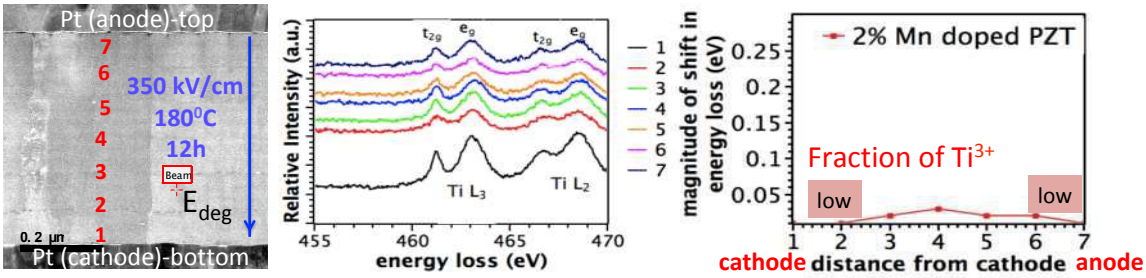

Figure 4.4 *Electron energy loss spectrum from different positions in the 2% Mn doped PZT film as a function of distance from the bottom interface (cathode). Ti $L_{2,3}$ of 2% Mn doped PZT films after degrading at 180°C under electric field of 350 kV/ cm for 12h.*

no modification in the Ti valence in the degraded films. Additionally, TSDC results of degraded Mn doped PZT films did not show a depolarization current peak arising from relaxation of trapped electrons from Ti^{4+}. This suggests that the multivalent Mn ions provide trap sites for electrons and holes; free electron generation due to compensation of oxygen vacancies at the cathode and free hole formation at the anode region might be suppressed by the valence changes from Mn^{3+} to Mn^{2+} and Mn^{2+} to Mn^{3+} respectively. In fact, the Mn_{Ti}^{x} and $Mn_{Ti}^{\prime}$ ions are more reducible than Ti_{Ti}^{x}.[39] Therefore, the compensated electrons are preferentially trapped on the manganese sites rather than Ti^{4+} ions.

$$Mn_{Ti}^{\prime} + e^{\prime} \rightleftarrows Mn_{Ti}^{\prime\prime} \qquad Mn_{Ti}^{x} + e^{\prime} \rightleftarrows Mn_{Ti}^{\prime} \qquad \text{Equation 4.6}$$

$$Mn_{Ti}^{\prime\prime} + h^{\bullet} \rightleftarrows Mn_{Ti}^{\prime} \qquad Mn_{Ti}^{\prime} + h^{\bullet} \rightleftarrows Mn_{Ti}^{x} \qquad \text{Equation 4.7}$$

To further explore the change in charge transport mechanism through chemical modification of PZT films, the conduction mechanism of pristine and degraded Mn doped PZT films was investigated. Figure 4.5 shows the fit of the I-V results to the equations for various conduction mechanisms. In the pristine state, the conduction

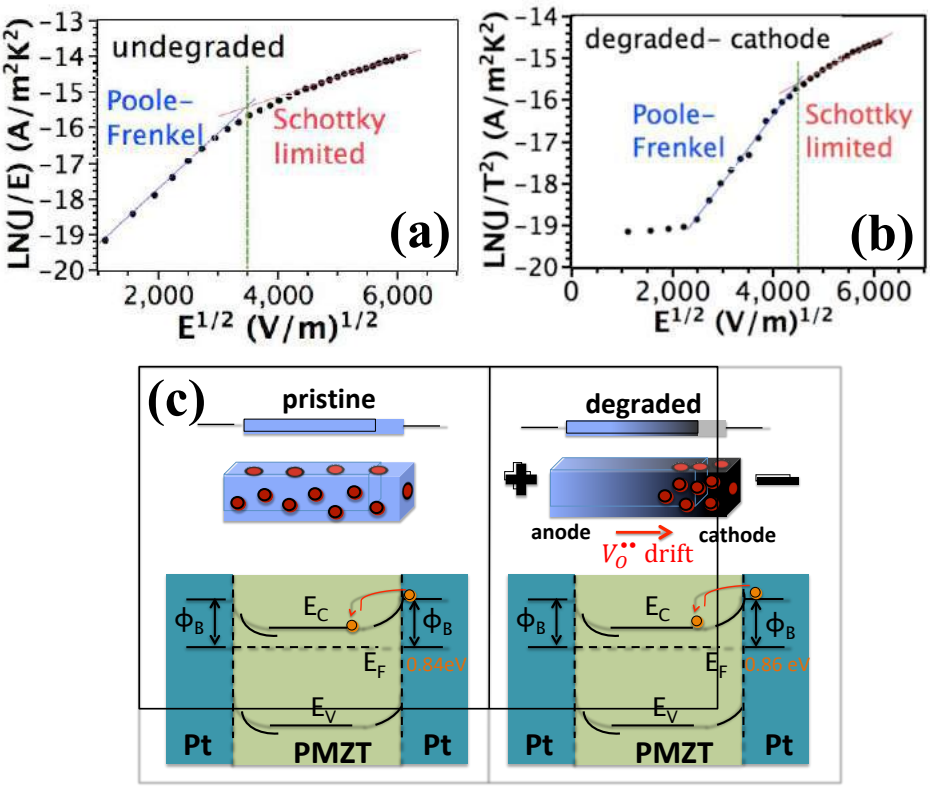

Figure 4.5 *Fitting of the leakage current-voltage data for distinct electric fields in 2% Mn doped PZT thin films (a) before, and (b) after degrading the thin film samples at 180°C with a DC field of 400 kV/cm for 12 h.*

mechanism below 145 kV/cm is dominated by Poole-Frenkel emission, whereas the high electric field range is controlled by Schottky emission. The Schottky barrier height was extracted from Schottky plots in the field range of 180-400 kV/cm and calculated to be 1.17±0.04, 1.06±0.05, 0.84±0.03, and 0.72±0.04 eV for 0.5, 1, 2, and 4 mol% Mn doped PZT films (Table 4.4). The experimental value is significantly lower than ideal value ($\phi_B = \phi_M - \chi_{PZT} = 1.8\,eV$), calculated based on the metal work function (5.3 eV) and the electron affinity of the PZT (3.5 eV), suggesting that the barrier height at the metal-PZT interface is strongly influenced by interface/surface states such as oxygen vacancies and/or impurity levels. The effect of surface/interface states on conduction of PZT was previously discussed via Scott et al.[40-41] It was reported that oxidation and reduction of the PZT/Pt interface leads to changes in E_f of more than 1 eV.[42] Reduction of the oxide

Table 4.4 *Schottky barrier heights of Mn doped PZT films*

	Experimental barrier height (eV)
0.5% Mn	1.17±0.04
1% Mn	1.06±0.05
2% Mn	0.84±0.03
4% Mn	0.72±0.04

surface creates a high concentration of defects, most likely oxygen vacancies, at the PZT/Pt interface that pin the Fermi energy level. This lowers the potential barrier height and enhances the probability of electron injection from the cathode to the PZT. In the same way, the barrier height decrease from 1.17 eV to 0.72 as the Mn concentration increased from 0.5 to 4 mol% due to modification of Schottky barrier through Fermi level pinning. The concentration of oxygen vacancies increases with Mn concentrations, resulting in a lower Schottky barrier height.

After degrading 2 mol% Mn doped PZT film under an electric field of 350 kV/cm at 180°C for 12 h, (1) the width of Poole-Frenkel regime increases, accompanied by a shrinkage in the field range for the Schottky regime; the transition electric field from Poole-Frenkel conduction to Schottky emission shifted from 145 to 182 kV/cm after degradation and (2) no significant change in potential barrier height for injecting electrons from cathode into PZT was observed after degradation; Schottky barriers of 0.84±0.05 and 0.86±0.07 eV were found in pristine and degraded states, respectively. It is also unexpected to observe that the Schottky barrier height remained the same after degradation.

The current density J under an applied electric field across a Schottky contact is given by:

$$J = J_0 \exp\left(\frac{qE}{nkT}\right)\left[1 - \exp\left(\frac{qV}{kT}\right)\right] \quad \text{Equation 4.8}$$

where J_0 is the reverse saturation current, and n and k are the ideality factor (which is 1 for the ideal Schottky contact) and the Boltzmann constant, respectively. V has positive and negative values for forward and reverse biases, respectively. J_0, the reverse saturation current is represented by:[43-44]

$$J_0 = A^* T^2 \exp\left(-q\frac{q\phi_B}{kT}\right) exp\left[\frac{q\sqrt{qE/4\pi\varepsilon_0\varepsilon_r w}}{kT}\right] \quad \text{Equation 4.9}$$

where A*, ϕ_B, $\varepsilon_0, \varepsilon_r$, and w are the Richardson's constant, the potential barrier height, vacuum permittivity, dielectric constant, and depletion layer thickness, respectively. In Eq. 4.9, it is assumed that E, which determines the barrier lowering, is uniform throughout the PZT film, which necessitates that the film is fully depleted. However, the electric field, E, is not equal to V/d in the case of partial depletion. Accumulation of oxygen vacancies at the negatively biased Schottky interface leads to a variation in E_m; high dopant concentration (N_D, oxygen vacancies) allows the applied electric field to be gradually dropped across a depletion layer near the cathode. In this case, a variation in E_m that relies on the built in bias, V_{bi}, is described by:[44-45]

$$E_m = \sqrt{\frac{2qN_D}{\varepsilon_s}(V - V_{bi} - \frac{kT}{q})} \quad \text{Equation 4.10}$$

where q, N_D, ε_o, ε_{DC}, V, V_{Bi}, k, T are electric charge, vacuum permittivity, dielectric constant, applied voltage, built-in potential, Boltzmann's constant, and temperature, respectively. The maximum field strength in the barrier, E_m, is directly proportional to exp ($q\Delta\phi_B$/kT), where $\Delta\phi_B$ is the lowering of the barrier due to the field. Upon degradation of 2 mol% Mn doped PZT films, oxygen vacancies accumulate near the cathode region. This leads to a decrease in the depletion layer width, $w = \sqrt{2\varepsilon_0\varepsilon_r(V_a - V_b)/qN_d}$[44, 46] The accumulation of oxygen vacancies near the cathode

exponentially increases the leakage current, accompanied by Schottky barrier lowering and eventually to electrical breakdown of the film. However, in this study, no change in Schottky barrier height was observed upon electrical degradation. This could be attributed to suppression of the electric field in the depletion layer via trapping of electronic charges by Mn sites near the interface, which screens the positively charged space charge due to accumulation of oxygen vacancies. This trapping creates a double electrical layer that is consisted of the negatively charged interfacial layer due to trapped electrons via Mn sites and positively charged space charge region as a result of accumulation of oxygen vacancies. When the carrier density is very high, the total space charge region near the interface becomes neutral by offsetting the positive space charge with the negative surface charge. Under this circumstance, barrier lowering, $\phi\Delta_B$ is limited by the suppressed electrical field due to the presence of trapped charges at Mn sites. Moreover, the distribution of trapped charges associated with Mn sites extends over long distances because the Mn concentration is low. This could also reduce the electric field in the depletion region, which in turn decreases barrier lowering and suppresses any leakage current increase upon electrical degradation.

To assess the different trap levels that contributes to Poole-Frenkel emission in Mn doped PZT films, charge-DLTS measurements and impedance analysis were conducted. Figure 4.6 depicts the DLTS signals of 2 mol% Mn doped PZT films at different discharging durations from 100-650K. The DLTS signals reveal three distinct peaks, referred to as traps 1, 2, and 3. The electron emission rate is given by:

$$e_n = \tau_n^{-1} = \sigma_n \gamma_n T^2 exp\left(-\frac{E_T}{kT}\right) \qquad \text{Equation 4.11}$$

where σ_n is the capture cross section, γ_n is a constant, τ_n is the emission time constant,

k is Boltzmann's constant, and E_t is the trap activation energy. The maximum temperature points for DLTS peaks are plotted on an Arrhenius plot for different rate

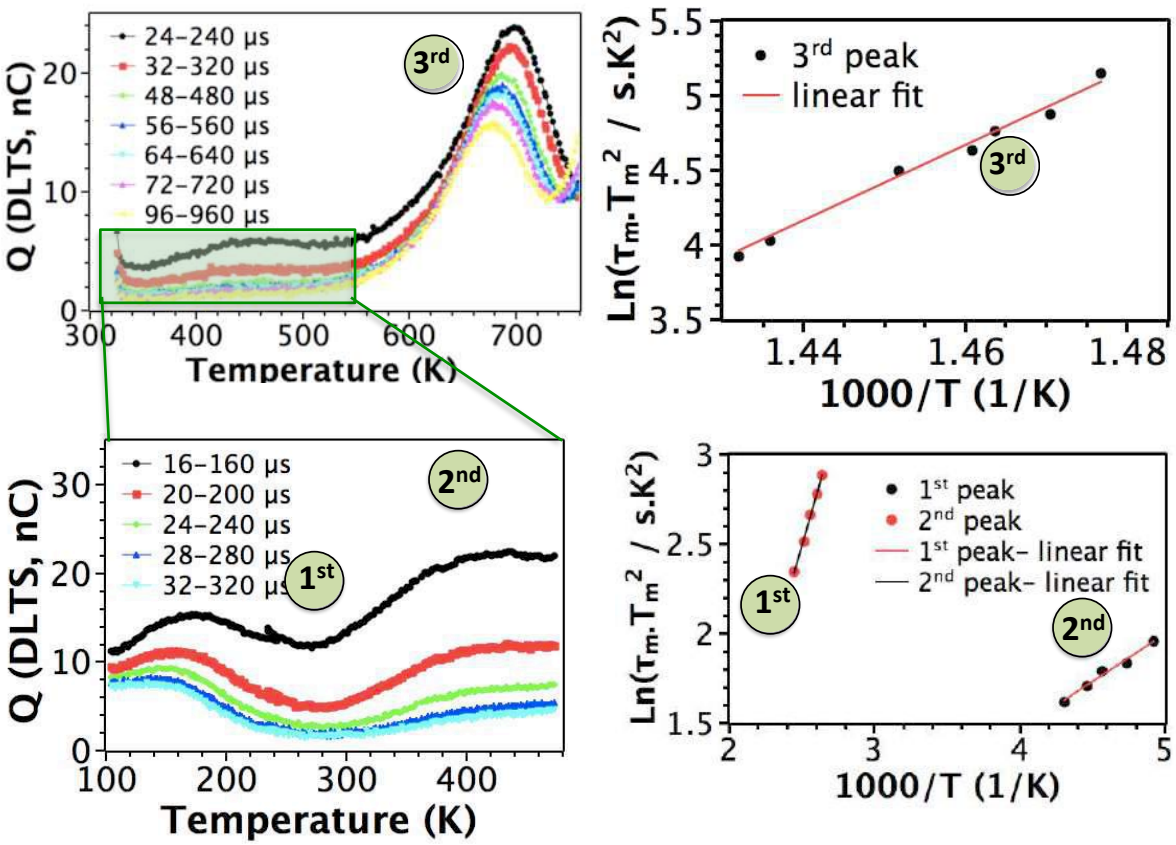

Figure 4.6 *(a) Q-DLTS of 2% Mn doped PZT films at temperatures from 300 to 750 K. The legend on Figure 5a indicates distinct rate windows. The DLTS signal was measured at seven different rate windows to resolve emission from different traps, A DLTS peak is generated when the thermal emission rate of the trap is the same as that of the rate window. (b) Arrhenius plot of the DLTS signal*

windows (Figure 4.6b). The activation energy and capture cross section of defect states were deduced from the slope and intercept of the Arrhenius plot, respectively; the results are shown in Table 4.5. The first DLTS peak with the small activation energy of 0.05 eV is most likely associated with hopping conduction. The second trap level with an activation energy of 0.26 eV was attributed by Smyth et al. to hole hopping between Pb^{2+} and Pb^{3+} sites.[17] The third DLTS peak with activation energy of 1.9 eV is associated

with $Mn^{2+/}Mn^{3+}$ impurity levels in the energy band diagram of PZT.[47]

$$Pb^{2+} + h^{\bullet} \longrightarrow Pb^{3+} \quad \text{Equation 4.12}$$
$$Mn^{2+} + h^{\bullet} \longrightarrow Mn^{3+} \quad \text{Equation 4.13}$$

In this study, $\frac{t_1}{t_2} = \alpha = 10$ was kept constant while scanning the rate window ($\tau_m = t_1(\alpha - 1) - \ln\alpha$). The maximum charge release $\Delta Q(\tau_m)$ is achieved when the rate window equals the emission rate of traps $t_1(\alpha - 1) - \ln\alpha = e_p$. The magnitude of released charge is then $Q_0[\alpha^{\frac{1}{1-\alpha}} - \alpha^{\frac{\alpha}{1-\alpha}}]$. For $\alpha = 10$, $\Delta Q_{max} = Q_0/1.29$. The density of traps can then be estimated using equation 9.[35]

$$N_t = 4\Delta Q_{max}/qAd \quad \text{Equation 4.14}$$

where q is the electron charge, A is the contact area and d is the thickness of the film.[33]

Table 4.5 *The activation energy and capture cross section of defect states in 2% Mn doped PZT films*

	E_a(eV)	$\sigma_n(cm^{-2})$
1st peak	0.05	$8.7x10^{-25}$
2nd peak	0.26±0.03	$2.8x10^{-16}$
3rd peak	1.9±0.06	$9.1x10^{-8}$

The density of $Mn^{2+/3+}$ traps was estimated to be $9.7x10^{17}$, and $1.98x10^{18}/cm^3$ for 1 and 2% Mn doped PZT films, respectively. The TSDC results demonstrate that the concentration of accumulated oxygen vacancies near the cathode region upon degradation is $1x10^{20}/cm^3$. In principle, a high concentration of oxygen vacancies, compensated via electrons $n \sim 2[V_O^{\bullet\bullet}] = 2x10^{20}/cm^3$ should exist near the cathode. These electrons could be trapped by Mn ions; each Mn ion can trap not more than two electrons. Most of the Mn ions need to act as trap sites to compensate the electrons near the cathode region. Since the Mn ions are widely distributed within the film due to their low concentrations, the trapped electrons at Mn sites are also spread out, which shifts the center of charge from

the cathode region through the bulk of the film. This prevents accumulation of electronic charges at the cathode/PZT film interface, which decreases barrier lowering and leakage current increase upon degradation, consistent with the experimental observations described above.

To further explore the variation in conduction mechanism with a change in defect chemistry of PZT films, impedance measurements were carried out. Figure 4.7 exhibits the imaginary part of the electric modulus and impedance of a pristine 2 mol% Mn doped PZT film measured at 340°C; *M″(f)* indicates the volume fraction with similar conductivity. The conductivity σ of the film is related to the relaxation frequency f(r) through the equation:

$$\sigma = 2\pi f_r \epsilon_0 \epsilon_r \qquad \text{Equation 4.15}$$

where ε_0 and ε_r are the vacuum and relative permittivities, respectively.

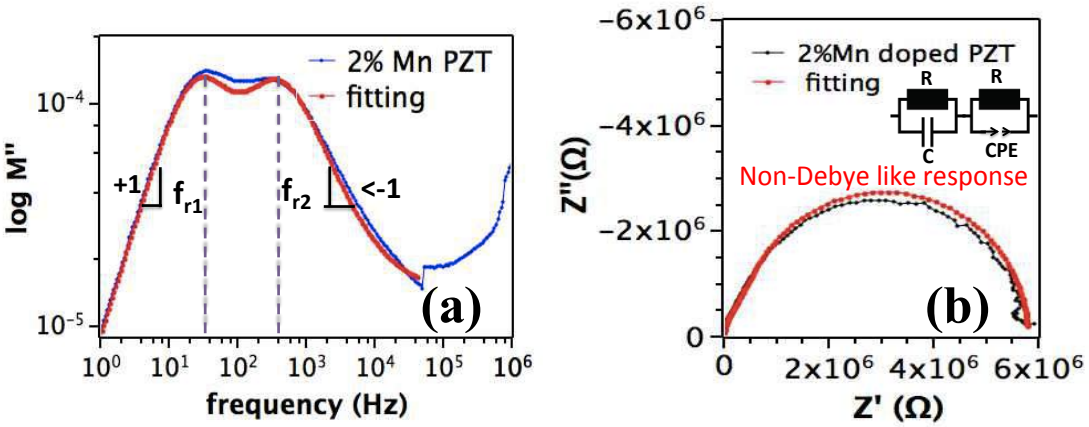

Figure 4.7 *Imaginary (a) modulus, and (b) impedance of 2% Mn doped PZT plotted as a function of frequency. The fit is for a Debye relaxation centered at frequency f_r.*

The frequency dependence of both imaginary modulus and impedance was found to be of the non-Debye type; the slopes of the log(M) – log(f) plots were +1 and <-1 below and above the relaxation frequency. As shown in Figure 4.7, the imaginary part of

the electric modulus for the 2 mol% Mn doped PZT film consists of two peaks, indicating the presence of two regions with different conductivities. This inhomogeneous conductivity might arise from (1) the presence of regions with distinct charge transport mechanisms and/or (2) non-uniform distribution of oxygen vacancies and other defects in the sample.

Figure 4.8 shows the imaginary part of the electric modulus as a function of frequency for 2 mol% Mn doped PZT films with different thicknesses. The magnitude of the modulus peak, which is inversely proportional to the permittivity of the PZT film at the relaxation frequency, is independent of thickness for films from 350–1200 nm. This indicates that the modulus peak is associated with bulk charge transport rather than an interface-controlled mechanism.

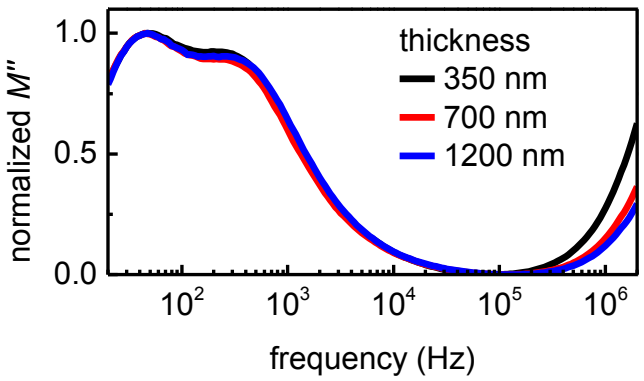

Figure 4.8 *Imaginary modulus of 2% Mn doped PZT with different thicknesses plotted as a function of frequency*

The magnitude of the imaginary part of the electric modulus peaks depends on the Mn concentration as shown in Figure 4.9. For the 0.5 mol% Mn doped PZT film, the modulus spectrum consisted of only one peak at 0.04 Hz, representing a homogeneous conductivity profile. As the Mn concentration increases to 1 mol% in PZT films, a second modulus peak appears at 20 Hz and the intensity of this peak gradually increased while the first peak is progressively suppressed with further increase in Mn concentration.

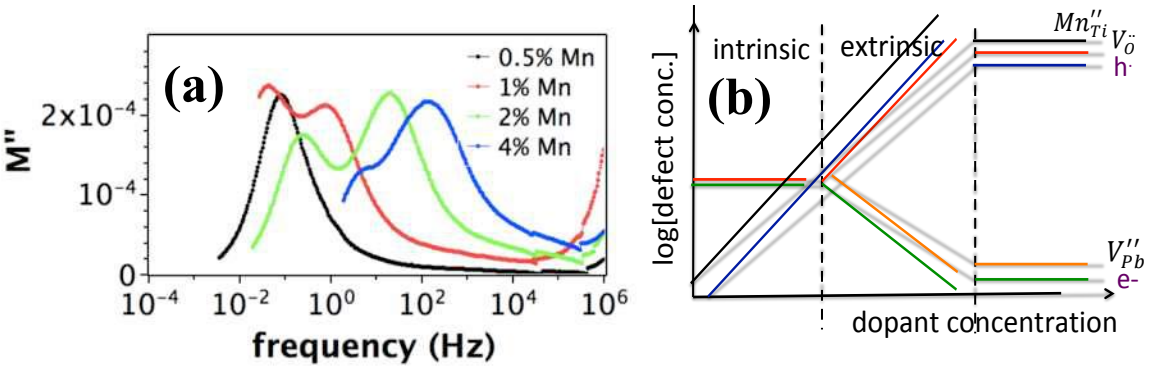

Figure 4.9**(a)** *Frequency dependence of modulus for 0.5, 1, 2, and 4% Mn doped PZT films, (b) Schematic representation of defect concentrations as a function of Mn doping level in PZT films*

The temperature dependence of the modulus peak was investigated to elucidate the origin of the dominant bulk charge transport mechanism (Figure 4.10). The activation energies extracted from the slope of Arrhenius plots for 0.5-4 mol% Mn doped PZT films are shown in Figure 4.10e. The activation energy for the low frequency modulus peak was found to be 1.39 ± 0.05 eV, which is associated with hole migration between V''_{Pb}; this peak is largely independent of the Mn concentration.[48] The activation energy of the higher frequency modulus peak, on the other hand, gradually decreases from 1.12 to 0.65 eV with increasing Mn concentration. This strongly indicates a gradual change in charge transport mechanism from the hole migration between V''_{Pb} to hole hopping and/or trapping between Mn ions. Indeed, as the Mn concentration increases in the PZT films, the hole concentration rises and $Mn^{2+/3+}$ ions start to serve as hole trapping sites (Figure 4.9b). Consequently, the contribution of V''_{Pb} to the total electronic conduction declines with addition of Mn.

To explore the nature of hopping conduction between Mn sites, the temperature dependent conductivity of 1-4 mol% Mn doped PZT films were fitted using the small

polaron hopping (SPH) model (Figure 4.11) proposed by Emin and Holstein. [49] It has

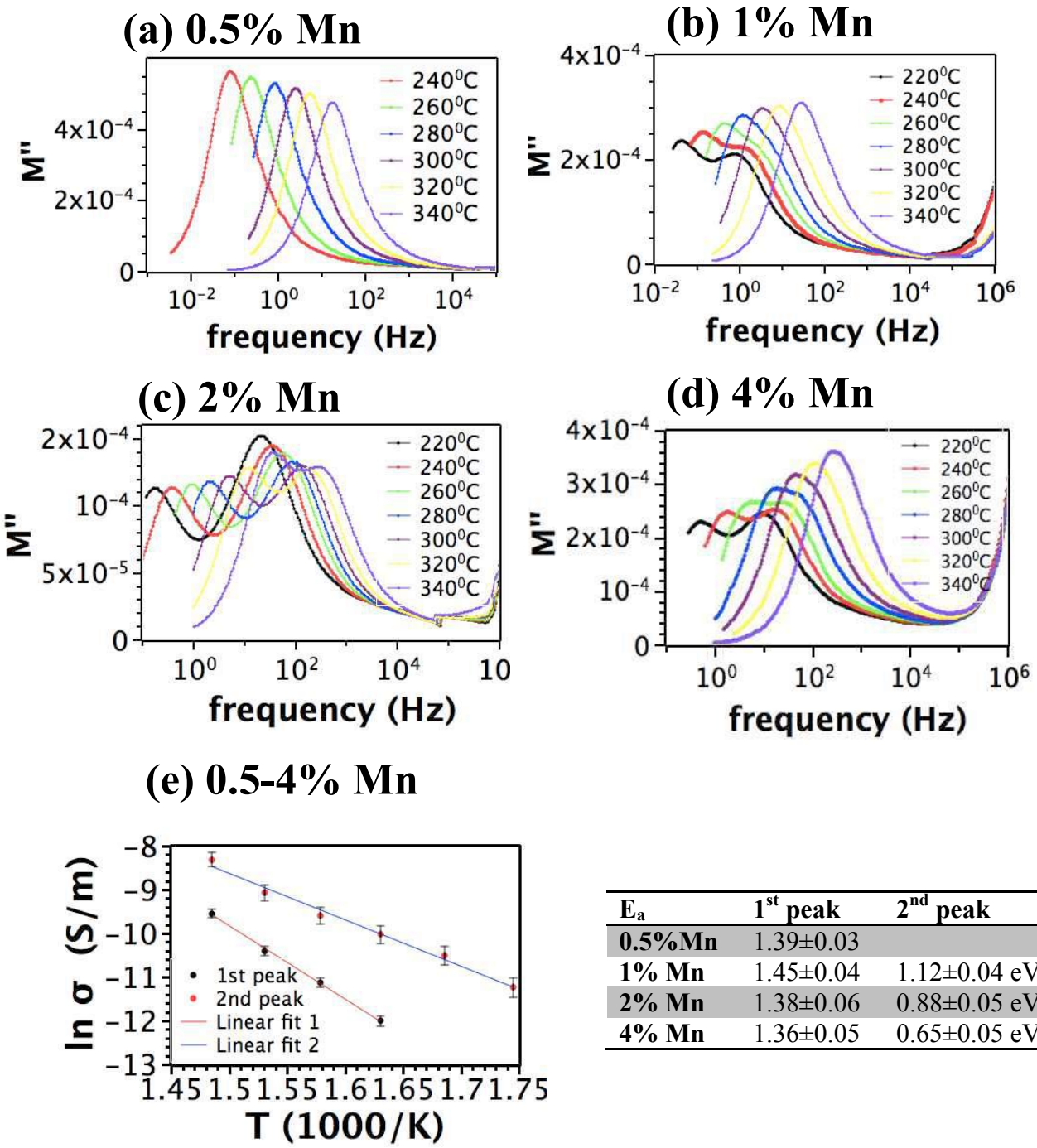

E_a	1st peak	2nd peak
0.5%Mn	1.39±0.03	
1% Mn	1.45±0.04	1.12±0.04 eV
2% Mn	1.38±0.06	0.88±0.05 eV
4% Mn	1.36±0.05	0.65±0.05 eV

Figure 4.10 *Temperature dependence of modulus in (a) 0.5, (b) 1, (c)2, and (d) 4% Mn doped PZT films, (e) Arrhenius plots for conductivity in Mn doped PZT films and corresponding activation energies for low and high frequency peaks*

been found that temperature dependence is consistent with the thermally activated hopping of small polarons, which can be expressed by,[50]

$$\sigma = ne\mu = \frac{\sigma_0}{T}\exp\left(\frac{-E_a}{k_B T}\right), \quad \sigma_{0=} \frac{gNc(1-c)e^2 r^2 \upsilon}{k_B}, \quad r = \left(\frac{1}{N}\right)^{1/3} \qquad \text{Equation 4.15}$$

where k is Boltzmann's constant, σ_o is the pre-exponential factor for small polaron conduction, e is the electronic charge, c is the fraction of sites occupied by polarons, n is the number of charge carriers [n=N•c•(1-c)], N is the density of conducting sites, r is the site-to-site hopping distance, ν is the characteristic vibrational frequency, and E_a is the hopping activation energy. The temperature dependence of conductivity was fitted to the equation for small polaron hopping conduction, where Ln (σ/T) should be proportional to 1/T. It was found that the plot showed good linearity. This suggests that the electrical transport in Mn doped PZT films is dominated by phonon-assisted hole hopping between Mn sites.

Conductivity at any temperature increases with increasing Mn concentration (Figure 4.11a). To establish the origin of this concentration dependence, the change in hopping distance (r) and the density of conducting sites with Mn addition was plotted in Figure 4.11b. The density of conduction sites, which is directly proportional to the Q-DLTS signal, increases by two times as the Mn concentration increased from 1 mol% to 2 mol% (Figure 11b). Given that the density of conducting sites for 1 and 2 mol% Mn doped PZT films are N= $9.7\text{x}10^{17}$ /cm^3 and 2N= $1.98\text{x}10^{18}$ /cm^3 (Q-DLTS results), the hopping distance, which is inversely proportional to the density of conducting sites r = $(N)^{-1/3}$, decreased from r(1mol%Mn)=$(9.7\text{x}10^{17})^{-1/3}$ = 95 Å to r(2mol%Mn) = $(2N)^{-1/3}$ = $0.79(N)^{-1/3}$ = $(1.98\text{x}10^{18})^{-1/3}$= 82 Å for 1 and 2 mol% Mn doped PZT films, respectively. Since c and ν are expected to vary only slightly with Mn doping, the factor responsible for the notable

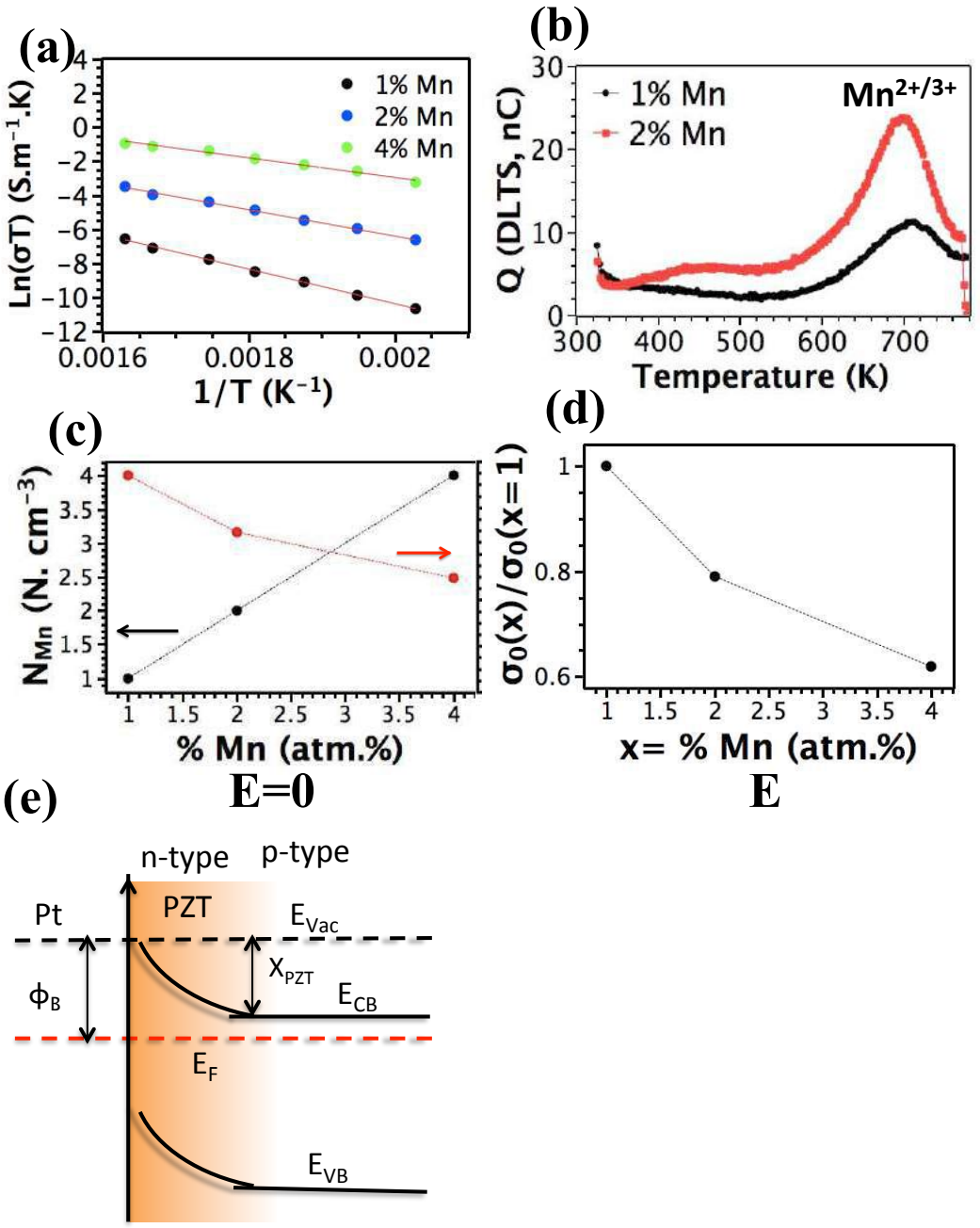

Figure 4.11 (a) *Temperature dependence of conductivity in 1, 2, and 4% Mn doped PZT films, (b) DLTS spectra of 1, and 2% Mn doped PZT films, Variation in (c) hopping distance between Mn sites and (d) pre-exponential factor with Mn doping level, (e) Schematic representation of Mn impurity sites in PZT energy band diagram.*

increase in conductivity with Mn doping is therefore N and r. The drop in hopping distance with Mn doping decreases the pre-exponential factor, σ_0 (Figure 4.11d) and the activation energy, E_a. These two factors enhance the small polaron hopping conduction

between $Mn^{2+/3+}$ and $Mn^{3+/4+}$ sites and result in a significant increase in the electronic conductivity.

The contribution of electronic conduction to the DC resistance degradation of Mn doped PZT films was further investigated using in-situ impedance spectroscopy. The imaginary part of the modulus $M''(f)$ during the degradation of the 0.5 and 4 mol% Mn doped PZT films is shown in Figure 4.12a and b. Only some frequency sweeps are shown for clarity. The pristine state of 0.5 mol% Mn doped PZT is characterized by only one maxima at 28 Hz (hence a homogenous conductivity profile) whereas two distinct maxima at 47.6 and 528 Hz were observed for 4 mol% Mn doped PZT films, indicating the existence of regions with distinct conductivities. A DC voltage of 40 kV/cm was applied at 320°C and continuous impedance measurements were acquired until the degradation process was finished. Both peaks shift to higher frequencies as degradation progresses in 4 mol% Mn doped PZT films; the magnitude of shift with degradation time is more noticeable in the first modulus peak. The bulk conductivity increases three orders of magnitude throughout the film on degradation. After 912s, the first peak started to merge with the second peak and the combined peak narrowed with increasing degradation time. This suggests that the conductivity profile of 4 mol% Mn doped PZT films became more homogenous as degradation progressed.

Similar to 4% Mn doped PZT films, the single modulus peak shifted through higher frequencies with degradation time in 0.5 mol% Mn doped PZT films, indicating a

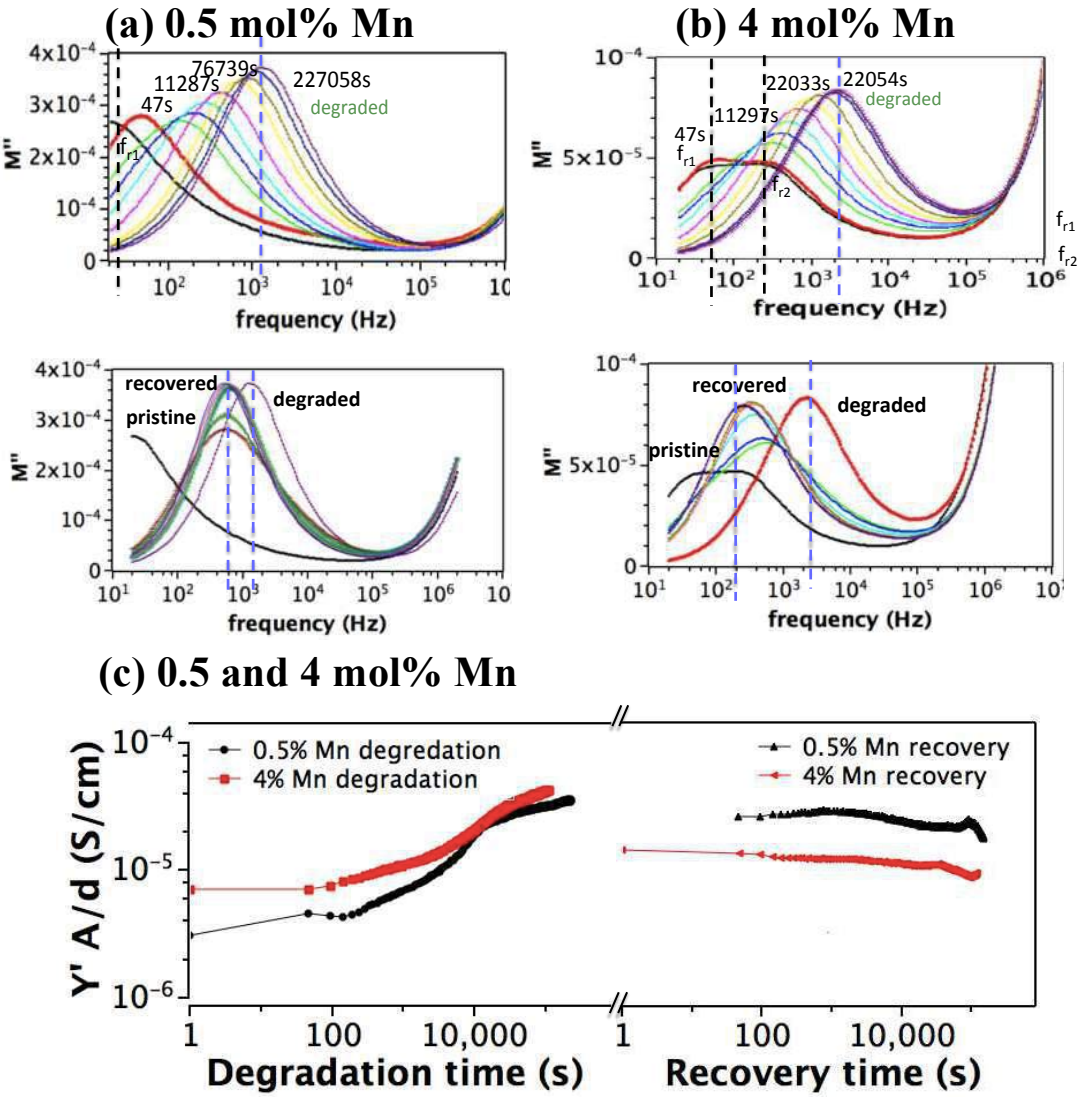

Figure 4.12 *(a) Imaginary modulus plotted as a function of frequency during degradation and recovery of 0.5 and 4 mol% Mn doped PZT films at 320°C, (b) change in admittance of 0.5 and 4 mol% Mn doped PZT films during degradation and recovery.*

gradual increase in the conductivity of the film. For both 0.5 and 4 mol% Mn doped PZT films, the modulus peak stabilized after 22054 s of degradation, indicating degradation reached a stable state.

Subsequent to degradation, the DC voltage was turned off to record the change in modulus during the recovery process. During recovery, the modulus peak decreases in relaxation frequency and increases in the magnitude. However, the modulus peak did not reach its original undegraded position within a recovery time of 77400 s at 320°C for 0.5

mol% Mn doped PZT films. This indicates that the conductivity of recovered state is still higher than that of the pristine sample. This suggests that a slow process like the drift of oxygen vacancies controls both degradation and recovery in 0.5 mol% Mn doped PZT films. For 4 mol% Mn doped PZT films, on the other hand, the recovery rate is much faster compared to 0.5 mol% Mn doped counterparts; an order of magnitude decrease in the conductivity was observed within 40s of recovery. This strongly suggests that the conductivity increase upon degradation is dominated by electronic conduction rather than ionic migration of defects. It is plausible that higher Mn concentrations increase small polaron hopping conduction, leading to a dramatic increase in the contribution of electronic conduction ($\frac{\sigma_{electronic}}{\sigma_{ionic}}$) to the conductivity.

Conclusions 4.4

0.5, 1, 2, and 4 mol% Mn-doped (PMZT) lead zirconate titanate films with a Zr/Ti ratio of 52/48 were deposited on Pt coated Si substrates by the sol-gel method. In the pristine state, the conduction mechanism below 145 kV/cm is dominated by the Poole-Frenkel emission, whereas, at higher electric fields, the conduction is controlled by Schottky emission. The potential barrier height was 1.17±0.04, 1.06±0.05, 0.84±0.03, and 0.72±0.04 eV for 0.5, 1, 2, and 4 mol% Mn doped PZT films. The variation in Schottky barrier height with Mn concentration is attributed to Fermi level pinning by interface states, mostly oxygen vacancies.

After degrading Mn doped PZT films under an electric field of 350 kV/cm at 180°C for 12 h, (1) the width of Poole-Frenkel regime increases, accompanied by a shrinkage in the field range for the Schottky regime; the transition electric field from Poole Frenkel conduction to Schottky emission shifted from 145 to 182 kV/cm after

degradation and (2) no significant change in potential barrier height for injecting electrons from cathode into PZT was observed after degradation; Schottky barriers of 0.84±0.05 and 0.86±0.07 eV were found in pristine and degraded states, respectively. This behavior might originate from the weakening of the electric field near the depletion region due to (1) partial cancellation of the positive space charge (due to accumulation of oxygen vacancies) in the PMZT film by the negative interface charge, which is created via trapped electrons at the Mn sites or/and (2) the shift in the center of charge, associated with Mn sites into the bulk of the film due to the wide distribution of Mn ions throughout the film. In principle, a high concentration of oxygen vacancies, compensated via electrons, should exist near the cathode, which should lower the Schottky barrier. Failure to observe a change in Schottky barrier height upon electrical degradation suggests that enhanced electric field during degradation is suppressed by trapping of electrons and holes via Mn ions. The presence of Mn ions in different valence states allows electron or hole hopping. Since the Mn ions are widely distributed within the film due to their low concentrations, the trapped electrons at Mn sites are also spread out, which prevents accumulation of electronic charges at the cathode/PZT film interface. This improves the resistance degradation behavior and lifetime of Mn doped PZT films.

4.5 References

[1]Polcawich R.G., Scanlon M., Pulskamp J., Clarkson J., Conrad J., Washington D., Piekarz R., Trolier-McKinstry S.E., Dubey M., "Design and fabrication of a lead zirconate titanate (PZT) thin film acoustic sensor," *Integr. Ferroelectr*. 54: 595-606 (2003).

[2]Zhou Q., Lau S., Wu D., and Shung K.K., "Piezoelectric films for high frequency ultrasonic transducers in biomedical applications," *Prog Mater Sci.* 56(2): 139–174 (2011).

[3]Qiu Y., Gigliotti J.V., Wallace M., Griggio F., Demore C.M.E., Cochran S. and Trolier-McKinstry S., "Piezoelectric Micromachined Ultrasound Transducer (PMUT) arrays for integrated sensing, actuation and imaging," *Sensors.* 15: 8020-8041 (2015).

[4]Yeo H.G., Ma X., Rahn C., Trolier-McKinstry S., "Efficient piezoelectric energy harvesters utilizing (001) textured bimorph PZT films on flexible metal foils," *Adv. Funct. Mater.* 26(32): 5940-46 (2016).

[5]Morimoto K., Kanno I., Wasa K., Kotera H., "High-efficiency piezoelectric energy harvesters of *c*-axis-oriented epitaxial PZT films transferred onto stainless steel cantilevers," *Sensors and Actuators A.* 163: 428-32 (2010).

[6]Kueppers H., Leuerer T., Schnakenberg U., Mokwa W., Hoffmann M., Schneller T., Boettger U., Waser R., "PZT thin films for piezoelectric microactuator applications," *Sens. Actuators. A.* 97-98: 680-684 (2002).

[7]Defay E., Millon C., Malhaire C., Barbier D., "PZT thin films integration for the realisation of a high sensitivity pressure microsensor based on a vibrating membrane," *Sensors and Actuators A*. 99: 64-7 (2002).

[8]Kanda T., Morita T., Kurosawa M., Higuchi T., "A rod-shaped vibro touch sensor using PZT thin film," *Proceedings of the IEEE Micro Electro Mechanical Systems (MEMS).* 378–383 (1998).

[9]Raymond M.V., Smyth D.M., "Defects and charge transport in perovskite ferroelectrics," *J. Phys. Chem. Solids*. 57: 1507-11 (1996).

[10]Hayashi K., Ando A., Hamaji Y., Sakabe Y., "Study of the valence state of the manganese ions in $PbTiO_3$ ceramics by means of ESR," *Jpn. J. Appl. Phys.* 37: 5237-40 (1998).

[11] Hennings D., Pomplun H., "Evaluation of lattice site and valence of Mn and Fe in polycrystalline $PbTiO_3$ by electron spin resonance and thermogravimetry," *J. Am. Ceram. Soc.,* 57: 527-30 (1974).

[12]Guiffard B., Boucher E., Eyraud L., Lebrun L., Guyomar D., "Influence of donor co-doping by niobium or fluorine on the conductivity of Mn doped and Mg doped PZT ceramics," *J. Eur. Cer. Soc.* 25: 2487-90 (2005).

[13]Polcawich R.G., Feng C-N, Kurtz S., Perini S., Moses P.J., Trolier-McKinstry S., "AC and DC electrical stress reliability of piezoelectric lead zirconate titanate (PZT) thin films," *Intl. J. Microcircuits Elect Pack*. 23: 85-91 (2000).

[14]Baude P.F., Ye C., and Polla D.L., "Deep level transient spectroscopy characterization of ferroelectric Pb(Zr,Ti)O_3 thin films," *Appl. Phys. Lett.* 64: 2670-72 (1994).

[15]Wang R-V., McIntyre P.C., "^{18}O tracer diffusion in Pb(Zr,Ti)O_3 thin films: A probe of local oxygen vacancy concentration," *J. Appl. Phys.* 97: 023508 (2005).

[16]Al-Shareef H.N., and Dimos D., "Leakage and Reliability Characteristics of Lead Zirconate Titanate Thin-Film Capacitors," *J. Am. Ceram. Soc.,* 80: 3127–32 (1997).

[17]Robertson J., Warren W.L., Tuttle B.A., Dimos D., Smyth D.M., "Shallow Pb^{3+} hole traps in lead zirconate titanate ferroelectrics," *Appl. Phys. Lett.* 63: 1519-21 (1993).

[18]Saremi S., Xu R., Dedon L.R., Mundy J.A., Hsu S-L., Chen Z., Damodaran A.R., Chapman S.P., Evans J.T., and Martin L.W., "Enhanced Electrical Resistivity and Properties via Ion Bombardment of Ferroelectric Thin Films," *Adv. Mater.* 28:10750–56 (2016).

[19]Pelaiz-Barranco A., Guerra JDS., Lopez-Noda R. and Araujo E.B., "Ionized oxygen vacancy related electrical conductivity in $(Pb_{1-x}La_x)(Zr_{0.90}Ti_{0.10})_{1-x/4}O_3$ ceramics," *J. Phys. D: Appl. Phys.* 41: 215503 (2008).

[20]Andrejs L., Fleig J., "Resistance degradation in donor-doped PZT ceramic stacks with Ag/Pd electrodes: I. Phenomenology of processes," *J. Eur. Ceram. Soc.* 33: 779-94 (2013).

[21]Nagaraj B., Aggarwal S., Song T.K., Sawhney T., and Ramesh R., "Leakage current mechanisms in lead-based thin-film ferroelectric capacitors," *Phys. Rev. B*. 59: 16022-27 (1999).

[22]Zhang T-F., Tang X-G., Liu Q-X., Jiang Y-P., Huang X-X., "Oxygen-vacancy-related high temperature dielectric relaxation in $(Pb_{1-x}Ba_x)ZrO_3$ ceramics," *J. Am. Ceram. Soc*. 98: 551-58 (2015).

[23]Wu X., Liu L., Li X., Zhang Q., Ren B., Lin D., Zhao X., Luo H., Huang Y., "Effect of annealing on defect and electrical properties of Mn doped $Pb(Mg_{1/3}Nb_{2/3})O_3$-0.28$PbTiO_3$ single crystals," *J. Cryst. Growth*. 318: 865–69 (2011).

[24]Zhao S., Zhang S.J., Liu W., Donnelly N.J., Xu Z. and Randall C.A., "Time dependent dc resistance degradation in lead-based perovskites: $0.7Pb(Mg_{1/3}Nb_{2/3})O_3 - 0.3PbTiO_3$," *J. Appl. Phys.* 105: 053705-1-7 (2009).

[25]Slouka C., Kainz T., Navickas E., Walch G., Hutter H., Reichmann K., and Fleig J., "The effect of acceptor and donor doping on oxygen vacancy concentrations in lead zirconate titanate (PZT)," *Materials*. 9: 945-967 (2016).

[26]Ossmer H., Slouka C., Andrejs L., Blaha P., Friedbacher G., Fleig J., "Electrocoloration of donor-doped lead zirconate titanate under DC field stress," *Solid State Ionics.* 281: 49–59 (2015).

[27]Bouyssou E., Leduc P., Guégan G., and Jérisian R., "Leakage current conduction in IrO_2/PZT/Pt structures," *J. Phys. Conf. Ser*. 10: 317-20 (2005).

[28]Holzlechner G., Kastner D., Slouka C., Hutter H., Fleig J., "Oxygen vacancy redistribution in $PbZr_xTi_{1-x}O_3$ (PZT) under the influence of an electric field," *Solid State Ionics*. 262: 625–29 (2014).

[29]Yoon S-H, Randall C.A., and Hur K-H., "Difference between resistance degradation of fixed valence acceptor (Mg) and variable valence acceptor (Mn)-doped $BaTiO_3$ ceramics," *J. Appl. Phys.* 108, 064101-1-9 (2010).

[30]Raj P.M., Xiang S., Kumar M., Abothu I.R., Hwang J-H. Liu Y., Yamamoto H., Tummala R., "Leakage current suppression in solution-deposited barium titanate films on copper foils," *J Mater Sci: Mater Electron*. 23: 901–908 (2012).

[31]Mori T. and Kakegawa K., "Improved reliability in thin-film capacitors fabricated with Mn-doped $Pb(Zr,Ti)O_3$ annealed at low temperatures," *Jpn. J. Appl. Phys.* 45: 7270-4 (2006).

[32]Yan Y., Cho K-H., and Priya S., "Piezoelectric properties and temperature stability of Mn-doped $Pb(Mg_{1/3}Nb_{2/3})$-$PbZrO_3$-$PbTiO_3$ textured ceramics," *Appl. Phys. Lett.*, 100, 132908 (2012).

[33]Akkopru-Akgun B., Zhu W., Lanagan M.T., Trolier-McKinstry S., "The effect of imprint on remanent piezoelectric properties and ferroelectric aging of Mn or Nb doped $PbZr_{0.52}Ti_{0.48}O_3$ thin films," *J. Am. Soc.* article in press, DOI: 10.1111/jace.16367 (2019).

[34]Prokopowicz T.I. and Vaskas A.R., "Research and development intrinsic reliability subminiature ceramic capacitors," Final Report Nos. ECOM-90705-F and NTIS AD-864068 (1969).

[35]Lang D.V., "Deep-level transient spectroscopy: A new method to characterize traps in semiconductors," *J. Appl. Phys.,* 45, 3023-32 (1974).

[36]Ma B., Narayanan M., Balachandran U.B., "Dielectric strength and reliability of ferroelectric PLZT films deposited on nickel substrates," *Mater. Lett.* 63: 1353–56 (2009).

[37]Akkopru-Akgun B., Marincel D., Bayer T., Tsuji K., Randall C., Lanagan M.T., Trolier-McKinstry S., "Thermally stimulated depolarization current measurements on degraded lead zirconate titanate films to be submitted to *Appl. Phys. Lett*.

[38]Akkopru-Akgun B., Bayer T., Tsuji K., Randall C., Lanagan M.T., Trolier-McKinstry S., "Thermally stimulated depolarization current measurements on degraded lead zirconate titanate films," to be submitted to *Adv. Elect. Mater*.

[39]Eichel R-A., "Structural and dynamic properties of oxygen vacancies in perovskite oxides--analysis of defect chemistry by modern multi-frequency and pulsed EPR techniques," *Phys. Chem. Chem. Phys.,* 13: 368-84 (2011).

[40]Scott J. F., Watanabe K., Hartmann A. J. and Lamb R. N., "Device models for PZT/PT, BST/PT, SBT/PT, and SBT/BI ferroelectric memories," *Ferroelectrics,* 225: 83-90 (1999).

[41]Klein A., "Interface properties of dielectric oxides*," J. Am. Ceram. Soc.,* 99: 369–387 (2016).

[42]Takatani S., Kushida-Abdelghafar K., Miki H., "Effect of H_2 annealing on a $Pb/PbZr_xTi_{1-x}O_3$ interface studied by x-ray photoelectron spectroscopy," *Jpn. J. Appl. Phys.,* 36: 435-38 (1997).

[43]Jaffe B., Cook W.R., and Jaffe H., Piezoelectric Ceramics, Academic, London (1971).

[44]Rhoderick E.H. and Williams R.H., Metal-Semiconductor Contacts, Clarendon, New York (1988).

[45]Sze S.M., Physics of Semiconductor Devices, 2nd ed., Wiley, New York (1981).

[46]Waser R.M., "Dielectric analysis of integrated ceramic thin film capacitors," *Integr. Ferroelectr*., 15: 39-51 (1997).

[47]Wechsler B.A., and Klein M.B., "Thermodynamic point defect model of barium titanate and application to the photorefractive effect," *J. Opt. Soc. Am. B- Optical Phys*, 5: 1711–23 (1988).

[48]Dih J. and Fulrath R.M., "Electrical conductivity in lead zirconate-titanate ceramics," *J. Am. Ceram. Soc.* 61: 448-51 (1978).

[49]Emin D., Holstein T., "Studies of small-polaron motion IV. Adiabatic theory of the Hall effect*," Annals of Physics*. 53: 439-520 (1969).

[50]Samara G.A., and Emin D., "Pressure and temperature dependences of the electronic conductivity of boron carbides," *Phys. Rev. B.* 2315-18 (1985).

Chapter 5

Thermally Stimulated Depolarization Current Measurements on Degraded Lead Zirconate Titanate Films

5.1 Introduction

Over the last few decades, ferroelectric thin films have been utilized in a variety of microelectromechanical (MEMS) devices, including adjustable optics,[1] ink jet printers,[2] ultrasound transducers,[3] resonators,[4] and energy harvesters.[5] MEMS are often driven at significantly higher electric fields than bulk piezoelectrics; therefore it is important to develop ferroelectric thin films which can operate under high electric fields. However, the use of high field operation imposes strict constraints on the DC resistance degradation in order to achieve reliable ferroelectric thin films with long lifetimes.

DC resistance degradation has been comprehensively studied in alkaline earth titanate perovskites such as acceptor doped $SrTiO_3$ and $BaTiO_3$. It is generally recognized that electromigration of oxygen vacancies under a DC bias field toward the cathodic region underpins electrical degradation in these materials. In $SrTiO_3$ and $BaTiO_3$, the primary source of both oxygen vacancies and holes is acceptor ions. To maintain electroneutrality, the concentration of electrons increases in the cathode region during degradation, while the hole concentration rises in the oxygen vacancy-depleted anodic region. As a result, the anodic region becomes a hole conductor, whereas in the cathodic region electron conductivity is dominant; in the titanates, the excess electrons can be trapped by Ti^{4+} to form Ti^{3+}.[7]

A comprehensive study on the evolution of defect distributions of PZT materials is needed. For PZT films, the high PbO volatility during crystallization leads to the

formation of oxygen vacancies and holes.[7-8] The situation becomes more complex by the hybridization of the lone electron pair in Pb^{2+} and also by the variation in oxidation states upon thermal treatment.[5] For example, the Pb^{2+} site can act as a shallow hole trap (to form Pb^{3+}). A greater knowledge of the behavior of mobile point defects is essential to better understand DC resistance degradation in PZT thin films. In practice, experiments that directly probe point defects in thin films are difficult to perform and only a few studies link the dominant charge transport mechanisms to the defect-chemistry of PZT films.[6-14]

In this work, thermally stimulated depolarization current measurements were employed to probe the defects that lead to electrical degradation in PZT films. Thermally stimulated depolarization current (TSDC) measurements have been widely utilized to study defects in semiconductors and organic materials. The nature and concentration of defects such as dipoles, trap charges, and mobile ions, can be determined via TSDC analysis. It also provides information on the activation energies and the concentration of those defects.[15-17]

TSDC analysis of ferroelectrics is complicated by the existence of background currents arising from the pyroelectric effect. Nonetheless, Wu and Sayer were able to explore the link between aging and the TSDC peak associated with oxygen vacancies in piezoelectric thin films by minimizing pyroelectric contributions to the signal.[18] Okino et al. used thermally stimulated current, reporting that polarization fatigue was caused by domain pinning from trapped charges. However, the physical origin of the trapped charges was not identified.[19]

The main objective of this study is to explore the changes in defect concentrations and defect distributions upon electrical degradation in undoped, donor (Nb) and acceptor (Mn) doped PZT films using TSDC. In particular, the manner in which defect type and concentration affect the electrical conduction and degradation phenomena in PZT films was investigated. The origins of dielectric relaxations in undoped, Mn and Nb doped PZT films were explored and linked to the time-dependent leakage current associated with oxygen vacancy migration upon degradation. The migration of oxygen vacancies under a dc bias is discussed and related to charge transport mechanisms in PZT films. Additionally, the electron polaron hopping between Ti^{3+} and Ti^{4+} was proved by complementary findings of TSDC and electron energy loss spectroscopy (EELS) analyses.

5.2. Experimental Plan

Preparation of undoped, Mn and Nb doped PZT thin films by sol-gel method

Undoped, acceptor-doped (Mn), and donor-doped (Nb) lead zirconate titanate (PZT) thin films with dopant concentrations varying from 0.5 to 4 mol% were grown on commercial Pt/Ti/SiO_2/Si substrates (Nova Electronic Materials, Flower Mound, TX) via chemical solution deposition. Solutions with a Zr/Ti ratio of 52/48 were prepared using 10 mol% Pb excess to compensate for lead loss during heat treatment. The preparation of solutions is similar to that described elsewhere.[20-21] The Mn and Nb doping concentration in solution was calculated presuming B site occupancy to reach final film compositions of: $PbZr_{0.52(1-x)}Ti_{0.48(1-x)}Mn_xO_{3-\delta}$, where x = 0.005–0.04 and $Pb_{\left(1-\frac{1}{2}x\right)}Zr_{0.52(1-x)}Ti_{0.48(1-x)}Nb_xO_3$, where x = 0.005–0.04, respectively.

To grow the film, PZT solution was spin coated on silicon substrates at 1500 rpm

for 30s. Then, each layer was exposed to two pyrolysis treatments for 3 min each at 250 and 450°C, respectively. The film was then crystallized at 700°C for 60 s by rapid thermal annealing (RTA) under O_2. The coating and drying process, as well as rapid thermal treatments were repeated until a desired thickness of 400 nm was reached. Finally, a single PbO layer was coated onto the surface of PZT films and annealed at 700°C in air, to remove surface pyrochlore. Remaining PbO was then eliminated by immersing the sample in a 4M acetic acid solution for 60 s.

Following crystallization, undoped PZT films were exposed to a second annealing treatment at 670°C under varying PbO partial pressures for 1 h. In this study, the range of tetraethyl lead partial pressures between 3.53 10^{-5} Torr and 2.85 10^{-4} Torr that promotes single phase PZT was used to control the lead nonstoichiometry in the perovskite phase.[22]

5.3. Materials Characterization

Characterization techniques used to explore structural and electrical properties of PZT films were described in Chapter 3.

5.3.1 TSDC measurements of PZT films

Thermally stimulated depolarization current (TSDC) differentiates relaxation currents originating from trapped charges, space charge, and defect dipoles based on their relaxation kinetics. The test conditions for the TSDC measurements in this work are shown in Figure 5.1(a). PZT thin films were wire bonded to two Pt pieces to facilitate electrical contacts. First, the sample was heated to a poling temperature (T_p) and then degraded under DC field to orient or move defects. After poling the sample for 12 h at 180°C under an electric field ranging from 250 to 400 kV/cm, the sample was cooled to room temperature (T_0) where the defect dipoles, space charges, and trapped charges were

frozen into the poled state. Subsequently, the sample was shorted and the electric field removed. Then, the sample was heated at a constant rate of 4, 6, 8, or 10 °C/min and the relaxation current from the depolarization of relaxing defects was recorded at temperatures ranging from 25 to 300°C with a HP 4140b PA meter. Electrical connections from the sample to PA meter were achieved by using BNC and triaxial cables in order to minimize the leakage current arising from the cable itself. The effect of poling field, heating rate, dopant type and concentration, and the annealing atmosphere on the depolarization current and associated trapped charges was investigated.

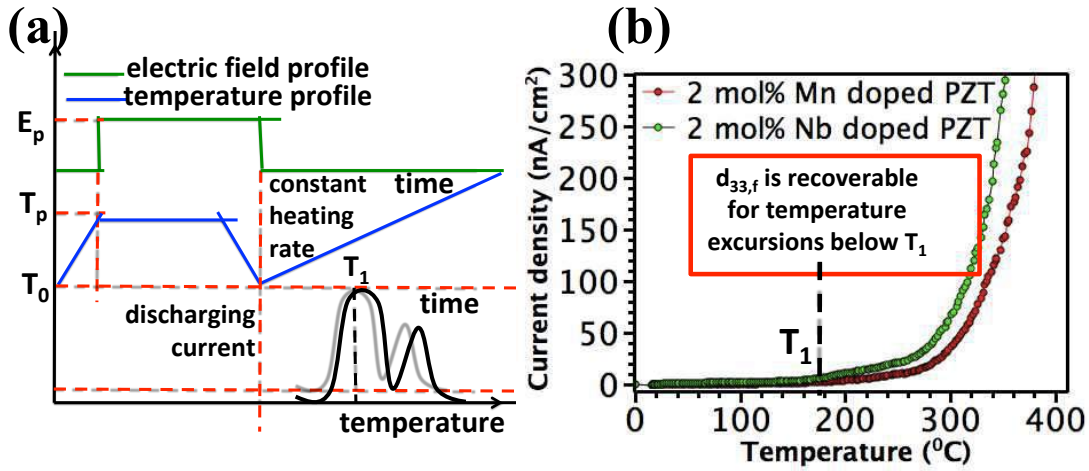

Figure 5.1 (a*)* TSDC measurement process, and (b**)** *The current response to increasing temperature in 2% Mn and 2% Nb doped PZT films.*

TSDC can be mathematically described for a single relaxation using the equation[23]

$$I(T) = n_0\, s\, exp\left(\frac{-E_A}{k_b T}\right) * exp\left[-s/\beta \int_{T_0}^{T}\left(\frac{-E_A}{k_b T^I}\right) dT^I\right] \qquad \text{Equation 5.1}$$

where E_a is the activation energy, T_m is the temperature corresponding to the peak maximum, β is the heating rate, n_0 is the concentration of dipoles and s is a geometrical factor relying on the dipole orientation. It is well known that the position and shape of TSDC peaks are affected by the heating rate. The TSDC peak becomes narrower and is

shifted to higher temperatures as the heating rate increases. High heating rates enhance the dipolar interaction process upon relaxation, leading to higher depolarization currents.[24] The concentration of dipoles, n_0, can also be evaluated from Equation 5.1, because the area under the dipolar peak is equal to the equilibrium polarization, P_e.

Before analyzing each peak to derive the activation energy and concentration of defects, the magnitude of the TSDC signal arising from depolarization of the ferroelectric polarization was investigated by assessing the piezoelectric response via Double Beam Laser Interferometer (DBLI). An equivalent sample was heated to a temperature just below 200°C, where the first TSDC peak emerged. It was found that for temperatures up to T_1, the piezoelectric $d_{33,f}$ coefficient recovered its original value on cooling to room temperature. (Figure 1b) Therefore, up to this temperature reorientation of the ferroelectric polarization is not expected to contribute to the measured TSDC signal in this temperature range.

5.4 Results and Discussion

5.4.1 Structural properties of PZT films

The surface morphology and structure of PZT films after annealing at 670°C under different PbO partial pressures were studied by GIXRD and FESEM. The GIXRD studies (Figure 5.2) reveal that undoped PZT films are approximately randomly oriented and have the perovskite structure. No peaks corresponding to secondary phases such as excess PbO or pyrochlore were observed in the XRD patterns. Moreover, the intensity and positions of XRD peaks are the same for all PbO contents, indicating that the crystallinity was governed by the initial crystallization step.

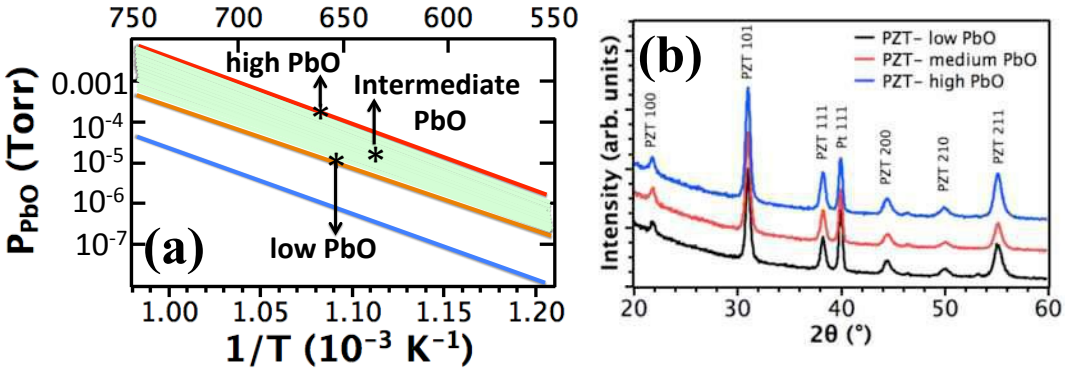

Figure 5.2 *The phase stability diagram of PbO, $PbTiO_3$, and $PbZrO_3$ at distinct temperatures. The red, orange, and blue lines denote the required equilibrium PbO partial pressure for $PbO(g) \rightarrow PbO(s)$, $PbZrO_3 \rightarrow PbO(g) + ZrO_2$, and $PbTiO_3 \rightarrow PbO(g) + TiO_2$, respectively. The shaded region represents the required range for PZT perovskite equilibrium,*[22, 25] *(b) XRD diffraction patterns of approximately randomly oriented PZT films indicating phase pure perovskite for (a) low, medium, and high PbO partial pressure.*

Figure 5.3 shows the FESEM micrographs of undoped PZT films annealed at different PbO activities. As shown in Figure 5.3, the deposited PZT films were smooth and homogeneous; no crack formation was observed. SEM results confirmed that grain size for undoped PZT films with different PbO content is similar and varies between 30-150 nm. This indicates that grain size remains relatively constant while annealing in a PbO-rich atmosphere.

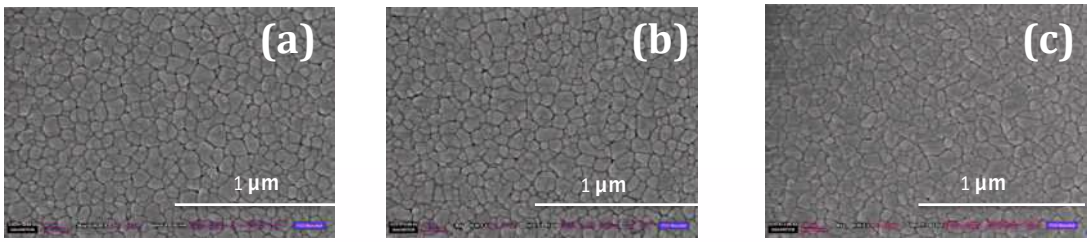

Figure 5.3 *Top surface SEM images of PZT films annealed at distinct PbO partial pressures: (a) low PbO partial pressure (yellow line), intermediate PbO partial pressure, and (red line) high PbO partial pressure. FESEM images were taken after patterning of Pt top electrodes*

As was the case for the undoped PZT films, no evidence for PbO or pyrochlore second phases was found by either XRD or FESEM for Mn or Nb doped PZT films. The deposited PZT films were smooth and homogeneous; no crack formation was observed.

FESEM results confirmed that grain size in both Mn and Nb doped PZT films is similar and varies between 40-160 nm. The details of structural characterization results of Mn and Nb doped PZT films can be found elsewhere.[21]

5.4.2 Thermally Stimulated Depolarization Current measurement results

Thermally stimulated depolarization current measurements were carried out on degraded Nb and Mn doped and undoped PZT films annealed under varying PbO partial pressures to probe electronic and ionic defects resulting in electrical degradation. Figure 5.4 shows the TSDC spectra obtained from degraded Mn and Nb doped PZT films that were polarized under electrical fields ranging from E_p=200 to 400 kV/cm at T_p=180°C for 12 h, measured with a heating rate of β=8°C/min.

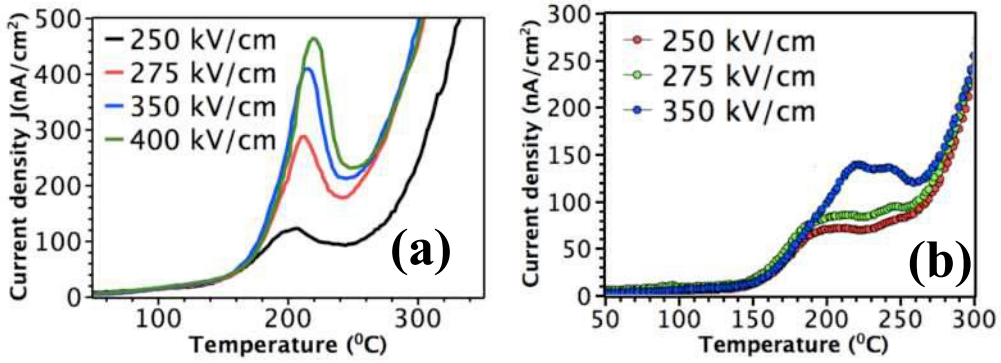

Figure 5.4 *Evolution of TSDC peaks with increasing polarization electrical field in (a) 2 mol% Mn, (b) 2mol% Nb doped PZT films using a ramp rate of 8°C/min. Samples were poled under a dc bias of 250-400 kV/cm at a temperature of 180°C for 12 h.*

The physical origin of the thermally stimulated current was explored by studying the dependence of T_m (Figure 5.4) on poling field. For a constant heating rate, the temperature of the current peak shifts in a well-defined manner with increasing polarization electric field; T_m can (1) shift to lower temperatures when the relaxation current is associated with trapped charges, (2) shift to higher temperatures when the physical origin of TSDC current is space charge, and (3) remain fixed when the TSDC

current arises from defect dipoles. As shown in Figure 5.4a, the TSDC data for Mn doped PZT films shows a single peak, with T_m from 204 to 220°C, for different polarization fields. It is readily seen in Figure 5.4a that T_m shifted to higher temperatures with increasing polarization electrical fields, suggesting that the origin of the TSDC depolarization peak is associated with a space charge, probably due to the migration of oxygen vacancies. This, coupled with the fact that the magnitude of this peak increases with Mn concentration, demonstrates that this peak is also not due to reorientation of the ferroelectric polarization.

Three distinct methods were used to determine the activation of the TSDC peak. In the first approach, the initial rise model, the first exponential term of equation (1) controls the temperature rise of the initial current. Thus, ln J_D versus 1/T, gives rise to a straight line, and the activation energy was estimated from the slope of this line as 0.65±0.04 eV (Figure 5.5a). In the second technique, the heating rate dependence of the TSDC peak position was used to estimate the activation energy of the TSDC relaxation current. The peak position, T=T_{max}, is related to the heating rate β through an Arrhenius equation.[26]

$$\ln \beta = \frac{-E_a}{k_b}\left(\frac{1}{T_{max}}\right) + const \qquad \text{Equation 5.2}$$

$$ln\left(\frac{{T_{max}}^2}{\beta}\right) = \frac{E_a}{k_b T_{max}} + ln\left(\frac{\tau_0 E_a}{k_b}\right) \qquad \text{Equation 5.3}$$

here k_b is Boltzmann's constant, E_a is the activation energy correlated with the TSDC peak. An activation energy of = 0.58±0.02 eV was derived from the plot of $ln\left(\frac{{T_{max}}^2}{\beta}\right)$ as a function of $1/T_{max}$ (Figure 5.5b).

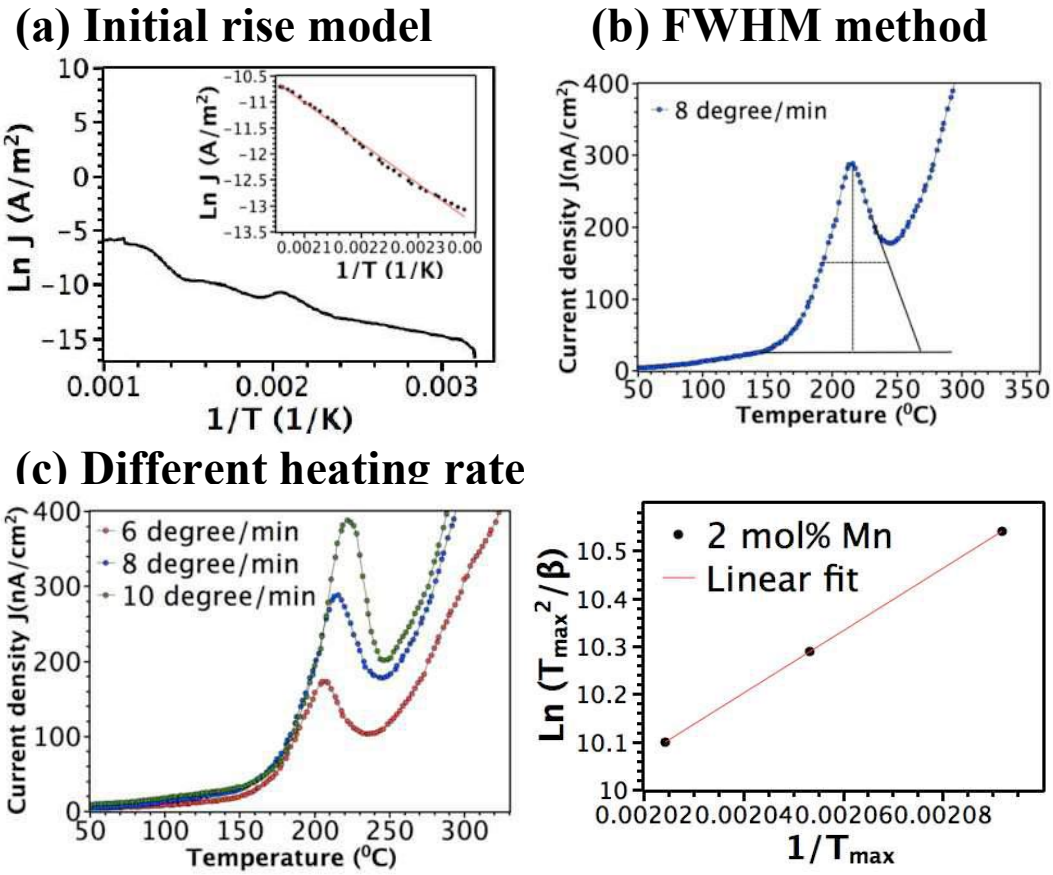

Figure 5.5 *Estimation of activation energies for TSDC peaks arising from 2 mol% Mn doped PZT films using three distinct methods: (a) initial rise model, (b) FWHM method, and (c) different heating rate (6-10°C/min). The films were degraded under an electric field of 275 kV/cm at 180°C for 12 h*

In the third method, the FWHM of TSDC peak was used to determine the activation energy (Figure 5.5c) via Equation 5.3:

$$W = 2.30\, kT_m^2/\Delta\, T_{1/2} \qquad \text{Equation 5.3}$$

where T_m is the temperature corresponding to the peak maximum, $\Delta\, T_{1/2}$ is the FWHM of TSDC peak. It should be noted that all the expressions in Equation 5.3 relate to a single Debye process where *W* has a unique value. An activation energy of 0.73±0.03 eV was found. Thus, the estimated activation energies from all three methods are in good agreement with that for the migration of oxygen vacancies as studied by Wang and

colleagues. (0.58 eV)[10]

In contrast to Mn doped PZT films, TSDC results of degraded Nb doped PZT films indicate two distinct relaxation current peaks with maxima around 220°C and 280°C. The two TSDC peaks in Nb doped PZT films exhibit distinctly different bias dependence behaviors. T_m of the low temperature peak shifts to higher temperature with increasing poling field, which is characteristic of space charge polarization. The position of the high temperature peak shifts slightly to lower temperatures with increasing poling field. A linear relation was found between the peak temperature T_m and the square root of

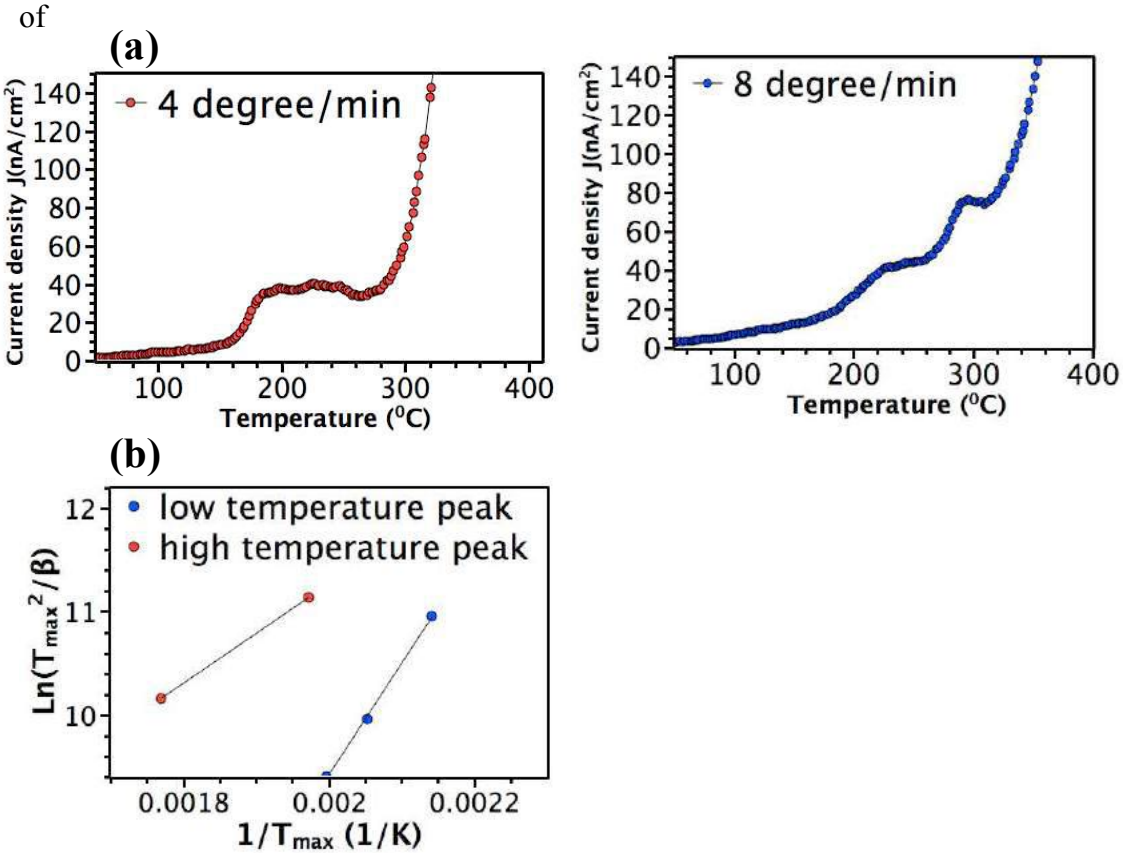

Figure 5.6 *(a) Thermally Stimulated Depolarization Current data of 2% Nb doped PZT films for different heating rates (4 and 8 degree/min), (b) Estimation of activation energies for the low and high temperature TSDC peaks using heating rate method. The films were degraded at 180°C under an electric field of 350 kV/cm for 12h*

the applied field, $E^{1/2}$, indicating relaxation of trapped charges. By using the heating rate method, the activation energies of low and high temperature peaks were estimated to be 0.61±0.06 and 0.18±0.05 eV, respectively. These values are similar to those previously reported for the diffusion of mobile oxygen vacancies and electron hopping between Ti^{3+} and Ti^{4+} in the perovskite structure.[15-16]

TSDC was also carried out on undoped PZT films annealed at varying PbO pressures. Figure 5.7 indicates TSDC data for undoped PZT films with low, medium, and high PbO contents. The magnitude of the TSDC peak attributed to relaxation of mobile oxygen vacancies diminishes gradually with increasing PbO content in PZT films, indicating that the oxygen vacancy concentration is lowest for films with the highest lead content. It is expected that annealing PZT films at high PbO activities minimizes PbO evaporation and therefore decreases the partial Schottky defect concentration in PZT films when lead vacancies are compensated by oxygen vacancies and holes.[11-14, 27-28]

Moreover, the high temperature TSDC peak at 280°C, attributed to electron hopping between Ti^{4+} and Ti^{3+} sites, was only observed in PZT films with low PbO contents. It is believed that a high concentration of oxygen vacancies accumulates near the cathode of PZT films with low PbO contents during electrical degradation. These vacancies are charge compensated by electrons trapped on Ti sites. It is possible that the inability to detect this signal in undoped PZT films with high PbO contents was due to a low concentration of oxygen vacancies, and hence a reduction in both the number of trapped electrons and the probability of electron hopping between Ti^{3+} and Ti^{4+}.

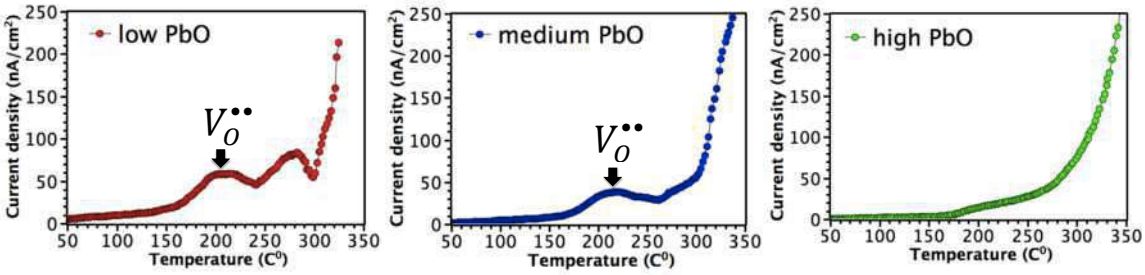

Figure 5.7 *TSDC spectra in PZT films annealed under low, medium, and high PbO activities. TSDC data were attained after degrading the films under an electric field of 275 kV/cm at 180°C for 12h. A 6 degree/min heating rate was used to attain TSDC peaks*

After identifying relaxation current peaks for undoped and doped PZT films, the TSDC peak associated with relaxation of mobile oxygen vacancies was further studied in Mn doped and Nb doped PZT films as a function of dopant concentration, as presented in Figure 5.7. The total amount of charge that relaxes due to diffusion of ions can be expressed as:[15]

$$Q_{TSDC} \approx 2avNqt_p \exp\left(-\frac{H}{kT}\right) \sinh\left(\frac{qaE_p}{2kT_p}\right) = Q_0 \sinh\left(\frac{qaE_p}{2kT_p}\right) \qquad \text{Equation 5.4}$$

where N is the density of diffusing ions, ν is ion jump frequency, k is the Boltzmann constant, q is the ionic charge, *a* is the ionic hopping distance between potential wells of depth H, T_p, E_p and t_p are the polarization temperature, electric field, and time, respectively.

The concentration of oxygen vacancies that undergo long-range migration during degradation at 180ºC under an electric field of 350 kV/cm for 12h was calculated by integrating the depolarization current peaks (Table 5.1). The magnitude of the depolarization current peak increases with increasing Mn concentration, suggesting (1) that any defect dipoles that might present, such as $(Mn_{Ti}'' - V_O^{\bullet\bullet})^X$ and/or $(Mn_{Ti}' - V_O^{\bullet\bullet})'$, dissociate during electrical degradation; mobile oxygen vacancies give rise to

increase of the ionic space charge peak (2) the concentration of mobile oxygen vacancies increases with increasing Mn concentration. When Mn is incorporated into PZT, it occupies the B-site (Ti or Zr) of the perovskite lattice and ionically compensated by oxygen vacancies. Thus, an increase in the magnitude of ionic space charge peak with increasing acceptor ion concentration is reasonable.

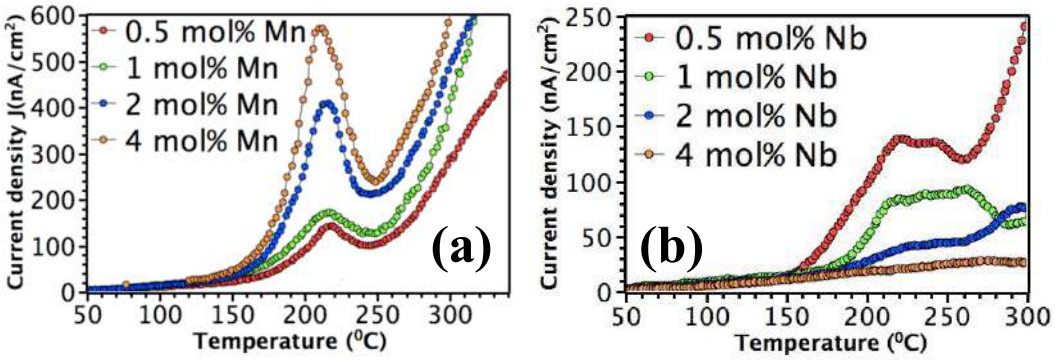

Figure 5.8 *Evolution of TSDC peaks in degraded PZT films with increasing (a) acceptor (Mn) dopant concentration, and (b donor (Nb) dopant concentration. The films were degraded at 180°C under an electric field of 350 kV/cm for 12h. TSDC data was obtained using a ramp rate of 8 °C/min.*

In contrast, the concentration of mobile oxygen vacancies decreases with increasing Nb concentration (Table 5.1). It is reasonable that the number of mobile oxygen vacancies diminishes as the concentration of Nb in PZT films rises, as Nb is a donor. The source of the remaining oxygen vacancies in Nb doped PZT films is likely to be the loss of the PbO during high temperature treatment. This creates lead and oxygen vacancy partial Schottky defect pairs.

$$Pb_{Pb}^{X} + O_{O}^{X} \rightarrow V_{Pb}'' + V_{O}^{\bullet\bullet} + PbO(g) \qquad \text{Equation 5.5}$$

$$2[V_{Pb}''] + [e'] = 2[V_{O}^{\bullet\bullet}] + [h^{\bullet}] \qquad \text{Equation 5.6}$$

The maximum temperature, T_{max}, of the TSDC peaks for relaxation of oxygen vacancies is higher for Nb doped PZT films than their Mn doped counterparts (Figure

5.8). T_{max} is closely related to the characteristic relaxation time for polarized charges and can be described as:[29]

$$T_{max} = \left[\frac{E_a}{k}\beta\tau_0 exp\left(\frac{E_a}{kT_{max}}\right)\right]^{1/2} \quad \text{Equation 5.7}$$

where E_a is activation energy, β is heating rate, k is Boltzmann's constant, and T_{max} is the relaxation peak temperature. As can be seen in Table 1, the characteristic time, $\tau_0 exp\left(\frac{E_a}{kT_{max}}\right)$ for relaxation of the migrated oxygen vacancies decreases with increasing Mn concentration or decreasing Nb concentration. Long-range migration of oxygen vacancies upon electrical degradation results in depletion of oxygen vacancies in the anodic region and accumulation of oxygen vacancies in the cathodic region. When the average oxygen vacancy concentration is high, as in Mn doped PZT films, even a small degree of electrical degradation results in a measurable depolarization current density; high oxygen vacancy concentrations are correlated with shorter relaxation times. In Nb doped PZT films with lower oxygen vacancy concentrations, however, longer-relaxation time and/or stronger

Table 5.1 *The concentration of polarized oxygen vacancies, diffusion coefficient, relaxation time, and T_{max} of TSDC results in Nb and Mn doped PZT films.*

	N (cm^{-3})	T_m (K)	τ_0 (10^{-4}s)	D_v (cm^2/s)
0.5% Nb	2.08±0.05 x10^{19}	498	8.11±0.09	8.77± 0.04 x10^{-15}
1% Nb	1.1±0.04 x10^{19}	502	8.32±0.09	8.63±0.05 x10^{-15}
2% Nb	4.8±0.03 x10^{18}	507	8.61±0.05	8.45±0.04 x10^{-15}
4% Nb	1.54±0.04 x10^{18}	514	9.46±0.07	8.24±0.06 x10^{-15}
0.5% Mn	3.1±0.03 x10^{19}	491	4.94±0.05	9.01±0.05 x10^{-15}
1% Mn	5.8±0.05 x10^{19}	488	4.51±0.06	9.13±0.04 x10^{-15}
2% Mn	1.4±0.03 x10^{20}	486	4.20±0.09	9.22±0.07 x10^{-15}
4% Mn	2.7±0.05 x10^{20}	483	3.84±0.06	9.32±0.03 x10^{-15}

polarization conditions are required to achieve the same magnitude of depolarization current density. The diffusion coefficient for long-range migration of oxygen vacancies

was calculated using the Nernst-Einstein equation assuming that the velocity is given by L/τ, where L is the film thickness and τ is time that is required for oxygen vacancy migration across the sample thickness of L.

$$D_V = \frac{kT}{2e} u_V = \frac{kTL}{2e\tau E},\ u_V = \frac{v}{E} \qquad \text{Equation 5.8}$$

where k is the Boltzmann constant, v and u_V are the velocity and the mobility of mobile ions, e is the elementary charge, T is the temperature, and E is the electric field. The estimated diffusion coefficients for Nb and Mn doped PZT films shown in Table 5.1 are in the range of 8-9 x 10^{-15} cm^2/s. This is two orders of magnitude smaller than the reported bulk diffusion coefficient value of 10^{-13} cm^2/s for oxygen vacancy migration in PZT ceramics at 580°C.[10] Based on the assumption that the activation energies for oxygen vacancy migration in these two systems are similar, a diffusion coefficient value of $7.2x10^{-15}$ cm^2/s was estimated at 180°C for PZT ceramics, which is very close to the diffusion coefficient measured in this work for PZT films.

Since more oxygen vacancies accumulate near the cathode upon electrical degradation in Mn doped PZT films compared to Nb doped samples, a higher concentration of compensating electrons is expected in Mn doped PZT films. In principle, each oxygen vacancy is compensated by two electrons ($n \sim 2[V_O^{\bullet\bullet}]$), which could be trapped by the Ti^{4+} to create Ti^{3+}, Subsequent electron polaron hopping between the Ti sites in the cathodic regions was shown by Liu et al. in Fe doped $SrTiO_3$ single crystals.[15] However, in this study, $Ti^{3+}$was only observed near the cathode of degraded Nb doped PZT films. The TSDC data of Mn doped PZT films did not show a depolarization current peak arising from relaxation of trapped charges, though the concentration of mobile oxygen vacancies and hence the amount of compensating electronic charge is much

higher compared to Nb doped samples.

To obtain additional evidence for changes in Ti valence in the cathodic region, Nb and Mn doped PZT samples were investigated using EELS. Figure 5.9 shows a series of Ti-L edges from different positions in the PZT film as a function of distance from the Pt bottom interface (cathode). A gradual shift to higher energy loss value was observed for the Ti $L_{2,3}$ edge of Nb doped PZT films. Moreover, Ti $L_{2,3}$ data taken close to the cathode shows that the t_{2g} and e_g peaks develop noticeable shoulders (See Figure 5.9b). Both the chemical shift of the Ti $L_{2,3}$ to lower energy losses and the appearance of shoulders on t_{2g} and e_g imply reduction of Ti cations.[30-31] The magnitude of shift in Ti-L edges is shown

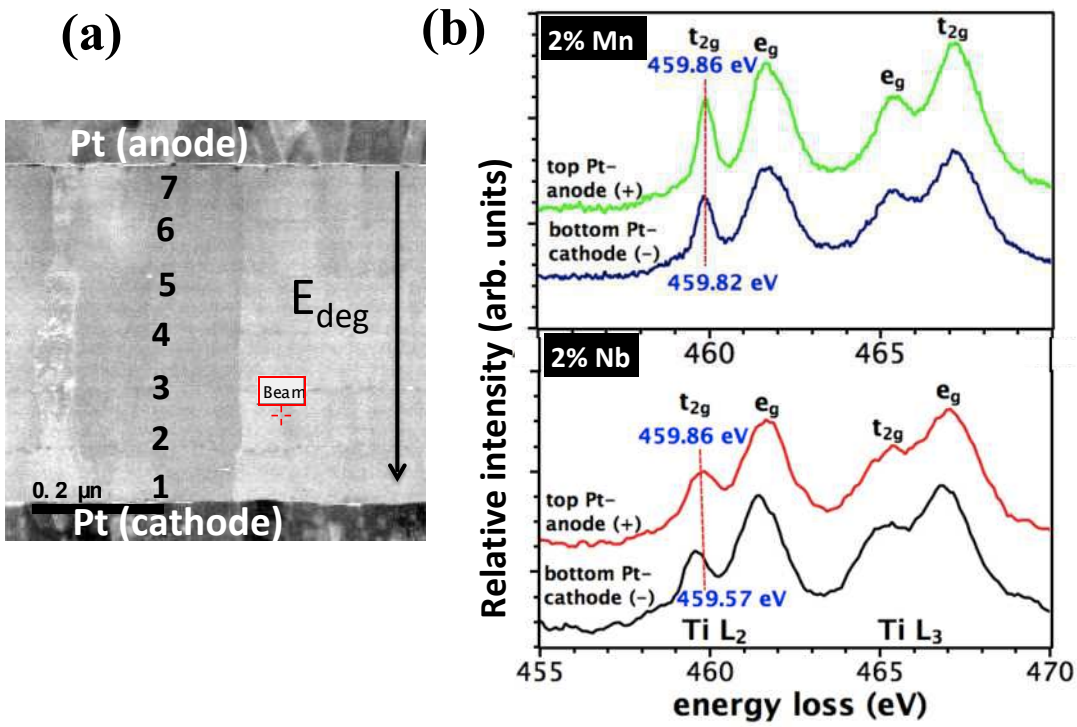

Figure 5.9 *(a) Cross sectional image of 2% Nb doped PZT films (b) Electron energy loss spectrum from different positions in the PZT film as a function of distance from the bottom interface (cathode). Ti $L_{2,3}$ of Mn, and Nb doped PZT films after degrading at 180°C under electric field of 350 kV/ cm for 12h.*

in Figure 5.9. This shows a progressive change in the Ti valence state towards the bottom

electrode (cathode), suggesting more electrons near the cathodic region of Nb doped PZT samples.

For Mn doped PZT, on the other hand, no apparent chemical shift is observed from a series of EELS spectra taken across the thickness of degraded samples, implying that there is no modification to the Ti valence in the degraded films. This suggests that although the acceptor ions increase the oxygen vacancy concentration in PZT films, free electron generation due to compensation of oxygen vacancies at the cathode and free hole formation at the anode region might be suppressed by the valence changes from $Mn^{3+/4+}$ to $Mn^{2+/3+}$ and $Mn^{2+/3+}$ to $Mn^{3+/4+}$ respectively. Mn can take multiple valence states and the ionization energy for 2+/3+ and 3+/4+ transitions are 1.2 and 1.9 eV,[32] respectively (Figure 5.10). Since the Mn_{Ti}^{x} and $Mn_{Ti}^{\prime}$ ions are more reducible than Ti_{Ti}^{x}, the electrons

$$Mn_{Ti}^{\prime} + e^{\prime} \rightleftarrows Mn_{Ti}^{\prime\prime} \qquad Mn_{Ti}^{x} + e^{\prime} \rightleftarrows Mn_{Ti}^{\prime} \qquad \text{Equation 5.9}$$

$$Mn_{Ti}^{\prime\prime} + h^{\bullet} \rightleftarrows Mn_{Ti}^{\prime} \qquad Mn_{Ti}^{\prime} + h^{\bullet} \rightleftarrows Mn_{Ti}^{x} \qquad \text{Equation 5.10}$$

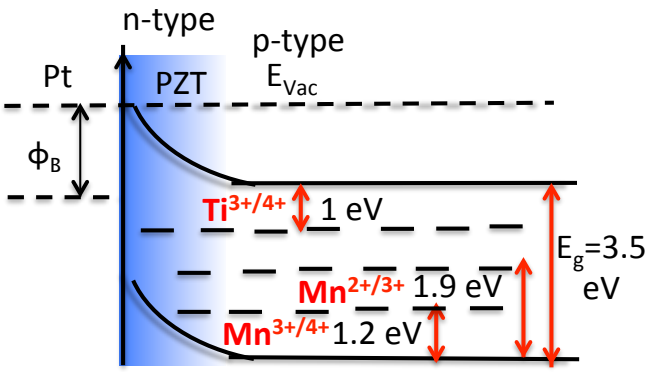

Figure 5.10 *Schematic representation of energy band diagram of PZT in contact with Pt electrode*

accumulated near the cathode region are trapped by Mn sites rather than Ti^{4+} ions. Due to the lower concentration of Mn with respect to Ti in PZT films, trapped electrons via Mn ions are distributed over a longer length scale. This diminishes the maximum electric field at the Schottky interface, which suppresses the potential barrier height lowering and

subsequent leakage current rise upon degradation. This leads to longer lifetime and lower electrical degradation rate in Mn doped PZT films.

5.4 Conclusions

It was demonstrated that thermally stimulated depolarization current (TSDC) is a useful technique to understand the type of defects leading to to DC resistance degradation in PZT films. Only one relaxation current peak near 200°C was observed for Mn doped PZT samples; this is associated with space charge polarization. The physical origin of the TSDC peak is due to relaxation of oxygen vacancies, the most mobile ions in PZT. Three distinct methods: the initial rise model, heating rate, and FWHM methods all gave activation energy of the TSDC peak in the range of 0.6-0.8 eV. This peak was attributed to migration of oxygen vacancies. The magnitude of the depolarization current peak increases with increasing Mn concentration. A similar but smaller TSDC peak attributed to relaxation of oxygen vacancies was also observed in Nb doped PZT films. An additional TSDC peak, associated with trapped charges, in the temperature range of 250-300°C, was observed in Nb doped PZT films. The trap depth is estimated to be 0.18±0.05 eV, which is attributed to electron hopping between B site ions Ti'_{Ti} and Ti^{X}_{Ti}. EELS results confirm the chemical shift in Ti $L_{2,3}$ to lower energy losses and appearance of shoulders on the t_{2g} and e_g peaks, implying reduction of Ti cations; this was observed only in degraded Nb doped samples. It is believed that free electron generation due to compensation of oxygen vacancies at the cathode and free hole formation at the anode region might be suppressed by the valence changes from Mn^{3+} to Mn^{2+} and Mn^{4+} to Mn^{3+} in Mn-doped films. This occurs preferentially to reduction of Ti in Mn doped PZT films, consistent with the location of the energy levels in the band structure.

5.5 References

[1]Wilke R.H., Johnson-Wilke R.L., Cotroneo V., Davis W.N., Reid P.B., Schwartz D.A., Trolier-McKinstry S., "Sputter deposition of PZT piezoelectric films on thin glass substrates for adjustable x-ray optics," *Appl. Opt.*, 52, 3412-9 (2013).

[2]Funakubo H., Dekkers M., Sambri A., Gariglio S., Shklyarevskiy I., and Rijnders G., "Epitaxial PZT films for MEMS printing applications," *MRS Bull.*, 37, 1030-8 (2002).

[3]Qiu Y., Gigliotti J.V., Wallace M., Griggio F., Demore C.M.E., Cochran S. and Trolier-McKinstry S., "Piezoelectric Micromachined Ultrasound Transducer (PMUT) arrays for integrated sensing, actuation and imaging," *Sensors*, 15, 8020-8041 (2015).

[4]Benoit R.R., Rudy R.Q., Pulskamp J.S., Polcawich R.G. and Bedair S.S., "Advances in piezoelectric PZT-based RF MEMS components and systems," *J. Micromech. Microeng.,* 27, 083002-1-13 (2017).

[5]Yeo H.G., Ma X., Rahn C., Trolier-McKinstry S., "Efficient piezoelectric energy harvesters utilizing (001) textured bimorph PZT films on flexible metal foils," *Adv. Funct. Mater.,* 26(32), 5940-46 (2016).

[6]Zhang S.J., Liu W., Donnelly N.J., Xu Z., and Randall C.A., "Time dependent dc resistance degradation in lead-based perovskites: 0.7 $Pb(Mg_{1/3}Nb_{2/3})O_3$−0.3$PbTiO_3$*," J. Appl. Phys.*, 105, 053705 (2009).

[7]Yoon S-H., Randall C.A., Hur K-H., "Difference between resistance degradation of fixed valence acceptor (Mg) and variable valence acceptor (Mn)-doped $BaTiO_3$ ceramics," *J. Appl. Phys.,* 108, 064101 (2010).

[8]Stolichnov I., Tagantsev A., Setter N., Okhonin S., Fazan P., Cross J.S., Tsukada M., Bartic A. & Wouters D., "Constant-current study of dielectric breakdown of $Pb(Zr,Ti)O_3$ ferroelectric film capacitors," *Integrated Ferroelectrics*, 32, 45 (2001).

[9]Zafar S., Hradsky B., Gentile D., Chu P., Jones R.E., Gillespie S., "Resistance degradation in barium strontium titanate thin films," *J. Appl. Phys.*, 86, 064101 (1999).

[10]Wang R-V., McIntyre P.C., "^{18}O tracer diffusion in $PbZrTiO_3$ thin films: A probe of local oxygen vacancy concentration," *J. Appl. Phys.*, 97: 023508-1-8 (2005).

[11]Prisedsky V.V., Shishkovsky V.I., Klimov V.V., "High-temperature electrical conductivity and point defects in lead zirconate-titanate," *Ferroelectrics* 17, 465 (1978).

[12]Waser R., Baiatu T., and Härdtl K. H., "dc electrical degradation of perovskite-type titanates: I, ceramics," *J. Am. Ceram. Soc.* 73, 1654 (1990).

[13]Smyth D.M., "Ionic transport in ferroelectrics," Ferroelectrics, 151 115 (1994).

[14]Raymond M.V., Smyth D.M," Defects and charge transport in perovskite ferroelectrics," *J. Phys. Chem. Solids,* 57, 1507 (1996).

[15]Liu W. and Randall C.A., "Thermally stimulated relaxation in Fe-doped $SrTiO_3$ systems: I. single crystals," *J. Am. Ceram. Soc.*, 91, 3245 (2008).

[16]Liu W. and Randall C.A., "Thermally stimulated relaxation in Fe-doped $SrTiO_3$ systems: II. degradation of $SrTiO_3$ dielectrics," *J. Am. Ceram. Soc.*, 91, 3251 (2008).

[17]Takeoka S., Morita K., Mizuno Y., and Kishi H., "Thermally stimulated current (TSC) studies on resistance degradation of Ni-MLCC," *Ferroelectrics*, 356, 370 (2007).

[18]Wu Z., Sayer M., "Defect structure and fatigue in ferroelectric PZT thin films," *Applications of Ferroelectrics, Proceedings of the Eighth IEEE International Symposium*, 244 (1992).

[19]Okino H., Shimizu M., Horiuchi T., Shiosaki T., Matsushige K., "A Study of the defect structures in MOCVD-grown $PbZr_xTi_{1-x}O_3$ thin films by thermally stimulated current measurements," *Integrated Ferroelectrics*, 18, 63 (1997).

[20]Wolf R.A. and Trolier-McKinstry S., "Temperature dependence of the piezoelectric response in lead zirconate titanate films," *J. Appl. Phys.*, 95 [3], 1397 (2004).

[21]Akkopru-Akgun, B., Zhu W., Lanagan M.T., Trolier-McKinstry S., "The effect of imprint on remanent piezoelectric properties and ferroelectric aging of Mn or Nb doped $PbZr_{0.52}Ti_{0.48}O_3$ thin films," *J. Am. Soc.* article in press, DOI: 10.1111/jace.16367 (2019).

[22] Marincel D.M., Belianinov S.J.A., Okatan M.B., Kalinin S.V., Jackson T.N., Randall C.A., and Trolier-McKinstry S., " A-site stoichiometry and piezoelectric response in thin film $PbZr_{1-x}Ti_xO_3$," *J. Appl. Phys.,* 117, 204104 (2015).

[23]Chen R. and Kirsh Y., "Analysis of thermally stimulated process," Pergamon Press, New York, 146 (1981).

[24]Torres A., Jimenez J., Vega B., and De Saja J.A., "Influence of heating rate in the dipolar relaxation," *Phys. Stat. Sol. (A),* 90, 749 (1985).

[25]Härdtl K.H. and Rau H., "PbO vapour pressure in the $Pb(Ti_{1-X})O_3$ system," Solid State Commun. 7 41 (1969).

[26]Moura Ramos J.J. and Correia N.T., "The determination of the activation energy of a relaxational process from thermally stimulated depolarisation currents (TSDC) data: an illustration with the β-relaxation of maltitol," *Thermochim. Acta*, 426, 185 (2005).

[27]Chen J., Harmer M.P, and Smyth D.M., "Compositional control of ferroelectric fatigue in perovskite ferroelectric ceramics and thin films," *J. Appl. Phys.*, 76, 5394 (1994).

[28]Zhao S., Zhang S.J., Liu W., Donnelly N.J., Xu Z., and Randall C.A., "Time dependent dc resistance degradation in lead-based perovskites $0.7Pb(Mg_{1/3}Nb_{2/3})O_3- 0.3PbTiO_3$," *J. Appl. Phys.*,105, 053705 (2009).

[29]Van Turnhout J., "Thermally Stimulated Discharge of Polymer Electrets," pp. 161 Elsevier, Amsterdam (1975).

[30]Leapman R.D., Grunes L.A., and Fejes P.L., "Study of the L_{23} edges in the 3d transition metals and their oxides by electron-energy-loss spectroscopy with comparisons to theory," *Phys. Rev. B*, 26, 614 (1982).

[31]Otten M.T., Miner B., Rask, J.H. and Buseck P.R., "The determination of Ti, Mn and Fe oxidation states in minerals by electron energy-loss spectroscopy," *Ultramicroscopy* 18, 285 (1985).

[32]Wechsler B.A., and Klein M.B., "Thermodynamic point defect model of barium titanate and application to the photorefractive effect," *J. Opt. Soc. Am. B- Optical Phys*, 5: 1711–23 (1988).

Chapter 6

Polarity Dependent DC Resistance Degradation and Electrical Breakdown in Nb Doped PZT Films

This chapter has been recently accepted to be published in Applied Physic Letters Materials.

6.1 Introduction

Lead zirconate titanate (PZT) films are used extensively in MEMS devices such as energy harvesters[1], inkjet printers[2], actuators[3], medical transducers[4], and resonators[5] due to their high piezoelectric properties. However, for MEMS actuators, the magnitude of the electric fields utilized often exceeds 100 kV/cm. As a result, DC resistance degradation, one of the limiting factors for the lifetime of PZT films, is of a great concern. Therefore, it is crucial to understand the causes of the leakage current increase to control electrical breakdown and device failure.

For PZT films with metal electrodes, electrons, holes, and ions can all contribute to conduction and DC resistance degradation. Various conduction models have been proposed for PZT films: from bulk-controlled mechanisms such as Poole–Frenkel emission[6], space charge-limited currents,[7] and ionic conduction[8] to interface-controlled conduction mechanisms such as Schottky emission[9] and Fowler–Nordheim tunneling[10]. It is probable that the wide range of models is a function of the fact that the electrical behavior depends explicitly on the stoichiometry and the defect chemistry, as well as the interface characteristics of PZT thin films and electrodes. One consequence of this is that films prepared under different conditions are likely to behave differently.

PZT is typically a p-type wide gap semiconductor due to unintentionally introduced acceptor ions and/or lead loss during processing.[11] There is debate in the literature as to whether holes or electrons are the majority carriers in PZT films; the fact that donor doping tends to reduce the leakage currents suggests p-type conductivity,[12-13] while experimental observations of Schottky barriers at the Pt/PZT films necessitate n-type surfaces, since the work function of Pt is higher than that of PZT.[14-15] Such n-type interfaces can develop due to accumulation of oxygen vacancies during electrode deposition or on annealing in a reducing atmosphere.[16-17] The oxygen vacancies act as a donor with an energy level 0.22-0.28 eV below the edge of the conduction band. Each oxygen vacancy is compensated by two electrons that are thermally excited at room temperature to form an n-type layer near the PZT surface,[16] as verified by the presence of Ti^{3+}at the Pt/PZT interface.[18] In previous work, it was demonstrated by electron energy loss spectroscopy that the concentration of Ti^{3+} ions gradually increases towards the cathode in degraded Nb doped PZT films.[18]

In the p-type bulk of PZT films,[18] a variety of different electronic conduction mechanisms can occur simultaneously; (1) hole hopping between Pb^{2+} and Pb^{3+} (0.24-0.38 eV) [19-20] (2) hole migration between lead vacancies (1.4 eV) [21-22] and (3) small polaron hopping between acceptor ion sites. (0.7-1 eV for hole hopping between Mn sites).[23] Because films often show Poole-Frenkel-dominated conduction in the bulk and a Schottky barrier at the interface, films behave as a pair of non-linear resistors in series.

Upon DC resistance degradation, $V_O^{\bullet\bullet}$ migrate towards the cathode. As $V_O^{\bullet\bullet}$ build up at the interface, they modulate the local charge distribution near the PZT/electrode interface and then modify the interface characteristics; the local accumulation of $V_O^{\bullet\bullet}$ can

reduce both the Schottky barrier height and the width of the depletion layer, which accelerates electron injection and charge trapping on the Ti^{4+} sites in the PZT film.[8, 18, 24-26] DC resistance degradation in PZT films could, in principle, be strongly influenced by interfacial defect chemistry. The interfacial defect chemistry can differ at the top and the bottom PZT/electrode interfaces due to (1) an inhomogeneous distribution of defects across the PZT film (e.g. a variation in PbO stoichiometry), (2) Ti/Zr segregation during film preparation, and/or (3) variation in the oxidation state of ions across the film that can act as charge trap sites. PZT films are prone to varying trap state densities near the top and bottom electrodes, with a potential for large gradients in defect concentration. For instance, Mihara et al. found that the $V_O^{\bullet\bullet}$ concentration in the interior of PZT films (10^{18} cm^{-3}) is lower than that near the surface (10^{20} cm^{-3}).[27] The variation in defect distribution near the electrode affects the interface barrier height and depletion width. These, in turn, influence electron conduction near the PZT/electrode interface. The presence of a higher concentration of $V_O^{\bullet\bullet}$ near the interface pins the Fermi level closer to the conduction band and decreases the potential barrier height for injecting electrons. Moreover, subsequent charge trapping processes leads to space charge gradients and to band bending. This could result in polarity-dependent lifetimes as well as asymmetric leakage current behavior. Al Shareef et al. showed that both leakage currents and breakdown fields can be strongly asymmetric in Nb doped PZT films with Pt top and bottom electrodes; the current increase was found to be more gradual when the top electrode was biased negatively with respect to the bottom electrode.[28] In another study, Tagantsev et al. attributed the polarity dependent electrical breakdown in PZT films to the polarization-dependence of the Schottky barrier.[29] Although a number of studies confirmed polarity

dependence in the time dependent resistance degradation, the role of interfacial defect chemistry on the charge transport mechanisms and DC resistance degradation characteristics of PZT films has not been fully elucidated.

This study aims to provide experimental evidence to demonstrate how the pristine state interfacial defect chemistry affects the transport mechanism upon electrical degradation in Nb doped PZT films. In particular, the roles of PbO stoichiometry and Ti/Zr segregation on the conduction properties of the PZT/Pt interfaces are described; this includes the band bending, potential barrier heights, the nature of majority carriers and the depletion layer thickness, and the bulk conduction mechanisms. The polarity dependence of lifetime was assessed using Highly Accelerated Lifetime Testing (HALT). I-V measurements were conducted both in the pristine state and after electrical degradation to investigate the variation in conduction mechanism with voltage polarity. The migration of $V_O^{\bullet\bullet}$ upon degradation and the resultant change in local chemistry near the Pt/PZT interfaces were explored using Thermally Stimulated Depolarization Current (TSDC) and Electron Energy Loss Spectroscopy (EELS). The local chemistry near the top and bottom interface was explored via Energy Dispersive X-ray (EDX) Mapping and correlated with the polarity dependent electrical degradation in Nb doped PZT films.

6.2 Experimental Procedure

The details of thin film preparation and characterization techniques used to explore structural and electrical properties of PZT films were described in Chapter 3.2.

6.3 Results and Discussion

Figure 6.1 shows the voltage polarity dependence of current density-time (J-t) response and the resistance degradation behavior of 2% Nb doped PZT films (PNZT) with Pt top and bottom electrodes. A noticeable difference in DC resistance degradation

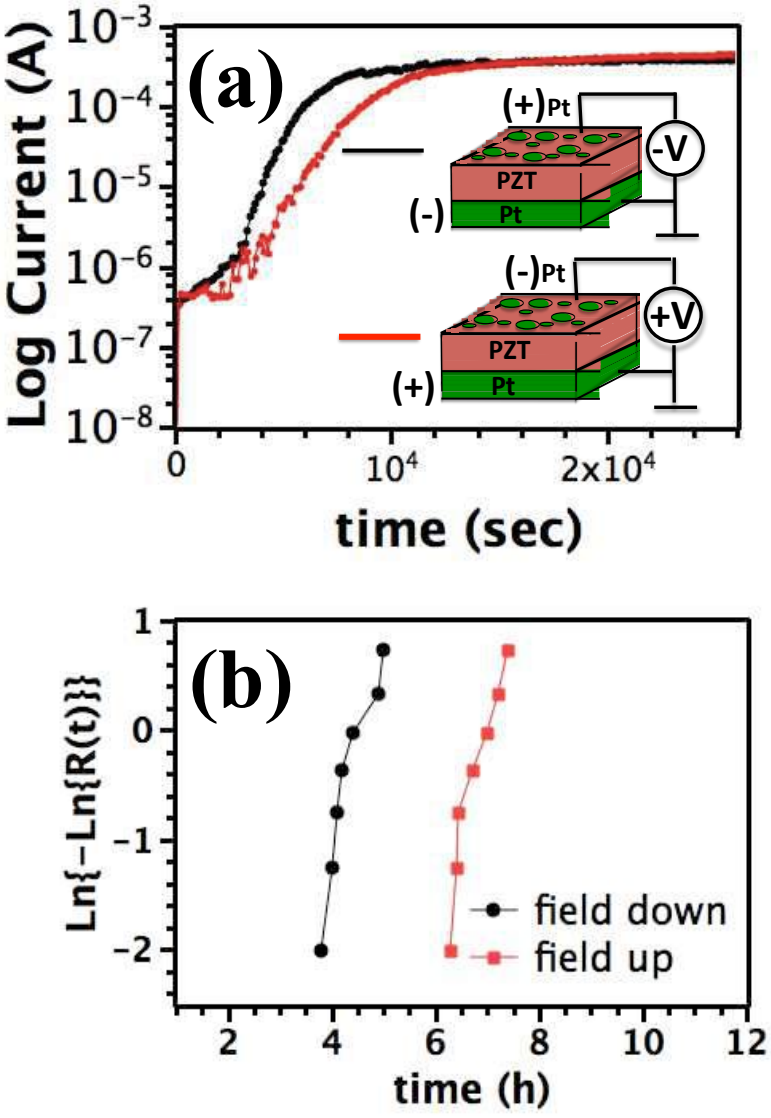

Figure 6.1*(a) Variation in leakage current with time, (b) the time to failure for 2% Nb doped PZT films. R(t) represents the probability of failure over time. The HALT measurement was conducted at 180°C with a DC field of either 400 or -400 kV/cm.*

behavior and time dependent electrical breakdown was observed for opposite bias

polarities. As can be seen in Figure 6.1, the steady-state current rises upon resistance degradation. Failure occurs abruptly when the bottom electrode was negatively biased with respect to the top electrode. On the other hand, a more gradual current increase was observed when the top electrode was biased negatively, accompanied by remarkable increase in the median time to failure (MTTF) from 4.8±0.7 to 7.6±0.4 hours. These results clearly indicate that the electrical reliability characteristics of Nb doped PZT films are superior when the top Pt electrode was biased negatively, for the PZT and Pt deposition conditions utilized.

To explore the variation in the charge transport mechanism with voltage polarity, I-V measurements were conducted on 2 mol% Nb doped PZT films before and after degradation at 180°C under an electric fields of -350 kV/cm (called field-down, since the direction of the electric field is from the top to the bottom Pt electrode, and the bottom electrode is negatively biased) and 350 kV/cm (called field-up, since the direction of the electric field is from the bottom to the top Pt electrode, and the top electrode is negatively biased) for 12 h (Figure 6.2). The leakage current of undegraded PNZT films shows insignificant voltage polarity dependence; the current-voltage characteristics are nearly

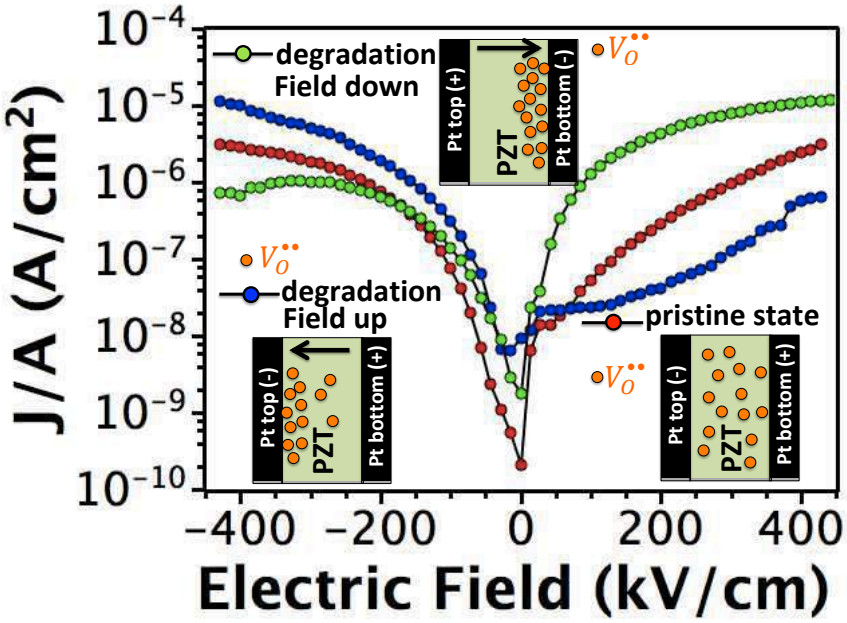

Figure 6.2 *Temperature dependence of conductivity for different polarities, as indicated by the arrows. The field direction for the current/voltage measurement is defined by the charge signs on the Pt electrodes.*

symmetric for negative and positive bias. However, the I-V characteristics become remarkably asymmetric after degrading the PNZT films. The absolute value of current after degradation was found to increase in the direction in which the PNZT films had been degraded; the leakage current increase upon DC resistance degradation was governed by the Pt/PNZT interface that was negatively biased (the cathode). To distinguish which Pt/PNZT interface dominated the leakage current, equivalent PNZT samples with asymmetric top IrO_2 and bottom Pt electrodes were used. Since IrO_2 has a lower work function than Pt, large differences were observed between I-V characteristics of top IrO_2 and bottom Pt contacts.

For degradation at -350 kV/cm, where the bottom Pt/PNZT interface was biased negatively, the leakage current increased at the bottom Pt/PNZT (cathode) interface, accompanied by a subtle change in the leakage current at the top Pt/PNZT interface (anode). In contrast, after degrading PNZT films at 350 kV/cm, a strong increase in the

leakage current at the negatively biased top Pt/PNZT interface (cathode) was detected with a trivial change in the leakage current for the positively biased bottom Pt/PNZT interface. Thus, the reverse biased cathode determines the leakage current behavior of PZT films.

The I-V response of PNZT films before and after degradation was fit to the equations for various conduction mechanisms. Figure 6.3a shows the disparity in the conduction mechanism near the bottom Pt/PZT interface in the pristine state and after degradation under an electric field of -350 and 350 kV/cm for 12 h. Current density-electric field (J-E) characteristics in the pristine state exhibited good linearity for both Poole-Frenkel (Ln (J/E) versus $E^{1/2}$) and Schottky emission (Ln (J/T^2) versus $E^{1/2}$) conduction mechanisms.

As a first approximation, a simple Schottky emission model, which assumes a homogeneous electric field in a fully depleted sample, was used to estimate the relative dielectric constant. The appropriate dielectric permittivity is limited by the optical permittivity when the carriers move through the insulating layer faster than the relaxation time and by the static dielectric permittivity when the carriers are slow. Assuming the electron movement across the film is faster than the relaxation time, the optical dielectric permittivity, ε_r, was extracted from the slope of the linear fits and the refractive index, $n = \sqrt{\varepsilon_r}$. At low electric fields (<122.5 kV/cm), n calculated from Poole-Frenkel plots ranged from 2.2 to 2.6, in good agreement with the refractive index of PZT (n~ 2.25).[30] This suggests that Poole-Frenkel emission controls the conduction at low electric fields; it has been previously shown that (1) electron trapping by Ti^{4+} and hole hopping between Pb^{2+} and Pb^{3+} sites are the main mechanisms that contribute to Poole-Frenkel conduction

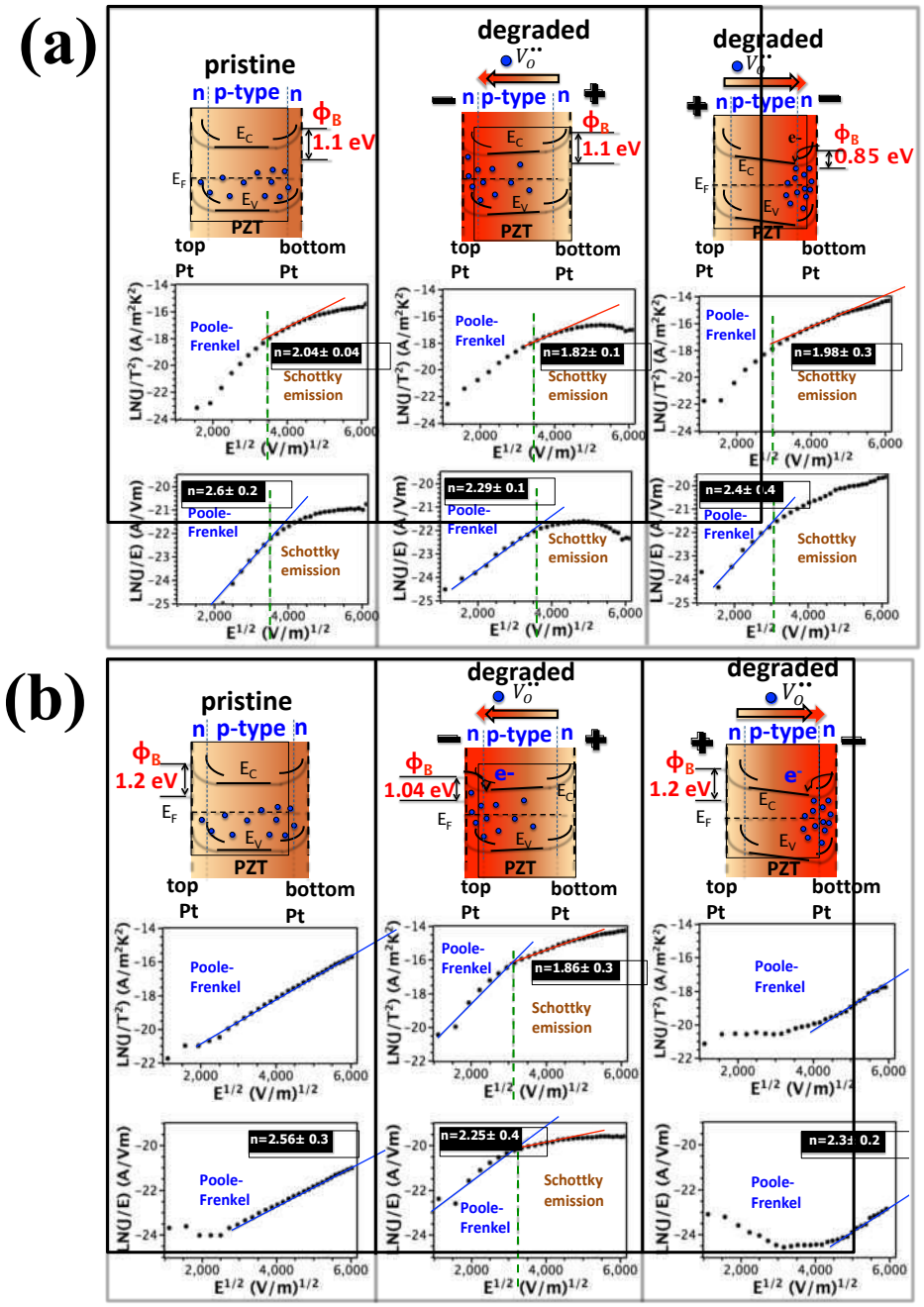

Figure 6.3 *Fitting of the leakage current-voltage data for distinct electric fields in 2 % Nb doped PZT thin films before (a) and after degradation (b) at 180°C under an electric field of 350 or -350 kV/ cm for 12h. Accumulation of oxygen vacancies near the interface during the deposition of the electrode makes the interface n-type though the bulk of the PZT films remain p-type.*

in PNZT films.[18] With increasing electric fields (>122.5 kV/cm), a refractive index of about 2.2 was obtained from the slopes of Schottky plots[30], indicating that Schottky emission dominates the leakage current.

In contrast to the bottom Pt/PNZT interface, the switch from Poole-Frenkel to Schottky emission occurs at higher electric fields (>360 kV/cm) for the top Pt/PNZT interface, accompanied by a larger potential barrier height (1.2±0.07 eV) for electron injection from the Pt electrode into the PNZT. Typically, the Schottky barrier height depends not only on the PZT work function and electron affinity, but also on the density and distribution of impurity sites at the interface due to Fermi-level pinning.[31-32] The role of $\boldsymbol{V_O^{\bullet\bullet}}$ on Schottky formation is critical in PZT films. Oxygen vacancies in PZT create electronic states that are 0.22-0.28 eV below the conduction band; these are reported to cause Fermi level pinning at the interface, reducing the Schottky barrer.[15, 18, 33] Two important sources for $\boldsymbol{V_O^{\bullet\bullet}}$ formation in Nb doped PZT films are (1) unintentionally introduced acceptor ions and (2) loss of PbO upon annealing.

Although the incorporation of donor ions (Nb) into PZT decreases the $V_O^{\bullet\bullet}$ concentration, it cannot entirely prevent $V_O^{\bullet\bullet}$ formation. Given that the pristine films are close to intrinsic, electroneutrality can be expressed as:

$$2[V_O^{\bullet\bullet}] + [Nb_{Ti}^{\bullet}] + [h^{\bullet}] = 2[V_{Pb}''] + [e'] \qquad \text{Equation 6.1}$$

PbO loss during deposition of film can occur at the surface of each layer of PZT films during annealing, as well as to the bottom electrode.[34] Figure 6.4a exhibits energy dispersive X-ray (EDX) mapping of Pb. The Pb/(Zr+Ti) ratio was found to be low in the PZT layers close to the bottom Pt electrode. Similar PbO loss was not observed in the

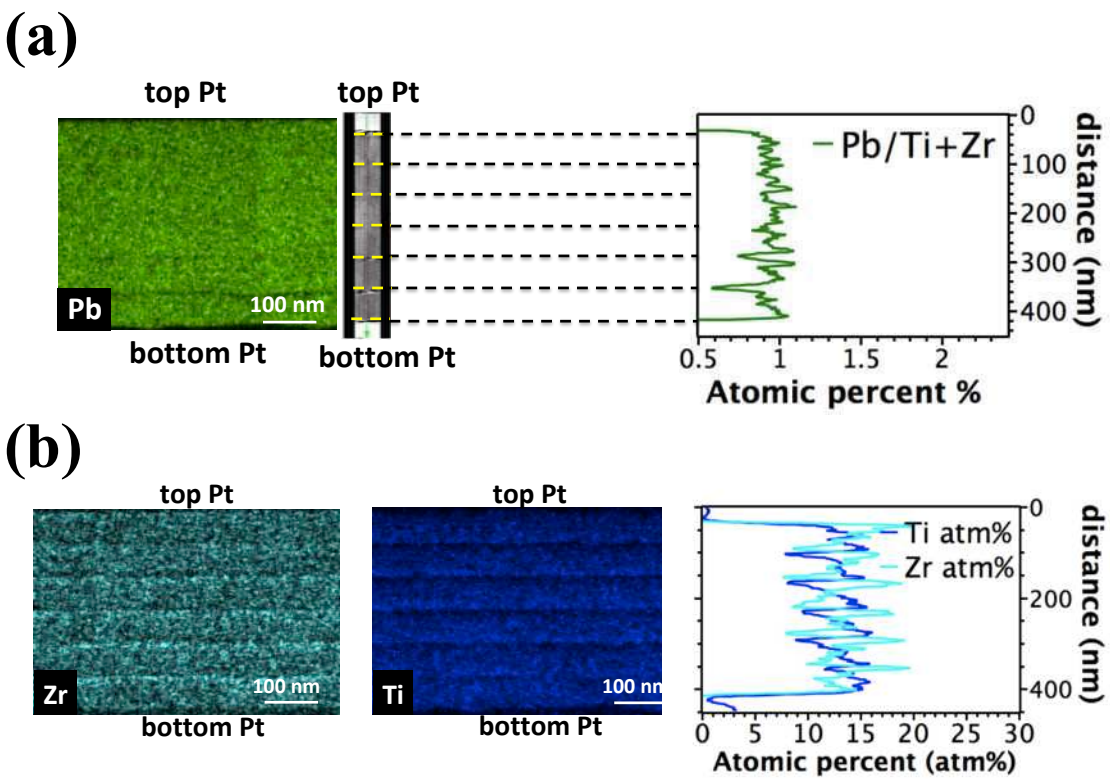

Figure 6.4 *Energy dispersive X-ray (EDX) mapping of (a) Pb, and (b) Ti, Zr*

PZT close to the top Pt electrode; any lead loss at this surface should have been compensated by the PbO overcoat. It is noted that in this work, PbO stoichiometry was attained by a kinetically controlled process. The variation in PbO stoichiometry through the PNZT films creates disparities in the interfacial defect chemistry near the top and bottom electrodes. Higher PbO loss near the bottom Pt/PZT interface leads to formation of oxygen and lead vacancies. It is believed that the higher concentration of $V_O^{\bullet\bullet}$ near the bottom Pt interface is one factor responsible for the low potential barrier height for electron injection and the low transition electric field from Poole-Frenkel to Schottky emission.

A second possibility is an asymmetry in the B-site stoichiometry at the top and bottom Pt/PNZT interfaces. Figure 6.4b illustrates EDX mapping of the Ti/Zr ratio across

the PNZT film. As shown in Figure 6.4b, there are strong Ti/Zr gradients through the thickness of each crystallized PNZT layer. The growth of PNZT thin films is strongly nucleation controlled. Since the crystallization temperature of $PbTiO_3$ is lower than $PbZrO_3$, a Ti-rich composition initially nucleates at the bottom of each layer and the composition gradually becomes enriched in Zr near the top surface. The Ti/Zr gradients lead to formation of Ti- and Zr-rich layers at the bottom and top Pt electrode interfaces, respectively.[35] Moreover, Zr is less reducible than Ti, and could result in a lower $V_O^{\bullet\bullet}$ concentration at the film top surface. It is plausible that Ti/Zr segregation can also change the charge distribution at the top and bottom Pt/PNZT Schottky contacts, which influence the Schottky barrier height and the transition electric field from Poole –Frenkel to Schottky emission. The existence of a Ti-rich layer near the bottom Pt/PNZT Schottky contact can induce a large amount of interfacial states (Ti^{3+}/Ti^{4+}) ~1 eV below the conduction band of PZT; this in turn enhance the partial Fermi-level pinning and lowers the potential height for charge injection. The possible effects of Ti segregation on the Schottky contact formation needs to be further studied to reveal the difference in the nature of contact between bottom Pt-Ti-rich PZT and top Pt-Zr-rich PZT layers.

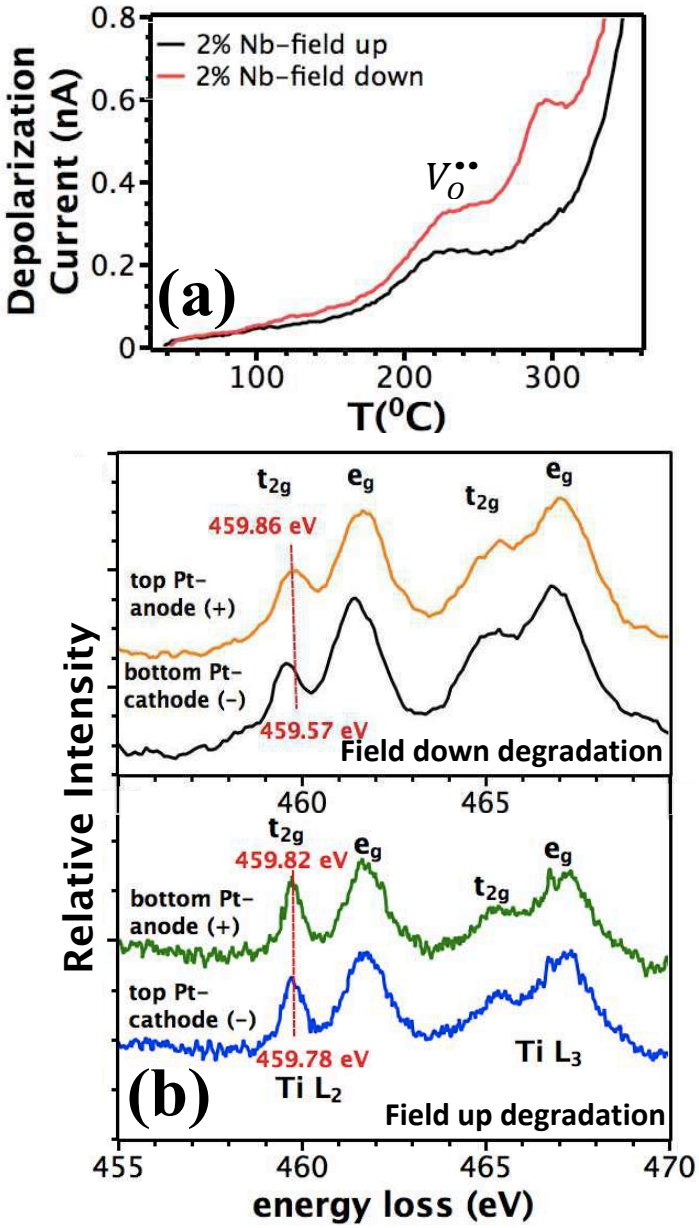

Figure 6.5 *Evaluation of* (a) *TSDC spectra and (b) electron energy loss spectra as a function of distance from the bottom interface (cathode) after degrading 2% Nb doped PZT films at 180°C with a DC field of 350 or -350 kV/cm.*

The I-V characteristic of the Pt/PNZT/Pt can be described via an equivalent circuit model comprised of two back-to-back Schottky diodes connected in series with the bulk (Poole-Frenkel dominated). Both forward and reverse biased interfaces were modeled using the Schottky equation, taking into consideration the potential barrier reduction due to image charges:[36]

$$J_F = A^{**}T^2 \exp\left(-\frac{q\emptyset_B}{kT}\right)\left[\exp\left(\frac{qV_F}{nKT}\right) - 1\right] \quad \text{Equation 6.2}$$

$$J_R = A^{**}T^2 \exp\left[-\frac{q(\emptyset_B - \sqrt{\frac{qE_m}{4\pi\varepsilon_s}}}{kT}\right] \quad \text{Equation 6.3}$$

where, A^{**}, V_{bi}, E_m, ε_s, $\emptyset_B$ and N_D are Richardson constant, built-in potential, maximum electric field at the interface, dielectric permittivity, the potential barrier height, and donor density at the interface, respectively. The potential barrier height at the bottom Pt/PNZT interface was calculated from the Schottky plot and found to be 1.1±0.05 eV in the pristine state. Following electrical degradation at 350 kV/cm, no significant change was observed in potential barrier height for the positively biased bottom Pt/PNZT interface (anode), and the leakage current was suppressed. When the bottom Pt/PNZT interface was negatively biased upon degradation (-350 kV/cm), on the other hand, a significant reduction in Schottky barrier height from 1.1±0.06 to 0.85±0.05 eV was observed. This was coupled with an expansion in the electric field range over which Schottky emission is dominant. This suggests that electron injection from the negatively biased Pt into PNZT films is the rate-limiting mechanism in electrical degradation of PNZT films (See Figure 6.3). If the leakage current was controlled by injection of holes and/or electron extraction at the anode, a significant increase in leakage currents should have been observed from the positively biased Pt/PNZT interface region upon degradation.

These findings are consistent with a well-known degradation mechanism in perovskite systems, as described by Baitu et al.[37] According to this model, field-driven ionic migration and subsequent accumulation of $V_O^{\bullet\bullet}$ near the cathode, with concurrent depletion of $V_O^{\bullet\bullet}$ near the anode are responsible for electrical degradation. The redistribution of $V_O^{\bullet\bullet}$ leads to increases in the electron and hole concentrations near the

cathode and anode regions, respectively. The leakage current in Pt/PNZT/PT thin films upon degradation is determined by the change in the height and the width of all of the potential barriers. As electrons accumulate in the space charge region near the cathode, mirror charges with the same magnitude and opposite polarity appear on the metal side of interface. This causes formation of an image force that opposes the potential in the space charge region, which significantly decreases the Schottky barrier height:[38]

$$\Delta\emptyset_B = (\frac{eE_m}{4\pi\varepsilon})^{1/2} \quad \text{Equation 6.4}$$

$$E_m = \sqrt{\frac{2qN_{eff}}{\varepsilon_s}(V_R + V_{bi} - \frac{kT}{q})} \quad \text{Equation 6.5}$$

where E_m is the maximum electric field at the interface. The Schottky barrier lowering is primarily determined by the maximum electric field at the interface. The large electric field in the depletion layer can both drive the diffusion of $V_O^{\bullet\bullet}$ and increase the likelihood of charge injection.

Another mechanism that contributes to the leakage current increase upon degradation is the change in the depletion width, which is given by:[39]

$$W = \sqrt{2\varepsilon(V_b - \frac{kT}{q})/(qN_d)} \quad \text{Equation 6.6}$$

where ε, V_{bi}, q, and N_d are dielectric permittivity, the built-in potential, the magnitude of an electron charge, and the donor concentration at the interface. The accumulation of $V_O^{\bullet\bullet}$ at the cathode interface upon electrical degradation is expected to cause severe band bending, which reduces the depletion width of the potential barrier. This makes it easier for electrons to overcome the barrier at the interface.

As was the case for the bottom Pt/PNZT interface, enhanced leakage current together with a decrease in potential barrier height from 1.20±0.07 to 1.04±0.08 was only observed when the top Pt/PNZT interface was negatively biased upon electrical degradation under an electric field of -350 kV/cm (Figure 6.3b). No significant change in either the leakage current or the potential barrier height were found when a positive voltage was applied to the top Pt/PNZT interface, suggesting that $V_O^{\bullet\bullet}$ accumulation and subsequent electron injection controls the leakage current enhancement during electrical degradation.

However, there are some discrepancies between the leakage current behavior arising from the top and bottom Pt/PNZT interfaces in the degraded states. The decrease in potential barrier height and resultant enhancement in leakage current upon electrical degradation is more severe when the bottom Pt/PNZT interface was negatively biased upon degradation. This is consistent with the possibility that the increase in leakage current upon degradation is influenced by the local chemistry near the Pt electrodes. In particular, the Schottky barrier lowering is related to the density of donor states, mainly $V_O^{\bullet\bullet}$, near the interface (Equation 6.4 and 6.5); this, in turn, induces additional injection of electrons. Furthermore, the electron depletion width may decrease due to the high density of $V_O^{\bullet\bullet}$.[36, 40-41]

To investigate the migration of $V_O^{\bullet\bullet}$ and resultant change in local interfacial defect chemistry near the top and the bottom Pt electrodes, TSDC analysis was performed on electrically degraded PNZT films. Figure 6.5a shows the TSDC results of PNZT films after degradation under an electric field of 350 (top electrode is negatively biased) or -350 kV/cm (bottom electrode is negatively biased) for 12 h. The temperature of the

current maximum for the TSDC peak around 200°C shifts higher with increasing poling electric field, suggesting that the TSDC peak corresponds to depolarization of space charges. An activation energy of 0.68±0.04 eV was found, which is associated with migration of oxygen vacancies.[42] However, the concentration of migrated $V_O^{\bullet\bullet}$, which is represented by the area under the TSDC peak, depends strongly on the electrical field polarity during degradation. The concentration of $V_O^{\bullet\bullet}$ accumulated near the bottom and the top interfaces after degradation at -350 and 350 kV/cm for 12 h at 180°C was found to be 6.2×10^{18} and 3.8×10^{18} /cm^3, respectively. The difference in the concentration of accumulated $V_O^{\bullet\bullet}$ most likely arises from inhomogeneous distribution of $V_O^{\bullet\bullet}$ across the PNZT film in the pristine state. It is suggested that additional PbO loss upon annealing in the layers close to bottom Pt/PNZT electrode causes a lead vacancy gradient through the film. Given that some of the lead vacancies are ionically compensated with oxygen vacancies, a gradient in $V_O^{\bullet\bullet}$ concentration through the thickness of the PNZT films is probable. This will increase the number of mobile $V_O^{\bullet\bullet}$ near the bottom interface, which accentuates accumulation of those vacancies when degraded at -350 kV/cm. This could be augmented by the existence of Ti-rich layers near the bottom surface that increase the propensity for reduction.

In either case, near the cathode, the high concentration of $V_O^{\bullet\bullet}$ is charge compensated by electrons via $n \sim 2[V_O^{\bullet\bullet}]$. Figure 6.5b presents the EELS spectra for the Ti-L edges acquired near the bottom and top Pt electrodes after electrical degradation. When the bottom electrode was biased negatively upon electrical degradation (-350 kV/cm), the Ti-$L_{2,3}$ edges shift to lower energy near the bottom interface. This is consistent with some reduction of Ti^{4+} to Ti^{3+}. As no comparable reduction was observed

in the pristine films, the lower Ti valence is likely to be due to the compensating electrons for the migrated $V_O^{\bullet\bullet}$.[18, 26] Moreover, no chemical shift is observed near the top Pt/PNZT electrode interface (cathode) after degradation under an electric field of 350 kV/cm, as shown in Figure 6.5. The result is a higher concentration of trapped charges near the bottom Pt/PNZT interface in the degraded state, accounting for the observed asymmetry in conductivity and lifetime.

6.4 Conclusions

The electrical reliability and associated charge transport mechanisms in PNZT films with identical Pt top and bottom electrode vary depending on voltage polarity; the HALT lifetime is significantly improved when the top electrode is biased negatively compared to the bottom Pt electrode. The underlying mechanism responsible for the improved electrical degradation behavior is correlated with a variation in interfacial defect chemistry. In the pristine state, the presence of higher concentration of $V_O^{\bullet\bullet}$ near the bottom Pt interface results in (1) a lower potential barrier height for electron injection, and (2) a decrease in transition electric field from Poole Frenkel to Schottky emission. Upon degradation, an increase in the absolute value of current is always observed in the direction in which the PNZT films had been degraded. This was accompanied by an increase in the electrical field range over which Schottky emission is dominant. This indicates that electron injection from the cathode into PNZT governs the leakage current rise upon electrical degradation. TSDC and EELS results confirmed that field-driven electromigration of $V_O^{\bullet\bullet}$ and subsequent electrons trapping by Ti^{4+} are primarily responsible for electrical degradation in PNZT films. A higher concentration of $V_O^{\bullet\bullet}$ was found near the bottom Pt/PNZT interface relative to the top interface. This causes more

severe Schottky barrier lowering at the bottom Pt/PNZT interface, which in turn accelerates injection of electrons and subsequent charge trapping process. This may be coupled with the fact that a Zr-rich layer near the top interface reduces the propensity for trapping electrons near the top Pt/PNZT interface.

6.4 References

[1] Yeager C.B., Trolier-McKinstry, S. "Epitaxial $Pb(Zr_x,Ti_{1-x})O_3$ ($0.30<x<0.63$) films on (100)MgO substrates for energy harvesting applications," *J. Appl. Phys.*, 112: 074107 (2012).

[2] Trolier-McKinstry S., Muralt P., "Thin film piezoelectrics for MEMS," *J. Electroceram*. 12: 7-17 (2004).

[3]Muralt P., Polcawich R.G., and Trolier-McKinstry S., "Piezoelectric thin films for sensors, actuators, and energy harvesting," *MRS Bull*. 34: 658-64 (2009).

[4]Muralt P., Ledermann N., Baborowski J., Bargezar A., Gentil S., Belgacem B., Petitgrand S., Bosseboeuf A., Setter N., "Piezoelectric micromachined ultrasonic transducers based on PZT thin films," *IEEE Trans. Ultrason. Ferroelectr. Freq. Control* 12:2"276-88 (2005).

[5]Pulskamp J.S., Polcawich R.G., Rudy R.Q., Bedair S.S., Proie R.M., Ivanov T., Smith G.L.," Piezoelectric PZT MEMS technologies for small-scale robotics and RF applications," MRS Bull 37:1062-70 (2012).

[6]Nagaraj B., Aggarwal S., Song T.K., Sawhney T., and Ramesh R., "Leakage current mechanisms in lead-based thin-film ferroelectric capacitors," *Phys. Rev. B*. 59: 16022-27 (1999).

[7]Zubko P., Jung D.J., and Scott J.F., "Electrical characterization of $PbZr_{0.4}Ti_{0.6}O_3$ capacitors," *J. Appl. Phys*. 100: 114112 (2006).

[8]Slouka C., Kainz T., Navickas E., Walch G., Hutter H., Reichmann K., and Fleig J., "The effect of acceptor and donor doping on oxygen vacancy concentrations in lead zirconate titanate (PZT)," *Materials*. 9: 945-967 (2016).

[9]Cho S.M., Jeon D.Y., "Effect of annealing conditions on the leakage current characteristics of ferroelectric PZT thin films grown by sol–gel process," *Thin Solid Films* 338: 149-54 (1999).

[10]Watanabe Y., "Tunneling current through a possible all-perovskite oxide p−n junction," *Phys. Rev. B* 57: R5563-6 (1998).

[11]Raymond M.V., Smyth D.M., "Defects and charge transport in perovskite ferroelectrics," *Integ. Ferroelec*., 4: 145-54 (1994).

[12]WoutersD.J., Willems G.J., and Maes H.E., "Electrical conductivity in ferroelectric thin films," *Microelectron. Eng.*, 29: 249-56 (1995).

[13]Stolichnov I., Tagantsev A., "Space charge influenced- injection model for conduction in $Pb(Zr_xTi_{1-x})O_3$ thin films," *J. Appl. Phys.*, 84: 3216-25 (1998).

[14]Scott J.F., "Device physics of ferroelectric memories", *Ferroelectrics*. 183: 51-63 (1995).

[15]Klein A., "Interface properties of dielectric oxides," *J. Am. Ceram. Soc*. 99(2): 369–387 (2016).

[16]Scott J.F., Watanabe K., Hartmann A.J. and Lamb R.N., "Device models for PZT/Pt, BST/Pt, SBT/Bi ferroelectric memories," *Ferroelectrics* 225: 83-90 (1999).

[17]Takatani S., Kushida-Abdelghafar K., Miki H., "Effect of H_2 annealing on a $Pb/PbZr_xTi_{1-}xO_3$ interface studied by x-ray photoelectron spectroscopy," *Jpn. J. Appl. Phys.,* 36: 435-38 (1997).

[18]Akkopru-Akgun B., Bayer T., Tsuji K., Randall C.A., Lanagan M.T., Trolier-McKinstry S., "Leakage current characteristics and DC resistance degradation mechanisms in Nb doped PZT films," to be submitted to Adv. Elect. Mater.

[19]Robertson J., Warren W.L., Tuttle B.A., Dimos D., and Smyth D.M., "Shallow Pb^{3+} hole traps in lead zirconate titanate ferroelectrics," *Appl. Phys. Lett.,* 63(11): 1519–21 (2012).

[20]Baude P.F., Ye C., and Polla D.L., "Deep level transient spectroscopy characterization of ferroelectric $Pb(Zr,Ti)O_3$ thin films," *Appl. Phys. Lett.* 64: 2670-72 (1994).

[21]Zhao S., Zhang S.J., Liu W., Donnelly N.J., Xu Z. and Randall C.A., "Time dependent dc resistance degradation in lead-based perovskites: $0.7Pb(Mg_{1/3}Nb_{2/3})O_3$ −$0.3PbTiO_3$," *J. Appl. Phys.* 105: 053705-1-7 (2009).

[22]Saremi S., Xu R., Dedon L.R., Mundy J.A., Hsu S-L., Chen Z., Damodaran A.R., Chapman S.P., Evans J.T., and Martin L.W., "Enhanced electrical resistivity and properties via ion bombardment of ferroelectric thin films," *Adv. Mater.* 28: 10750–56 (2016).

[23] Akkopru-Akgun B., Bayer T., Tsuji K., Randall C.A, Lanagan M.T., Trolier-McKinstry S., "The influence of Mn doping on the leakage current mechanisms and resistance degradation behavior in lead zirconate titanate (PZT) films," to be submitted to *Advanced Electronic Materials*

[24]Boukamp B.A., Pham M.T.N., Blank D.H.A., and Bouwmeester H.J.M., "Ionic and electronic conductivity in lead-zirconate-titanate (PZT)," *Solid State Ionics*, 170:239 (2004).

[25]Ossmer H., Slouka C., Andrejs L., Blaha P., Friedbacher G., Fleig J.,"Electrocoloration of donor-doped lead zirconate titanate under DC field stress," *Solid State Ionics*, 281: 49-59 (2015).

[26]Robertson J., Warren W.L., Tuttle B.A., "Band states and shallow hole traps in $Pb(Zr,Ti)O_3$ ferroelectrics," *J. Appl. Phys*. 77: 3975-80 (1995).

[27]Mihara T., Watanabe H., Yoshimori H., Paz de Araujo C.A., Melnick B., MacMillan I.D., "Process dependent electrical characteristics and equivalent circuit model of sol-gel based PZT capacitors," *Integr. Ferroelec.,* 1: 269-91 (1992).

[28]Al-Shareef H.N., and Dimos D., "Leakage and reliability characteristics of lead zirconate titanate thin-film capacitors," *J. Am. Ceram. Soc.,* 80: 3127–32 (1997).

[29]Tagantsev A.K., Kholkin A.L., Colla E.L., Brooks K.G., Setter N., "Effect of ferroelectric polarization on current response of PZT thin films," *Integ. Ferroelect.,* 10: 189-204 (1995).

[30]Trolier-McKinstry S., Chen J., Vedam K., and Newnham R.E., "In situ annealing studies of sol-gel ferroelectric thin films by spectroscopic ellipsometry," *J. Am. Ceram. Soc.*, 78: 1907-13 (1995).

[31]Robertson J. and Chen C.W., "Schottky barrier heights of tantalum oxide, barium strontium titanate, lead titanate, and strontium bismuth tantalite," *Appl. Phys. Lett.* 74: 1168-1170 (1999).

[32]Hwang C.S., Lee B.T., Kang C.S., Kim J.W., Lee K.H., Cho H.J., Horii H., Kim W.D., Lee S.I., Roh Y.B., and Lee M.Y., "A comparative study on the electrical conduction mechanisms of $(Ba_{0.5}Sr_{0.5}TiO_3$ thin films on Pt and IrO_2 electrodes," *J. Appl. Phys.* 83: 3703-13 (1998).

[33]D.C. Lupascu, *in Fatigue in Ferroelectric Ceramics and Related Issue*s (Springer,-Verlag Berlin Heidelberg, pp. 115-116 (2004).

[34] Marincel D.M., Belianinov S.J.A., Okatan M.B., Kalinin S.V., Jackson T.N., Randall C.A., and Trolier-McKinstry S., "A-site stoichiometry and piezoelectric response in thin film $PbZr_{1-x}Ti_xO_3$," *J. Appl. Phys.,* 117: 204104 (2015).

[35]B.A. Tuttle and R.W. Schwartz, "Solution deposition of PZT ferroelectric thin films," *MRS Bull.*, 7: 1876-82 (1996).

[36]S.M. Sze, K.K. Ng, *in Physics of Semiconductor Devices* (Wiley- Interscience, Hoboken, NJ, 2007), pp. 153-70.

[37]T. Baiatu, R. Waser, K.H. Härdtl, "dc electrical degradation of perovskite-type titanates: III, a model of the mechanism," *J. Am. Ceram. Soc*. 73(6): 1663–73 (1990).

[38]Rhoderick E.H. and Williams R.H., *in Metal-Semiconductor Contacts* (Clarendon, New York, pp. 36 (1988).

[39]Dey S., Lee J.-J., and Alluri P., "Electrical properties of paraelectric $(Pb_{0.72}La_{0.28})TiO_3$ thin films with high linear dielectric permittivity Schottky and Ohmic contacts," *Jpn. J. Appl. Phys. Part 1*, 34: 3142-52 (1995).

[40]Zubko P., Jung D.J., and Scott J.F., "Electrical characterization of $PbZr_{0.4}Ti_{0.6}O_3$ capacitors," *J. Appl. Phys*. 100: 114112 (2006).

[41]Dawber M., Scott J.F., "Calculation of Schottky barrier height of platinum/lead zirconate titanate interface," *Integ. Ferroelec.*, 38: 161-9 (2001).

[42]Akkopru-Akgun B., Marincel D., Bayer T., Randall C., Lanagan M.T., Trolier-McKinstry S., "Thermally stimulated depolarization current measurements on degraded lead zirconate titanate films," to be submitted to *Appl. Phys. Lett.*

Chapter 7

Conclusions and Future Work

7.1 Conclusions

This study investigated the role of defect chemistry in the development of imprint, the aging of ferroelectric properties, and the DC resistance degradation of PZT films. Defects that can contribute to ionic and electronic conductivity in PZT films were explored using EELS, TSDC, DLTS and in-situ impedance analysis in order to provide a deeper understanding of electrical breakdown and the aging characteristics of PZT films. The variation in nature and concentration of defects was controlled by introducing different levels of acceptor (Mn) and donor (Nb) ions into PZT films; 0.5-4% Nb and Mn doped PZT (Zr/Ti: 52/48) thin films were produced using chemical solution deposition. Phase pure, randomly oriented, and crack free PZT films were obtained. Lifetime-determining defect sites and associated charge transport mechanisms responsible for aging and electrical degradation were revealed for both acceptor and donor doped PZT films.

The underlying mechanism responsible for formation of internal field upon thermal poling of PZT films was elucidated in Nb and Mn doped PZT films and the link between imprint and high temperature aging was investigated. A higher magnitude of internal field was generated in Mn doped PZT films compared to their Nb doped counterparts after thermal poling at temperatures from 25°C to 200°C under an electric field of -240 kV/cm (the electrical field was driven from top Pt to bottom Pt electrode) for 30 min.; the internal field ranged from 3 to 32 kV/cm and 0.5 to 18 kV/cm for PMZT and PNZT films, respectively. The larger internal field in Mn doped PZT films were

related to a higher oxygen vacancy concentration on Mn doping. Depending on the Mn concentration in the PZT films, the estimated activation energy for formation of the internal field changed from 0.5±0.06 to 0.8±0.1 eV, suggesting that short range migration of oxygen vacancies and defect dipole alignment are responsible for the induced imprint in PMZT films. For Nb doped PZT films, on the other hand, higher activation energies in the range between 0.8±0.1 and 1.2±0.2 eV that are similar to the potential barrier height for charge injection were found, suggesting that thermionic emission of electrons and subsequent trapping by Ti^{4+} contributes to the formation of imprint in PNZT films.

The thermally induced internal field films enhances remanent piezoelectric properties, $d_{33,f}$, in both PMZT and PNZT films. However, the enhancement in properties is more noticeable in PMZT films due to larger internal fields introduced upon thermal poling. The $d_{33,f}$ almost doubled in 4% Mn doped PZT thin films following thermal poling at 200°C. For 4% Nb doped PZT films, on the other hand, $d_{33,f}$ only increased by 30% after the same poling treatment. The thermally induced imprint also significantly reduces aging in PMZT films, indicating higher stability of the polarization state possibly due to a strong defect association between $Mn_{Ti}^{\acute{}}$ and $V_O^{\bullet\bullet}$ ions. The higher aging rates in Nb doped PZT films indicate that poled state was not retained with time, presumably due to relaxation of trapped charges upon high temperature aging.

The correlation between defect chemistry, leakage currents, and DC resistance degradation was also investigated for Nb and Mn doped PZT films. The dominant conduction mechanism and associated charge transport mechanisms responsible for leakage current rise upon DC resistance degradation were explored. In the pristine state, the Poole-Frenkel mechanism controls the leakage current at lower electric fields for both

Nb and Mn doped PZT films. To elucidate bulk controlled conduction mechanisms, DLTS and Impedance spectroscopy were used. Nb doped PZT films were found to be nearly intrinsic; (1) hole hopping between Pb^{2+} and Pb^{3+} and electron trapping by Ti^{4+} were observed. In contrast to findings of Nb doped PZT films, no signature for electron trapping by Ti^{4+} sites was detected for Mn doped PZT films. Instead, (1) hole hopping/trapping between Pb^{2+} and Pb^{3+}, (2) hole trapping by Mn^{2+}/Mn^{3+}, as well as (3) hole migration between lead vacancies were three main mechanisms that contribute to bulk controlled Poole-Frenkel conduction in Mn doped PZT films. The contribution of lead vacancies to the electronic conduction diminishes with Mn concentration due to increased concentration of hole trapping Mn^{2+}/Mn^{3+} sites.

Beyond a critical electrical field, Schottky emission is responsible for the leakage current in Nb and Mn doped PZT films. The transition electric field from Poole-Frenkel to Schottky emission varies depending on oxygen vacancy concentration in the PZT films; it decreases from 172 to 82 kV/cm, accompanied by a concurrent change of Schottky barrier height from 1.24 to 0.95 eV with decreasing Nb concentrations, which is attributed to Fermi level pinning by oxygen vacancies. Similarly, the potential barrier height gradually decreased from 1.17±0.04 to 0.72±0.04 eV with increasing Mn content in PZT films due to strong Fermi level pinning by oxygen vacancies.

The major carrier type that leads to the increase in leakage current upon electrical degradation and the associated charge transport mechanisms were also explored. The drift of oxygen vacancies under a DC bias was monitored using TSDC and the change in the defect distribution that occurs during electrical degradation was investigated. A

depolarization current peak with an activation energy of 0.6 eV was found for both Mn and Nb doped PZT films, which is associated with drift of oxygen vacancies.

Significant differences were found between DC resistance degradation characteristics of Mn and Nb doped PZT films. In Nb doped PZT films, the electromigration and subsequent accumulation of oxygen vacancies under a DC bias result in reduction in potential barrier height, which in turn accelerates electron injection from the cathode into the bulk of the PZT films. The electrons that compensate for oxygen vacancies near the cathode are trapped on Ti atoms. As a result, electron hopping between Ti^{3+} and Ti^{4+} was confirmed by TSDC and electron energy loss spectroscopy (EELS). The chemical shift in Ti $L_{2,3}$ to lower energy losses and appearance of shoulders on the t_{2g} and e_g near the cathode Pt/PNZT interface proves the presence of Ti^{3+} cations. The electrical degradation rate drops with increasing Nb concentration due to lower oxygen vacancy concentrations at higher Nb levels in PZT films. The number of accumulated oxygen vacancies near the cathode region of degraded Nb doped PZT films drastically decreased from 2.08 ± 0.05 x10^{19}/cm^3 to 1.54 ± 0.04 x10^{18}/cm^3 with increasing Nb concentration from 0.5 to 4 mol%.

In contrast to Nb doped PZT films, no significant change in the potential barrier height for charge injection was observed after electrical degradation of Mn doped PZT films. The transition electric field from Poole Frenkel conduction to Schottky emission shifted from 145 to 182 kV/cm after degradation, which could be attributed to suppression of the maximum electrical field in the depletion region, which determines the potential barrier height lowering and thus leakage current increase upon electrical degradation. It is possible that electrons needed to compensate for the charge of the

oxygen vacancies at the cathode are trapped at Mn sites. EELS results confirm that the oxidation state of Ti remains the same towards to the cathode of degraded Mn doped PZT films. Moreover, no depolarization current peak associated with electron hopping between Ti^{3+} and Ti^{4+} sites was observed in electrically degraded Mn doped PZT films. This strongly implies the electrons can be preferentially trapped at Mn sites rather than Ti atoms, consistent with the location of the energy levels in the energy band diagram. Since the Mn ions are widely distributed within the PZT film due to their low concentration, the trapped electrons are also spread out, which prevents accumulation of electronic charges at the Pt/PMZT interface. This modifies the electric field distribution in the depletion region; the maximum electric field drastically diminishes at the Pt/PMZT interface, which in turn decreases Schottky barrier lowering and leakage current rise upon degradation. The improvement in electrical degradation becomes more noticeable with increasing Mn concentration from 0.5 to 4 mol% despite higher oxygen vacancy concentrations at higher Mn levels in PZT films; The MTTF escalates remarkably from 1.47±0.2 to 21.4±0.8 hr with increasing Mn concentration from 0.5 to 4 mol%. It is possible that higher Mn concentrations enhance hopping conduction, leading to a dramatic increase in the hole concentrations near the depletion region that might act as recombination centers for electrons that compensate the oxygen vacancies, which in turn improves electrical degradation.

The role of interfacial defect chemistry on charge transport and DC resistance degradation was also investigated in 2% Nb doped PZT films with top and bottom Pt electrodes. The electrical reliability characteristic of Nb doped PZT films was found to be strongly dependent on the voltage polarity; the MTTF remarkably increased from 4.8±0.7

to 7.6±0.4 hours when the top Pt electrode was biased negatively. The polarity dependent lifetime is correlated with variation in the interfacial defect chemistry near the top and bottom Pt/PNZT interfaces. EDX mapping studies revealed that (1) more severe PbO loss near the bottom Pt electrode leads to an oxygen vacancy gradient across the film thickness. The higher initial oxygen vacancy concentration near the bottom Pt electrode is responsible for lower potential barrier height for electron injection and a lower transition electric field from Poole Frenkel to Schottky emission in the pristine state, (2) Ti/Zr segregation in PZT films also alters the interfacial defect chemistry with formation of Ti-rich and Zr-rich layers near the bottom and top Pt/PNZT interfaces, respectively. This reduces propensity for electron trapping by Ti^{4+} near the top Pt interface.

Upon degradation, a strong increase in leakage current was always observed in the direction in which PNZT films were degraded. This strongly indicates that an electron injection from reverse biased Pt electrode (cathode) into the bulk of the films determines the leakage current increase upon degradation. The Schottky barrier lowering and resultant enhancement in leakage current is more pronounced when the bottom Pt electrode was biased negatively due to higher initial oxygen vacancy concentration that induce additional injection of charges. Moreover, the depletion width may decrease due to higher donor concentrations, mostly oxygen vacancies. Both lower potential barrier height and depletion width accelerates charge injection upon electrical degradation, which in turn leads to a higher leakage current rise upon degradation and shorter lifetime.

7.2 Future Work

7.2.1 Electronic and ionic conductivity of PZT films annealed under different PbO activities

In this study, it has been shown that oxygen vacancy migration and subsequent charge redistribution near the cathode and anode regions contribute to the electrical degradation in PZT films. This occurs through multiple pathways. First, the effective density of charges in the depleted regions depends on the oxygen vacancy concentration. Second, oxygen vacancies contribute to ionic conductivity. Third, a high oxygen vacancy concentration in PZT films modulates the potential barrier height for electron injection through Fermi level pinning, which accelerates charge injection upon electrical degradation. Fourth, a distribution in oxygen vacancy concentration through the thickness of PZT films leads to voltage polarity dependent lifetime in Nb doped PZT films.

Thus, controlling oxygen stoichiometry in PZT films is crucial to improve the DC resistance behavior. However, it is very difficult to control stoichiometry absolutely in PZT films due to PbO volatility upon annealing above 400°C. As shown above, even donor doped PZT films have a significant concentration of oxygen vacancies, increasing both ionic and electronic conductivity. Electronic conductivity changes from p-type to n-type at temperatures around 150°C; this transition is strongly dependent on the oxygen stoichiometry. Below 150°C, hole hopping between Pb^{2+} and Pb^{3+} as well as hole trapping by lead vacancies dominate electronic conduction; electronic trapping by Ti^{4+} controls the electronic conduction above 150°C. Therefore, control of the nature and concentration of the majority carriers as a function of the PbO stoichiometry is essential to better understanding charge transport mechanisms leading to electrical degradation.

Preventing such degradation will improve the performance and reliability of piezoMEMS.

The oxygen partial dependence of the conductivity in PZT ceramics was studied by a number of researchers to understand the predominant charge carriers at different temperatures. Nonaka et al. investigated the influence of Pb-deficiency on the conductivity of PZT with a Zr/Ti molar ratio of 50/50.[1] A significant increase in conductivity was observed in Pb deficient PZT films. Furthermore, Boukamp et al. found that both ionic and electronic conductivity are strongly influenced via thermal treatment and the oxygen partial pressure; the lead vacancies are compensated by oxygen vacancies and holes trapped on the lead sites, resulting in hopping conduction for PZT samples annealed in N_2.[2] Recently, Slouka et al. showed that Nd doped PZT exhibit hole conduction at high oxygen partial pressures, while under reducing atmosphere, electron conduction becomes predominant.[3] However, the correlation between PbO stoichiometry and the electrical conductivity of PZT films has not been investigated in detail. A systematic study on the role of annealing temperature and PbO activity on the n-p transition is needed for PZT films. It is anticipated that the PbO partial pressure dependence of electrical conductivity will yield important information about the charge carriers and/or dominant point defects responsible for the electrical current in PZT films.

To pursue such a study, it is suggested that PZT films be grown using established routes for chemical solution deposition or sputter deposition. Of particular concern is the possibility of PbO loss either to the bottom electrode or to the atmosphere during the high temperature crystallization steps. Following growth, the PbO content should be adjusted using thermodynamic, rather than kinetic control of the defect chemistry. This could be

done using the PbO control furnace shown in Figure 7.1. For example, large PZT-coated wafers could be subdivided and each piece annealed at different PbO activities. This will allow the PbO partial Schottky defect concentration of films prepared by any method to be controlled without significantly changing the grain size or grain orientation. All samples will then be characterized by X-ray diffraction and field emission scanning electron microscopy to ensure that no second phases develop.

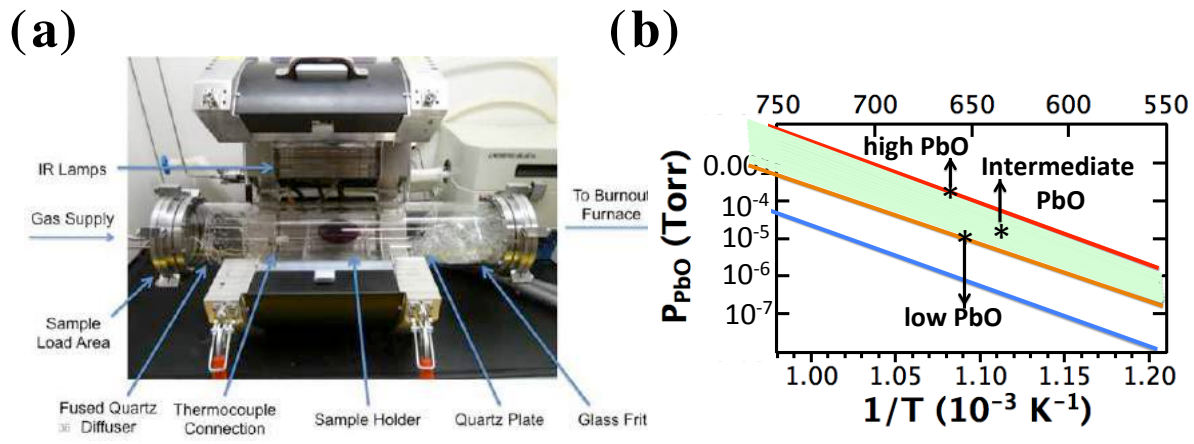

Figure 7.1 *Lead oxide annealing furnace built at Penn State in order to control PbO stoichiometry in thin films, (b) The partial pressure of PbO required for equilibrium of* $PbO(g) \rightarrow PbO(s)$ *(red line),* $PbZrO_3 \rightarrow PbO(g) + ZrO_2$ *(orange line), and* $PbTiO_3 \rightarrow PbO(g) + TiO_2$ *(blue line) at different temperatures.*

The PbO pressure dependence of the PZT conductivity could be assessed via impedance spectroscopy in order to determine the dominant charge carriers. The conductivity as a function of partial pressure of PbO can be described via:

$$\sigma = \sigma_e + \sigma_h + \sigma_i \qquad \text{Equation 7.1}$$

$$\sigma = en\mu_e + ep\mu_h + en_i\mu_i \qquad \text{Equation 7.2}$$

where the subscripts e, h, i represents the electrons, holes, and ions respectively and strongly depends on the concentration n_j, charge e_j and mobility μ_j of the charge carriers.

When PbO evaporates, charge compensation is achieved either by creation of oxygen vacancies or by change in the concentrations of holes and electrons.

$$Pb_{Pb}^{X} + O_{O}^{X} \rightarrow V_{Pb}'' + V_{O}^{\bullet\bullet} + PbO(g) \qquad \text{Equation 7.3}$$

$$2[V_{Pb}''] + [e'] = 2[V_{O}^{\bullet\bullet}] + [h^{\bullet}] \qquad \text{Equation 7.4}$$

Equilibration with oxygen from the atmosphere during cooling or sintering may suppress oxygen vacancies by:[3, 4, 5]

$$\frac{1}{2}O_2 + \rightleftarrows V_{Pb}'' + O_{O}^{X} + 2h^{\bullet} \qquad \text{Equation 7.5}$$

and thus hole conduction could dominate and the PZT films become slightly p-type even when donor doped.[4, 6] It is anticipated that the slope of log σ versus log PbO will depend on the PbO activity. A positive slope (associated with p-type conduction) is expected in PZT films annealed at higher PbO (Figure 7.2). The transition from p-type to n-type conduction at different PbO activities and temperatures will be explored. The comparison between experimental plots of log σ versus log PbO and the theoretical isotherms using the Brouwer approximation will be done to describe the nature of predominant point defects at distinct PbO activities.

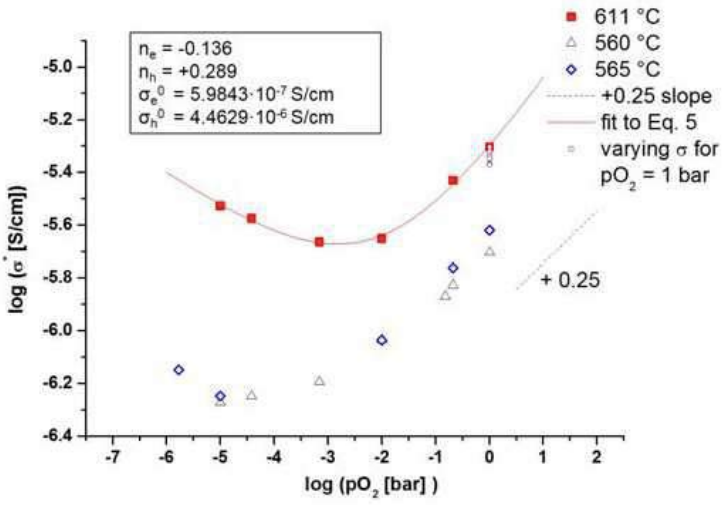

Figure 7.2 *The dependence of conductivity on oxygen partial pressure at 560, 565, and 611°C. Figure reproduced from reference 3.*

Further information regarding ionic contributions to the conductivity of PZT films could be attained using ^{18}O-tracer exchange measurements and secondary ion mass

spectroscopy (SIMS) to explore ionic defects, mainly oxygen vacancies, and ionic conduction in PZT films annealed at different PbO activities.

Analysis of oxygen vacancy transport via Time-of-Flight Secondary Ion Mass Spectrometry (ToF-SIMS):

ToF-SIMS can quantify ion diffusion and provides 2D and 3D information about surface chemical composition as well as depth concentration profile. Slouka et al. studied the composition dependence of the ^{18}O tracer concentration in PZT ceramics. Depth profiles of the concentration for undoped, acceptor, and donor doped PZT ceramics are shown in Figure 7.3.[7] Higher ^{18}O tracer concentrations were observed at a depth of 125 nm in Fe doped PZT ceramics compared to donor-doped or undoped PZT ceramics. Furthermore, higher tracer concentrations were found at grain boundaries, indicating fast grain boundary diffusion in La doped PZT ceramics.[7] Similar ^{18}O tracer exchange experiments can be performed in PZT thin film samples annealed under different PbO activities to attain more detailed insight into field driven migration of oxygen vacancies in PZT films, as suggested by Wang et al.[8] At 450°C, tracer distribution exhibited two distinct regions; the tracer diffusion in the near-surface region is faster compared to the bulk of the polycrystalline PZT film. This was attributed to an equilibrium depletion of oxygen vacancies near the surface.

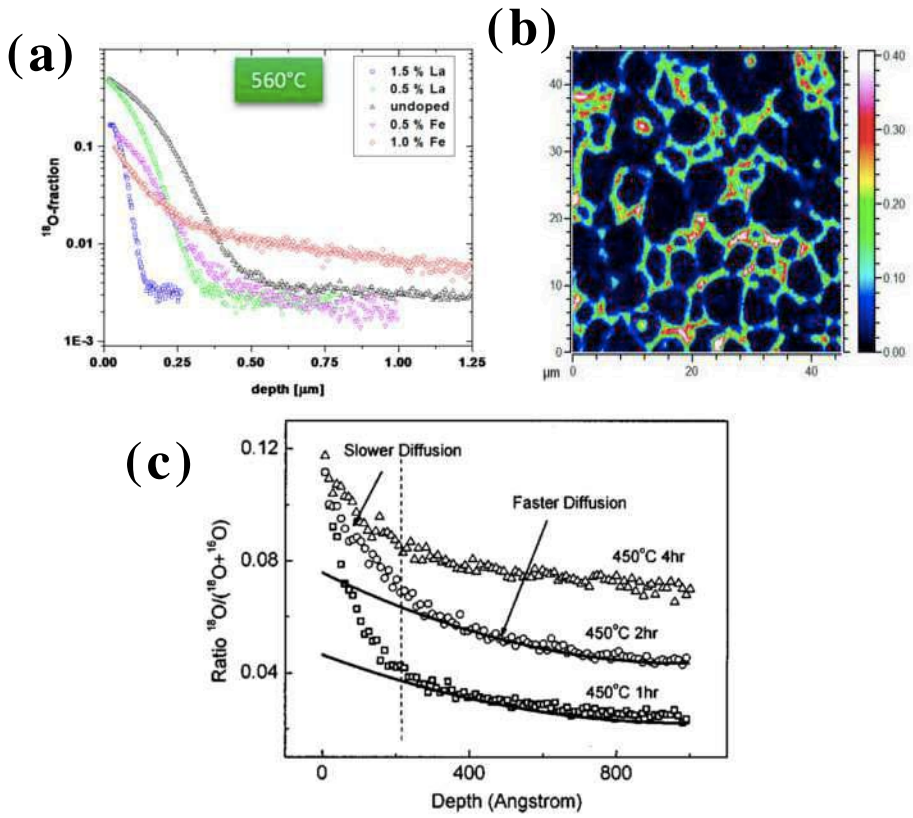

Figure 7.3 *(a) Tracer depth profile of undoped, La, and Fe doped PZT at 560°C* [7]*, (b) top view image of tracer distribution after tracer exchange experiments at 560°C for 30 minutes* [7]*, (c) Tracer depth profile of PZT film after exchange experiment at 450°C for 1, 2, and 3h.*[8]

The thin film samples should be first exposed to tracer oxygen at different temperatures and subsequently monitored via SIMS. The oxygen isotropic fractions can be estimated from measured secondary ion intensities (I_{18_O} and I_{16_O})[7, 9]

$$f_{18_O} = \frac{I_{18_O}}{I_{16_O} + I_{18_O}} \qquad \text{Equation 7.6}$$

The tracer depth profile can be determined via monitoring sputtering times and normalizing it to measured sputter crater depths. Since lower PbO pressures enhance the oxygen vacancy concentration, a higher tracer concentration is expected. Then, bulk tracer diffusion coefficient can be calculated using equation 7:[9]

$$\frac{f_{^{18}O}-f_{bg}^{\ 18}O}{f_{gas}^{\ 18}O-f_{bg}^{\ 18}O}=(1-\mathrm{erf}\left(\frac{X}{2\sqrt{D_b^*\,t}}\right))-e^{\frac{k^*X}{D_b^*}+\frac{k^{*2}t}{D_b^*}}\,[1-\mathrm{erf}\,(\frac{X}{2\sqrt{D_b^*\,t}}+k^*\sqrt{\frac{t}{D_b^*}})]$$ Equation 7

where $f_{bg}^{\ 18}O$ is the natural abundance of tracer oxygen, t is the diffusion time, x is the depth, D_b^* is the bulk tracer diffusion coefficient, $f_{gas}^{\ 18}O$ is the fraction of tracer oxygen in the gas phase, k^* is the oxygen exchange factor, and $f_{bg}^{\ 18}O$ the natural abundance of tracer oxygen.

Relative changes in tracer concentration and diffusion coefficients with variation in PbO partial pressure would enhance understanding of the ionic conductivity in PZT films. The variation in depth of tracer concentration with PbO activity near surface region and the bulk of the film could be explored, which provides insight into interfacial defect chemistry effect on ionic conductivity. Together with the impedance results, the required PbO partial pressure that suppress ionic and electronic conductivity can be revealed, leading to better understanding of the processing parameters needed to control the leakage current rise and electrical breakdown in PZT films.

7.2.2. The contribution of electron/hole trapping to DC resistance degradation in acceptor doped PZT films

The findings in this thesis indicate that while charge injection from Pt electrode into Mn doped PZT films is controlled by Schottky emission, the drift of injected charges is dominated by bulk Poole-Frenkel conduction. Transport of injected charges in Mn doped PZT films takes place via carrier hopping between redox active Mn trap sites (Mn^{2+}, Mn^{3+}, Mn^{4+}) upon DC resistance degradation. Electromigration of oxygen vacancies along the applied electric field results in generation of holes near the anodic regions and electrons near the cathodic regions. In the presence of redox active acceptor

ions, formation of free electrons and holes can be suppressed by valence change from $A_{Ti}^{X} \rightarrow A_{Ti}'$, $A_{Ti}' \rightarrow A_{Ti}''$ in the cathodic region and $A_{Ti}' \rightarrow A_{Ti}^{x}, A_{Ti}'' \rightarrow A_{Ti}'$ in the anodic region, respectively. It is believed that electron/hole trapping at redox active acceptor ions is responsible for improvement in resistance degradation behavior of PZT ceramics. This yielded a significant improvement in the resistance degradation of Mn doped PZT films with increasing Mn concentration, even though incorporation of Mn increases the concentration of mobile oxygen vacancies.

The contribution of electron/hole trapping to electrical degradation is strongly dependent on the relative concentration of A_{Ti}^{X}, A_{Ti}', and A_{Ti}''. Formation of electrons and holes can be equivalently suppressed when acceptor ions with different oxidation states exist in the same ratio. In this thesis, it was found that the $Mn^{2+/3+}$ ions in PZT films are ionized to $Mn^{3+/4+}$ ions through absorbing oxygen from the atmosphere upon heating at 320°C. This leads to a variation in the valence state of Mn ions through the thickness of the PZT films and contribytes to polarity dependent electrical degradation and lifetimes. The questions that need to be further clarified are: (1) how the annealing atmosphere, PO_2, influences the distribution of valence states for Mn ions in PZT films, (2) the optimal concentrations of different Mn valence states to suppress electrical degradation in PZT films, and (3) whether similar lifetime increases can be observed in PZT films doped with fixed valence state acceptors like Mg. To elucidate these questions, Mn and Mg doped PZT films should be prepared by chemical solution deposition. Subsequently, the films should be annealed under oxidizing and reducing atmosphere for different times. The relative ratio of different valence state of Mn ions is expected to be strongly dependent on both the PO_2 and post-annealing time.[11-14] Hayashi et al. reported that the

concentration of Mn^{4+} ions significantly reduced after annealing $PbTiO_3$ in a reducing atmosphere (Figure 7.4).[11]To assess the valence state, EPR (Electron Paramagnetic Resonance) analysis should be utilized.

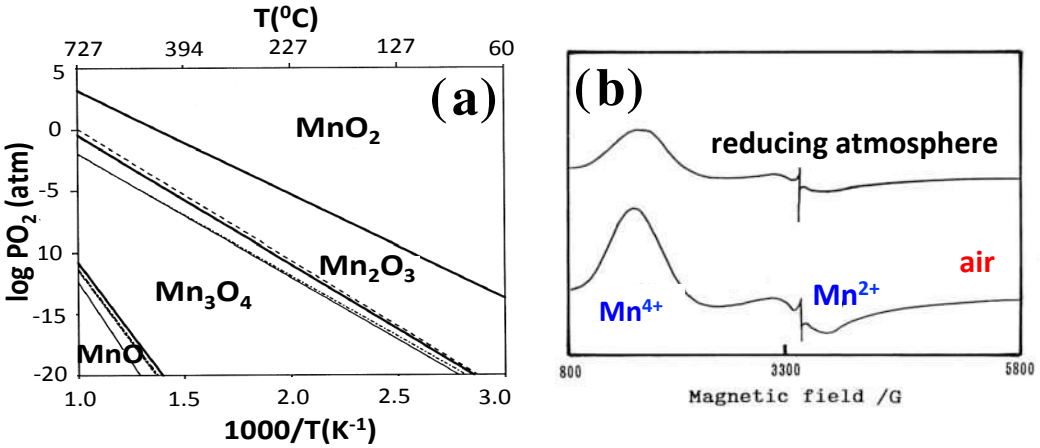

Figure 7.4 (a) *Phase diagram of manganese dioxide, plotted for temperature versus oxygen partial pressure,*[10] *4(b) EPR spectra of $PbTiO_3$ films annealed under reducing atmosphere and air.*[11]

Additionally, the dissociation of defect dipoles, i.e. $(Mn'_{Ti} - V_O^{\bullet\bullet})^{\bullet}$ and $(Mn''_{Ti} - V_O^{\bullet\bullet})$ upon electrical degradation should be monitored using in-situ EPR measurements. It is anticipated that the EPR resonance signal attributed to any defect complexes will decrease with increasing degradation time. Because of the Jahn-Teller distortion between Mn^{3+} and oxygen vacancies, higher association energy and therefore longer degradation times would be required for dissociation of $(Mn'_{Ti} - V_O^{\bullet\bullet})^{\bullet}$ compared to $(Mn''_{Ti} - V_O^{\bullet\bullet})$ defect dipoles. In-situ EPR measurements will also provide insight into the real time change in local defect distribution throughout the PZT films upon electrical degradation. Because the local concentration of oxygen vacancies will increase in the cathode region, accompanied by creation of electrons, it is expected that this will change the local electrical field distribution in the sample.

The maximum electric field at Schottky interface, which is responsible for potential barrier lowering and the leakage current rise upon DC resistance degradation, is

influenced by the density of electron or hole traps and by the dopant concentrations in the depletion layer as described in equation 8 and 9.[15]

$$E_m = \sqrt{\frac{2qN_{eff}}{\epsilon_i \epsilon_0}\left(V + V_{bi} - \frac{kT}{q}\right)} \quad \text{Equation 8}$$

$$N_{eff}(T) = \sum h_i(T) - \sum n_j(T) + N_{doping} \quad \text{Equation 9}$$

where h_i is the density of the i^{th} trap level for holes, n_j is the density of the j^{th} trap level for electrons, and N_{doping} is the doping density. In the presence of Mn trap sites, suppression of either free electron and holes or carriers trapped on Ti^{3+}, for example, could change the electrical field in the depletion layers. Depending on the relative densities of different valence states for the Mn ions and their energy depth in the band diagram, the magnitude of N_{eff} and thereby E_m at the interface as well as density of injected charges would differ. The variation in electrical field distribution near the cathode and anode upon DC resistance degradation could be investigated using Kelvin Probe Microscopy.[16] This would also any change in the electric field distribution in the depletion layer as a result of electron/hole trapping via Mn ions to be probed. Furthermore, the local electric field enhancement at the interface with increasing degradation time can be monitored.

7.2.3 The influence of DC electrical degradation on ferroelectric properties in PZT films

Preliminary work has demonstrated that the functional properties or PZT films are adversely affected by DC resistance degradation. Figure 7.5 shows the change in reversible and irreversible Rayleigh coefficients in Mn and Nb doped PZT films after degrading under an electric field of 350 kV/cm at 180°C for 4, 7, or 14h. It can be seen

that both the reversible and irreversible Rayleigh response of PZT films gradually decreased with increasing degradation time. The reduced reversible Rayleigh parameter in Mn and Nb doped PZT films can attributed to (1) the loss of switchable units or/and the effective electrode area that contributes to the polarization response as a result of delamination and/or burning of electrodes, (2) the development of a DC bias. On the other hand, the irreversible Rayleigh coefficient, α, decreased considerably in Mn and Nb doped PZT films. However, the decrease in irreversible Rayleigh parameter is more pronounced at lower frequencies, indicating that the slowest moving domain walls are being lost from the distribution as the film was degraded.

Migration and subsequent redistribution of charges, especially oxygen vacancies, upon electrical degradation leads to domain wall pinning (immobilization of domain walls), which in turn suppresses the domain wall mobility. Oxygen vacancies that accumulate at domain walls upon degradation tailor the domain wall charge distribution and polarization within the domain due to interaction between bound charges on the domain walls and oxygen vacancies.[17-19] To better understand the microscopic mechanism underlying the interaction between mobile oxygen vacancies and domain walls, it is proposed that Single Beam Laser Interferometer (SBLI) measurements could be used to quantify the piezoelectric nonlinearities locally upon electrical degradation.[18] The Rayleigh law could be used to evaluate the variation in irreversible contribution of the domain walls movement to the nonlinear response as degradation progresses.[17]

The spatial variation in the effective piezoelectric $d_{33,f}$ coefficients could be measured using SBLI, as described elsewhere.[20] The amplitude dependence of the dielectric permittivity should be measured simultaneously using an LCR meter. When

motion of purely ferroelectric domain walls contributes to the piezoelectric response due to the Rayleigh behavior for amplitude dependence can be described as:[19]

$$d = d_{init} + \alpha_d E_0 = d_0[1 + (\beta + \beta' E_0)\sin(wt)] + \alpha_d E_0 \qquad \text{Equation 10}$$

where d is the piezoelectric coefficient, w is the angular frequency, t is the time, E_0 is the amplitude of the ac electric field, β and β' are scaling factors for the frequency and field dependence of the reversible Rayleigh coefficient d_{init} and α_d is the irreversible piezoelectric Rayleigh coefficient. $\frac{\alpha_d}{d_{init}}$ and $\frac{\alpha_\varepsilon}{\varepsilon_{init}}$ should be extracted from the ac field dependence of the piezoelectric and dielectric response on degradation.

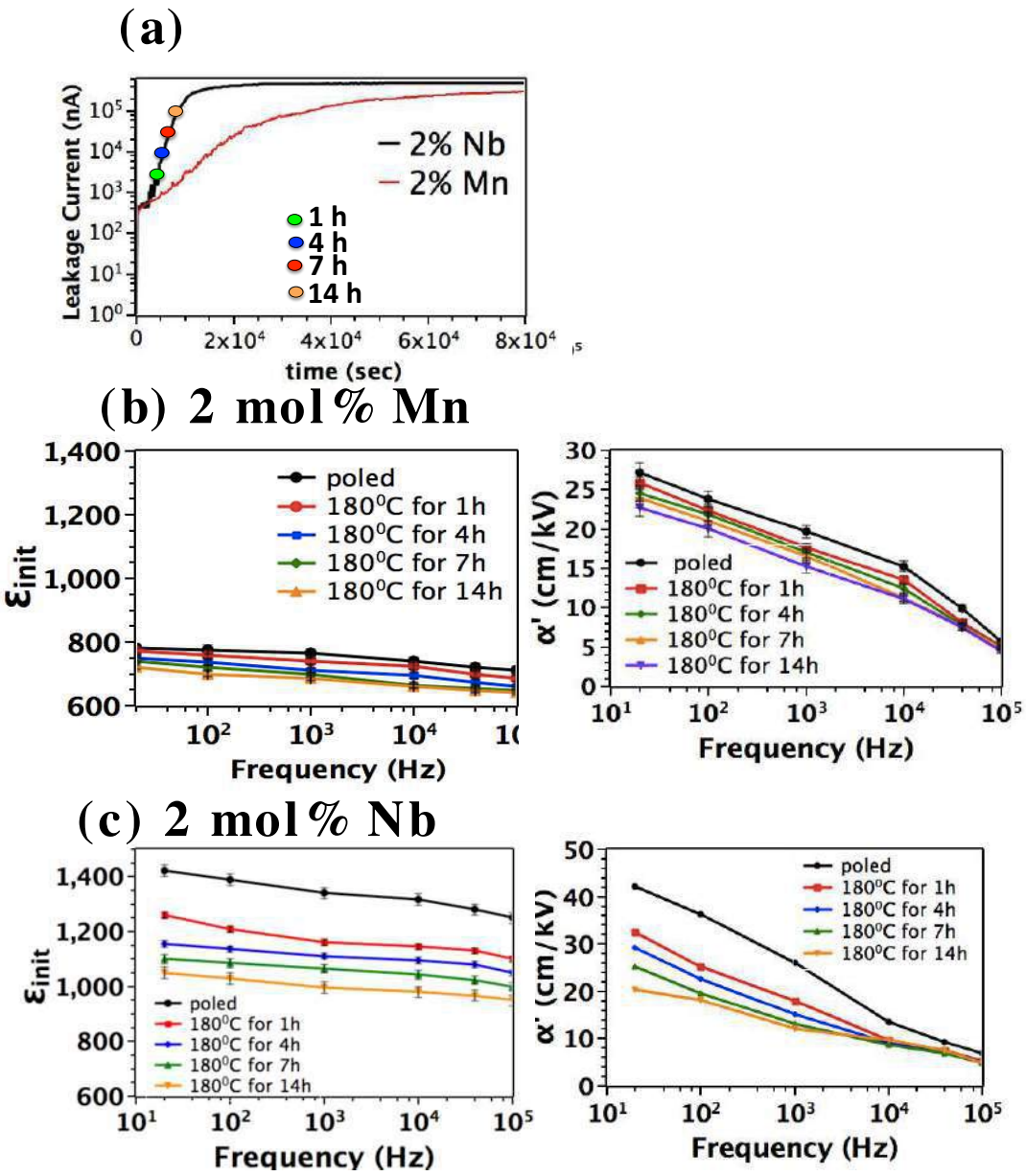

Figure 7.5 *(a) Time dependence of leakage current in 2% mol Mn and Nb doped PZT films, The change in reversible and irreversible Rayleigh parameters in (b) 2 mol% Mn , (c) 2 mol% Nb doped PZT films after electrical degradation under an electric field of 350 kV/cm at 180°C for 1,4, 7, or 14h.*

7.3 References

[1]Nonaka K., Akiyama M., Hagio T., Takase A., "Effect of Pb/(Zr+Ti) molar ratio on the photovoltaic properties of lead zirconate-titanate ceramics", *J. Europ. Ceram. Soc.*, 19: 1143-48 (1999).

[2]Boukamp B.A., Pham Mai T.N., Blank Dave H.A., Bouwmeester Henny J.M., "Ionic and electronic conductivity in lead–zirconate–titanate (PZT)," *Solid State Ionics,* 170: 239–254 (2004).

[3]Slouka C., Andrejs L., and Fleig J., "Defect chemistry and transport properties of Nd doped $Pb(Zr_xTi_{1-x})O_3$," *J. Electroceram.*, 33: 221-39 (2014).

[4]Donnelly N.J. and Randall C.A., "Pb loss in $Pb(Zr,Ti)O_3$ ceramics observed by in situ ionic conductivity measurements," *J. Appl. Phys.*, 109: 104107-1-6 (2011).

[5]Pan M-J., Park S-E., Park C.W., Markowski K.A., Yoshikawa S., Randall C.A., "Superoxidation and electrochemical reactions during switching in $Pb(Zr,Ti)O_3$ ceramics," *J. Am. Ceram. Soc.*, 79:2971-74 (1996).

[6]Prisedsky V.V., Shishkovsky V.I. and Klimov V.V. "High-temperature electrical conductivity and point defects in lead zirconate-titanate," *Ferroelectric*s 17: 465-68 (1978).

[7]Slouka C., Kainz T., Navickas E., Walch G., Hutter H., Reichmann K., and Fleig J., "The effect of acceptor and donor doping on oxygen vacancy concentrations in lead zirconate titanate (PZT)," *Materials*," 9: 945-1-22 (2016).

[8]Wang R-V., McIntyre P.C., "^{18}O tracer diffusion in $PbZrTiO_3$ thin films: A probe of local oxygen vacancy concentration," *J. Appl. Phys.*, 97: 023508-1-8 (2005).

[9]Holzlechner G., Kubicek M., Hutter H. and Fleig J., "A novel ToF-SIMS operation mode for improved accuracy and lateral resolution of oxygen isotope measurements on oxides," *J. Anal. At. Spectrom.*, 28: 1080–1089 (2013).

[10]Fritsch S., Navrotsky A., "Thermodynamic properties of manganese oxides," J. Am. Ceram. Soc. 79: 1761-68 (1996).

[11]Hayashi K., Ando A., Hamaji Y., Sakabe Y. "Study of the valence state of the manganese ions in $PbTiO_3$ ceramics by means of ESR," *Jpn. J. Appl. Phys*., 37: 5237-40 (1998).

[12] Keeble D.J., Li Z., and Paindexter E.H., "Electron paramagnetic resonance of Mn^{4+} in $PbTiO_3$," *J. Phys: Condens. Matter*., 7: 6327-33 (1995).

[13]Ikushima H., Hayakawa S., "Electron Spin resonance of Mn^{2+} in lead titanate," *J. Phys. Soc. Japan*, 27: 414-419 (1969).

[14]Eichel R-A., "Structural and dynamic properties of oxygen vacancies in perovskite oxides—analysis of defect chemistry by modern multi-frequency and pulsed EPR techniques," *Phys. Chem. Chem. Phys.*, 13: 368–384 (2011).

[15]Pintille L., Vrejoiu I., Hesse D., LeRhun G., and Alexe M., "Ferroelectric polarization-leakage current relation in high quality epitaxial $Pb(Zr,Ti)O_3$ films, *Phys. Rev. B*, 75: 104103 (2007).

[16]Son J.Y., Bang S.H., and Choa J.H., "Kelvin probe microscopy study of $SrBi_2Ta_2O_9$ and $PbZr_{0.53}Ti_{0.47}O_3$ thin films for high-density nonvolatile storage devices," *Appl. Phys. Lett.,* 82: 3505-7 (2003).

[17]Tagantsev A.K., Stolichnov I., Colla E.L., and Setter N., "Polarization fatigue in ferroelectric films: Basic experimental findings, phenomenological scenarios, and microscopic features," *J. Appl. Phys.*, 90: 1387-1402 (2001).

[18]Morozov M.I., and Damjanovic D., "Hardening-softening transition in Fe-doped ceramics and evolution of the third harmonic of the polarization response," *J. Appl. Phys.*, 104: 034107 (2008).

[19]Bassiri Gharb N., Trolier-McKinstry S., and Damjanovic D., "Piezoelectric nonlinearity in ferroelectric thin films," *J. Appl. Phys*., 100: 044107 (2006).

[20]Shetty S., Yang J.I., Stitt J., and Trolier-McKinstry S., "Quantitative and high spatial resolution d_{33} measurement of piezoelectric bulk and thin films," *J. Appl. Phys.*, 118: 174104 (2015).

Appendix: The role of interfacial defect chemistry in DC resistance degradation of Mn doped PZT films

Figure A.1 illustrates the voltage polarity dependence of current density-time (J-t) response of 2% Mn doped PZT films (PMZT) with Pt top and bottom electrodes. As shown in the Figure A.1, the current increase is strongly dependent on the sign of applied voltage. When a positive voltage was applied to bottom Pt electrode (field-up), leakage current rise upon electrical degradation occurs more abruptly. On the other hand, when a positive bias was applied top Pt electrode (field-down), a more gradual current increase with time was observed. Median time to failure (MTTF) for field-up and field-down polarities is 9.8±0.7 and 3.1±0.4, respectively. These results clearly demonstrates that interfacial defect chemistry determines the I-t characteristics and lifetime of 2% Mn doped PZT films.

To further investigate the variation in the charge transport mechanism with voltage polarity, I-V measurements were conducted on 2 mol% Mn doped PZT films before and after degradation at 180°C under an electric fields of -350 kV/cm (field-down) and 350 kV/cm (field-up) for 12 h (Figure A.2). The leakage current of undegraded PMZT films exhibits significant voltage polarity dependence; the current-voltage characteristics are remarkably asymmetric for negative and positive bias. This presumably occurs due to variation in (1) the oxygen vacancy concentration, and (2) the Mn valence state through the thickness of PMZT films. After field-up electrical degradation, the absolute value of current was found to increase in the direction in which the PMZT films had been degraded; the leakage current increase upon DC resistance

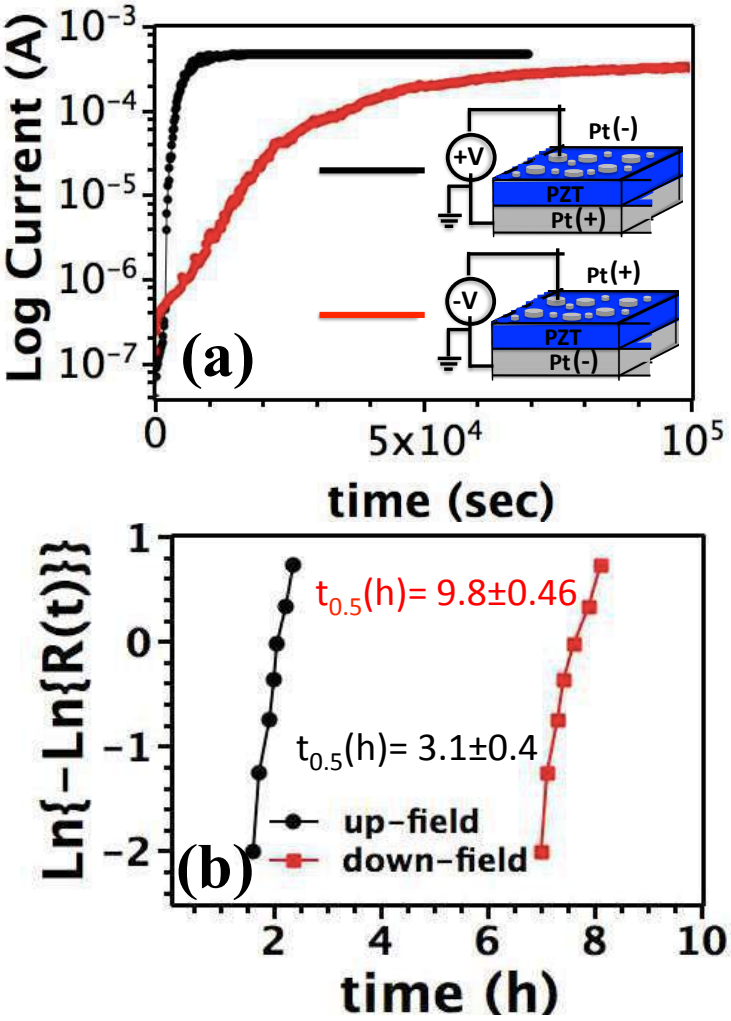

Figure 1 *(a) Variation in leakage current with time, (b) the time to failure for 2% Mn doped PZT films. R(t) represents the probability of failure over time. The HALT measurement was conducted at 180°C with a DC field of either 350 or -350 kV/cm.*

degradation was governed by the Pt/PMZT interface that was negatively biased (the cathode). Under field-down electric fields, on the other hand, the magnitude of leakage current at the negatively biased top Pt/PNZT interface (cathode) was significantly suppressed with a small change in the leakage current for the positively biased top Pt/PMZT interface.

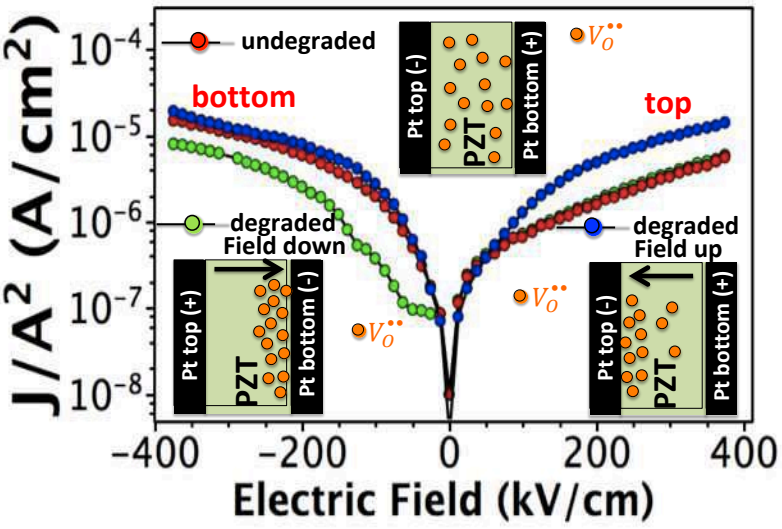

Figure 2 *Temperature dependence of conductivity for different polarities, as indicated by the arrows. The field direction for the current/voltage measurement is defined by the charge signs on the Pt electrodes.*

To elucidate the electronic conduction mechanisms governing electrical degradation, the I-V response of PMZT films before and after degradation was fit to the equations for various conduction mechanisms. Figure A.3a shows the disparity in the conduction mechanism near the top Pt/PMZT interface in the pristine state and after degradation under an electric field of -350 and 350 kV/cm for 12 h. Current density-electric field (JE) characteristics in the pristine state exhibited good linearity for both Poole-Frenkel (Ln(J/E) versus $E^{1/2}$) and Schottky emission (Ln (J/T^2) versus $E^{1/2}$) conduction mechanisms. The refractive index, n, was estimated from the slope Poole-Frenkel and Schottky plots. At low electric fields (<32 kV/cm), *n* calculated from Poole-Frenkel plots ranged from 2.7 to 2.9, in good agreement with the refractive index of PZT (n~ 2.25). This suggests that Poole-Frenkel emission controls the conduction at low electric fields; it has been previously shown that (1) hole hopping between Pb^{2+} and Pb^{3+}

sites, (2) hole migration between lead vacancies, and (3) hole trappig by $Mn^{2+/3+}$ are the main mechanisms that contribute to Poole-Frenkel conduction in PMZT films. With increasing electric fields (>50 kV/cm), a refractive index of about 1.8 was obtained from the slopes of Schottky plots, indicating that Schottky emission dominates the leakage current.

In contrast to the top Pt/PMZT interface, the switch from Poole-Frenkel to Schottky emission occurs at higher electric fields (>186 kV/cm) for the bottom Pt/PMZT interface, accompanied by a lower potential barrier height (0.95±0.05 eV) for electron injection from the Pt electrode into the PMZT. Typically, the Schottky barrier height depends not only on the PZT work function and electron affinity, but also on the density and distribution of impurity sites at the interface due to Fermi-level pinning. The most possible candidate that causes potential barrier lowering through Fermi level pinning, is oxygen vacancies in PZT films. Acceptor ions like $Mn^{2+/3+}$ in PZT films are ionically compensated by oxygen vacancies and create defect dipoles represented as $(Mn''_{Ti} - V_O^{\square\square})^x$, $(Mn'_{Ti} - V_O^{\square\square})'$. The variation in oxidation state of Mn ions through the thickness of the PMZT films results in oxygen vacancy gradient through the film. This can modify (1) the number of oxygen vacancies accumulated near the cathode region upon electrical degradation, (2) the local hole concentration near the cathode and anode Pt regions.

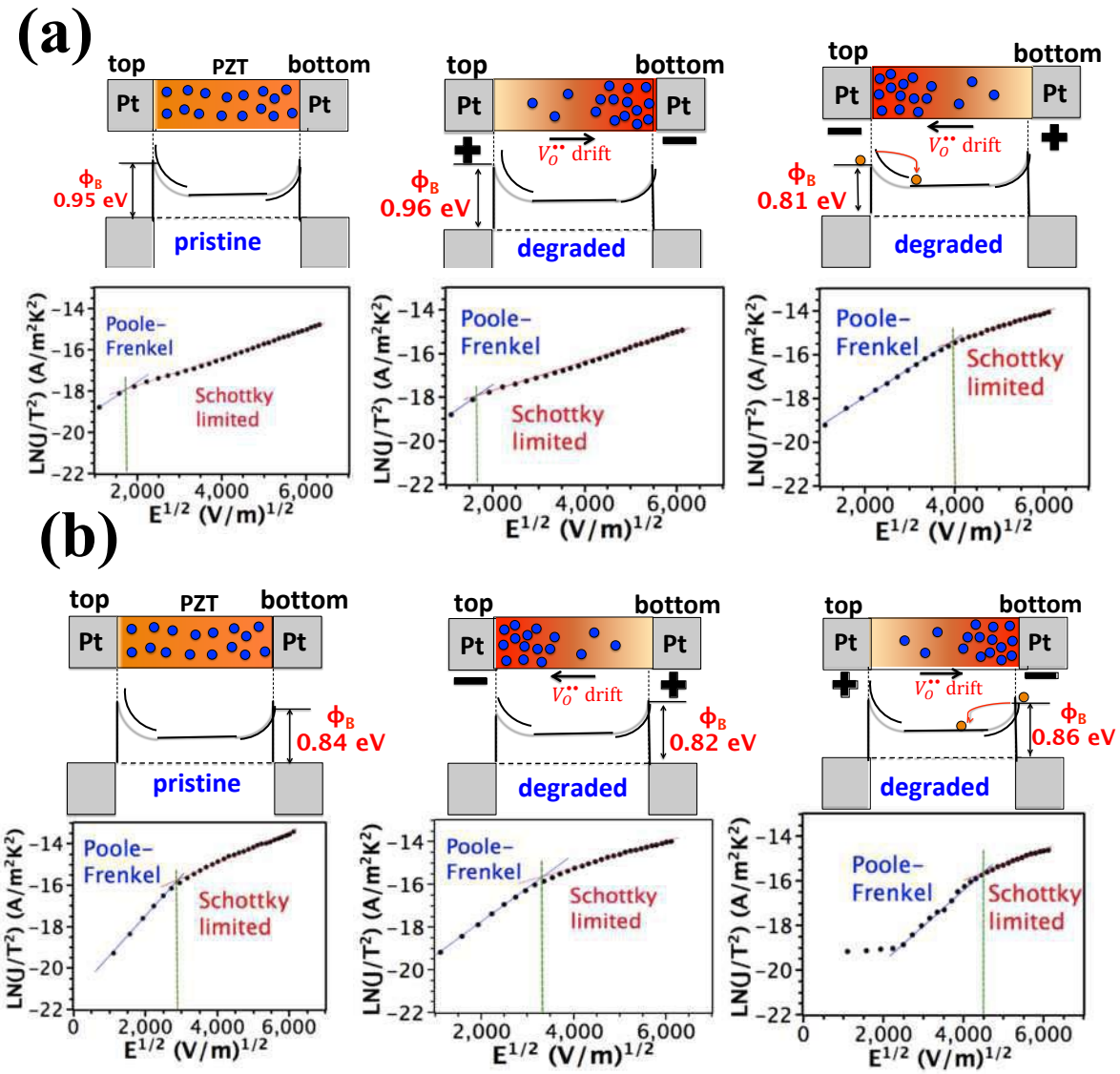

Figure 3 *Fitting of the leakage current-voltage data for distinct electric fields in 2 % Mn doped PZT thin films before (Figure 3a) and after degradation (Figure 3b) at 180°C under an electric field of 350 or -350 kV/ cm for 12h.*

To investigate the variation in Mn valence state through the film and resultant change in local defect chemistry, impedance and DLTS analyses were performed on 2% Mn doped PZT thin films before and after heating at 320°C for 3 weeks (Figure A.4). Figure A.4 (a) exhibits the imaginary modulus of 2% Mn doped PZT films as a function

of frequency after holding at 320°C for distinct times. The magnitude of conductivity of 2% Mn doped PZT film increased approximately two orders of magnitude after holding at 320°C for 366 h. The enhanced conductivity after heating for 2 weeks is attributed to ionization of Mn. Some of the Mn^{2+} ions in PZT films can be ionized to Mn^{3+} ions through absorbing oxygen from the atmosphere (Figure A.4(b) and (c)).

$$Mn'_{Ti} \longrightarrow Mn''_{Ti} + h^{\cdot} \qquad \Delta H = 1.9 \text{ eV}$$

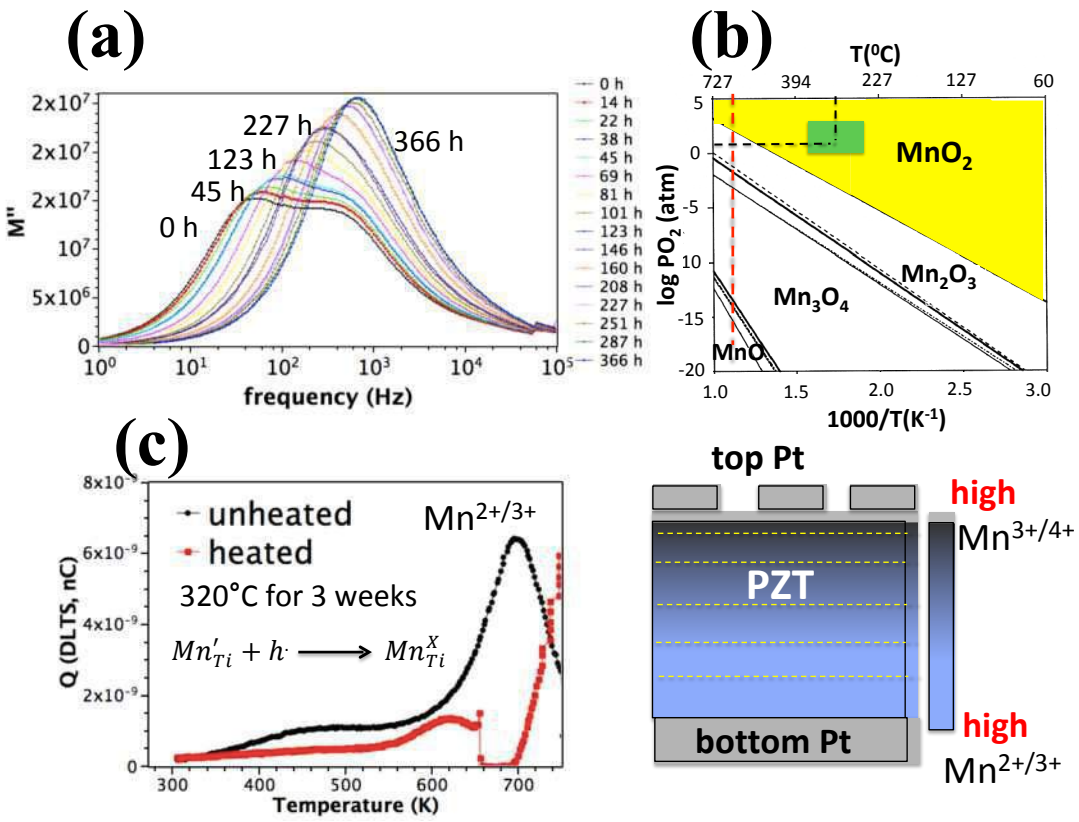

Figure 5 (a) *Imaginary modulus of 2% Mn doped PZT plotted as a function of frequency after heating at 320°C for distinct times, (b) Mn-O phase stability diagram, and (c) Q-DLTS of 2% Mn doped PZT films before and after heating at 320°C for 3 weeks.*

Since the likelihood of oxygen absorption in the PMZT layers close to the top Pt upon heating at 320°C is higher than that of PMZT layers close to the bottom Pt

electrode, one could expect existence of higher Mn oxidation state in the upper PMZT layers close to the top Pt electrode. This also leads to oxygen vacancy gradient through the film.

To investigate the migration of oxygen vacancy and resultant change in local interfacial defect chemistry near the top and the bottom Pt electrodes, TSDC analysis was performed on electrically degraded PMZT films. Figure A.5 shows the TSDC results of PMZT films after degradation under an electric field of 350 (top electrode is negatively biased) or -350 kV/cm (bottom electrode is negatively biased) for 12 h. The temperature of the current maximum for the TSDC peak around 200°C shifts higher with increasing poling electric field, suggesting that the TSDC peak corresponds to depolarization of space charges. An activation energy of 0.56±0.06 eV was found, which is associated with migration of oxygen vacancies. However, the concentration of migrated oxygen vacancies, which is represented by the area under the TSDC peak, depends strongly on the electrical field polarity during degradation. The concentration of oxygen vacancies accumulated near the bottom and the top interfaces after degradation at -350 and 350 kV/cm for 12 h at 180°C was found to be $1X10^{20}$ and $6X10^{19}$ /cm^3, respectively. The difference in the concentration of accumulated oxygen vacancies most likely arises from variation in Mn valence state across the PMZT film in the pristine state. Given that some of the Mn ions are ionically compensated with oxygen vacancies, lower oxidation state of Mn ions near the bottom Pt/PMZT interface results in higher oxygen vacancy concentration in PMZT layers close to the bottom Pt electrode. This will increase the number of mobile oxygen vacancies near the bottom Pt/PMZT interface upon electrical degradation. It is believed that higher oxygen vacancy concentration near the bottom

Pt/PMZT is responsible for lower potential barrier height for electron injection from Pt electrode into PMZT films.

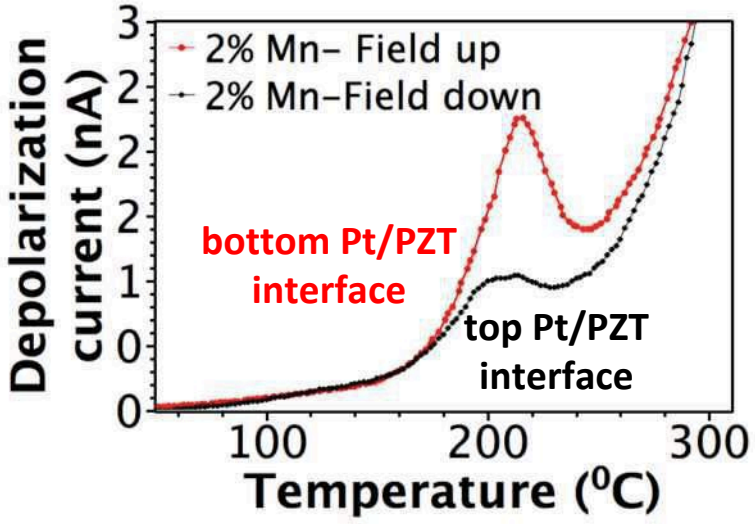

Figure 5 *Evaluation of TSDC spectra of 2% Mn doped PZT films after degrading the films at 180°C with a DC field of 350 or -350 kV/cm.*

In spite of lower potential barrier height and higher oxygen concentration near the bottom Pt/PMZT interface, higher lifetime and lower electrical degradation rates were observed under field-down electric fields. This unexpected electrical degradation behavior might arise from electron/hole trapping effect of Mn ions in PZT films. Mn ions can act as both electron and hole traps. The concentration of free electrons and holes accumulated near the cathode and anode regions can be effectively suppressed in the presence of Mn ions. In fact, the Poole-Frenkel regime is effective over larger electric fields near the bottom Pt/PMZT layer both in pristine and degraded state. Mn ions in PZT films can be either ionically compensated via oxygen vacancies or/and electronically compensated by holes. Lower oxidation states of Mn ions near the bottom Pt./PMZT interface increases the local hole concentration, which enhances the Poole-Frenkel

reactions, like hole hopping between Mn ions. The hole concentration rise near the bottom Pt/PMZT films might suppress the effective density of charges, which determines the maximum electric field at the Schottky contact, as a result of annihilation of injected electrons and holes. This will reduce potential barrier lowering for electron injection and improves the resistance degradation of PMZT films under field-down electric fields.

Vita

Betul Akkopru-Akgun

Betul Akkopru-Akgun was born in Eskisehir, Turkey on December 2nd, 1982. Before beginning her doctoral degree program at Penn State University, she received summa cum laude in Ceramic Engineering from the Dumlupinar University in Turkey and M.S. degree in Metallurgical and Materials Engineering from Middle East Technical University in Turkey. She also completed a second M.S. in the department of Materials Science and Engineering at Penn State University. Additionally, she stayed as a visiting scholar in the department of Ceramic Engineering at Alfred University.